Using human embryonic stem cells (hESCs) as an *in vitro* model for environmental contaminant embryotoxicity testing

Bai Li

Thesis submitted in partial fulfillment of the requirements for the
Doctorate in Philosophy degree in Biology.

Department of Biology
Faculty of Science
University of Ottawa

Abstract

Early embryo development is one of the most sensitive stages to environmental chemicals during the whole life. Prenatal exposures to many environmental chemicals have been shown to impact fetal development and be associated with adverse health outcomes in later life stages. However, the effects of chemical mixture exposure on developing embryos, especially in early developmental stages, have yet to be fully studied. To fulfill this research gap, my thesis was divided into three data chapters and mainly aimed at investigating the effects of a chemical mixture on human early-stage embryo development. In Chapter 2, I chose methylmercury (MeHg) as the main study toxicant to establish procedures for embryotoxicity testing using human embryonic stem cells (hESCs). I then characterized the effects of low doses of MeHg on this stem cell model by screening a set of cell fate decision-related makers and found MeHg is embryotoxic, which is consistent with epidemiological and *in vivo* findings. In Chapter 3, I studied the embryotoxicity of a chemical mixture that consists of 23 individual environmental chemicals (including MeHg) detected from the maternal blood samples of pregnant women in Nunavik, labelled as Nunavik Contaminant Mixture (NCM), using the same cell model. The effects of NCM exposure on hESCs were compared to MeHg exposure alone. NCM exposure adversely affected cell viability and adhesion, induced apoptosis, disrupted the cell cycle, altered the expression of cytoskeleton and autophagy proteins, and changed the levels of lineage marker gene and protein expressions in a dose-dependent manner. Some distinct effects on hESCs between NCM exposure and MeHg alone exposure were noticed, and the potential interactions among the chemical components within a chemical mixture were indicated. In Chapter 4, I studied the effects of MeHg exposure during the formation of definitive endoderm (DE) cells from hESCs and compared that to MeHg's effects on undifferentiated hESCs. I found that cell

specification towards endoderm could be affected by MeHg exposure, mainly through disrupting calcium homeostasis and over-generating reactive oxygen species, leading to increased ribosome biogenesis and protein synthesis. Moreover, MeHg effects are state-dependent; MeHg enhances pluripotency in undifferentiated hESCs, but it promotes differentiation during DE induction. Taken together, this thesis verifies the value of hESCs in testing the embryotoxicity and developmental toxicity of environmental chemicals, enriches the understanding of the toxicity of MeHg and NCM, emphasizes the necessity of evaluating the effects of chemical mixtures and provides new directions in studying environmental chemical toxicity using stem cells. Findings from my thesis could hopefully contribute to predicting the potential effects of prenatal environmental chemical exposures and aid in developing evidence-based public health policy.

Résumé

Le développement précoce de l'embryon est l'une des étapes les plus sensibles aux produits chimiques environnementaux tout au long de la vie. Il a été démontré que les expositions prénatales à de nombreux produits chimiques environnementaux ont un impact sur le développement du fœtus et que elles sont associées à des effets néfastes sur la santé aux stades ultérieurs de la vie. Cependant, les effets de l'exposition aux mélanges chimiques sur les embryons en développement, en particulier aux premiers stades de développement, n'ont pas encore été pleinement étudiés. Pour combler cette lacune de recherche, ma thèse a été divisée en trois chapitres de données et visait principalement à étudier les effets d'un mélange chimique sur le développement de l'embryon humain à un stade précoce. Au chapitre 2, j'ai choisi le méthylmercure (MeHg) comme principal toxique d'étude pour établir des procédures de test d'embryotoxicité à l'aide de cellules souches embryonnaires humaines (CSEh). J'ai ensuite caractérisé les effets de faibles doses de MeHg sur ce modèle de cellules souches en examinant un ensemble de décideurs liés au destin cellulaire et j'ai découvert que le MeHg est embryotoxique, ce qui est cohérent avec les résultats épidémiologiques et *in vivo*. Dans le chapitre 3, j'ai étudié l'embryotoxicité d'un mélange chimique composé de 23 produits chimiques environnementaux individuels (dont MeHg) détectés dans des échantillons de sang maternel de femmes enceintes au Nunavik, étiquetés Nunavik Contaminant Mixture (NCM), en utilisant le même modèle cellulaire. Les effets de l'exposition au NCM sur les CSEh ont été comparés à l'exposition au MeHg seul. L'exposition au NCM a affecté négativement la viabilité et l'adhérence des cellules, induit l'apoptose, perturbé le cycle cellulaire, altéré l'expression des protéines du cytosquelette et de l'autophagie et modifié les niveaux d'expression des gènes marqueurs de lignée et des protéines de manière dose-dépendante. Certains effets distincts sur les

CSEh entre l'exposition au NCM et l'exposition au MeHg seul ont été remarqués, et les interactions potentielles entre les composants chimiques d'un mélange chimique ont été indiquées. Dans le chapitre 4, j'ai étudié les effets de l'exposition au MeHg lors de la formation de cellules endodermiques définitives (DE) à partir de CSEh et j'ai comparé cela aux effets du MeHg sur des CSEh indifférenciées. J'ai découvert que la spécification cellulaire vis-à-vis de l'endoderme pouvait être affectée par l'exposition au MeHg, principalement en perturbant l'homéostasie du calcium et en surgénérant des espèces réactives de l'oxygène, entraînant une augmentation de la biogenèse des ribosomes et de la synthèse des protéines. De plus, des effets dépendants de l'état de différenciation de l'exposition au MeHg sur les cellules souches ont été trouvés, car le MeHg favorise probablement la différenciation pendant l'induction de DE tandis que le MeHg améliore la pluripotence dans les CSEh indifférenciées. Pris ensemble, cette thèse vérifie la valeur des CSEh pour tester l'embryotoxicité et la toxicité pour le développement des produits chimiques environnementaux, enrichit la compréhension de la toxicité du MeHg et du NCM, souligne la nécessité d'évaluer les effets des mélanges chimiques et fournit de nouvelles orientations dans l'étude des produits chimiques environnementaux. toxicité à l'aide de cellules souches. Les résultats de ma thèse pourraient, espérons-le, contribuer à prédire les effets potentiels des expositions prénatales aux produits chimiques environnementaux et contribuer à l'élaboration d'une politique de santé publique fondée sur des données probantes.

Acknowledgements

A Ph.D journey is not smooth sailing, I cannot complete my project confidently without countless external supports. There are so many people that I should thank, but first and foremost, I must thank with my deepest gratitude my supervisor Dr. Laurie Chan. It is not only because the countless mentorships you have provided to me on research, but also the encouragements and supports you offered me when I faced difficult issues out of research. Your enthusiasm and perseverance on work showed me what a real scientist be like, and your wisdom in life led me to know how to live a happier and balanced life. Words are too powerless to express my gratitude and admiration, I cannot thank you enough.

Secondly, I was very lucky to have opportunity to do a part of my project in Dr. Dawn Jin's lab in Health Canada. Dawn, thank you for the patience you offered to discuss experimental problems with me, the efforts you made to revise the manuscripts and the care you gave to my daily life in the past several years. Especially, thank you so much for sharing your stories in both work and life with me that allowed me to broaden my horizons and improve faster in a new environment. I am also grateful to my committee members Dr. William Willmore and Dr. Tuan Bui for their thoughtful comments and suggestions throughout the project.

A big thank you must be given to all our lab members, especially Drs. Emmanuel Yumvihoze and Xuefeng Hu for the technical expertise and suggestions, and Ms. Kayla Greydanus, Lynn Barwin and Amada Loura for your help in the administrative components. With your help, the process of my project got much smoother.

Most importantly, I would like to thank my parents that always support me. Without my parents, this thesis would be impossible to achieve. A heartful thank to my husband, Yihang. He gives me unconditional love, understanding and respect which makes me stronger and more

confident. Last but most specially, I would say “thank you” to my first baby who is just two-month-old but have touched me a lot and makes me fearless. This thesis will be the birth gift to you. Welcome to the world, my little one!

This world is not gentle, but I hope you will be treated gently by this world.

这世界并不温柔，但，愿你被这世界温柔以待。

Table of Contents

List of Figures

List of Tables

List of Abbreviations

"3R" rules	Replacement, Reduction and Refinement
ANOVA	analysis of variance
BMD	benchmark dose
BSA	bovine serum albumin
CMA	chaperone-mediated autophagy
CO_2	carbon dioxide
DAPI	4',6-diamidino-2-phenylindole
DE	definitive endoderm
DEG	differentially expressed gene
DEPC	diethyl pyrocarbonate
DMSO	dimethyl sulfoxide
ECL	enhanced chemiluminescence
ELISA	enzyme-linked immunosorbent assay
EST	embryonic stem cell test
FC	fold change
GO	gene ontology
GSH	reduced glutathione
Hcy	homocysteine
hESC	human embryonic stem cell
Hg	mercury
hPSC	human pluripotent stem cell
HRP	horseradish peroxidase

ICM	inner cell mass
KEGG	kyoto encyclopedia of genes and genomes
MeHg	methylmercury
mESC	mouse embryonic stem cell
NCM	Nunavik contaminant/chemical mixture
NFDM	non-fat dry milk
NOAEL	no observed adverse effect level
NPC	neuroprogenitor cell
O_2	oxygen
OCs	organochlorines
OTA	ochratoxin A
PBS	phosphate-buffered saline
PCA	principal component analysis
PCBs	polychlorinated biphenyls
PCR	polymerase chain reaction
PFASs	perfluoroalkyl substance
PI	propidium iodide
POPs	persistent organic pollutants
PPI	protein-protein interaction
PVDF	polyvinylidene fluoride
RIPA	radioimmunoprecipitation assay buffer
ROS	reactive oxygen species
TBST	tris-buffered saline with 0.1% tween 20

TCDD	2,3,7,8-tetrachlorodibenzo-p-dioxin
β-ME	β-mercaptoethanol
HO-1	hemeoxygenase-1
LC3B	microtubule associated proteins 1A/1B light chain 3B
SQSTM1	sequestosome 1
GATA4	GATA binding protein 4
IL6ST	interleukin 6 cytokine family signal transducer
NANOG	Nanog homeobox
OCT4	octamer-binding transcription factor 4
POU5F1	POU domain, class 5, transcription factor 1
PRDM1	PR domain-containing protein 1
SOX2	SRY-box transcription factor 2
FOXA2	forkhead box A2
KLF5	Kruppel-like factor 5
PAX3	paired box 3
TRPM8	transient receptor potential cation channel subfamily M member 8
MYC	Myc proto-oncogene protein
SOX17	SRY-Box transcription factor 17
PDGFRA	platelet-derived growth factor receptor-alpha
NPPB	natriuretic peptide B
RGS4	protein expression of regulator of G protein signaling 4
DRD4	dopamine receptor D4
CC3	cleaved caspase 3

FCN3	ficolin 3
LEFTY2	left-right determination factor 2
EOMES	eomesodermin
COLEC10	collectin subfamily member 10
HNF1B	hepatocyte nuclear factor-1 beta
TM4SF1	transmembrane 4 L six family member 1
TBX3	T-Box transcription factor 3
TRIM56	tripartite motif containing 56
ABCA4	ATP binding cassette, subfamily A, member 4
CDH9	cadherin 9
BHMT	betaine-homocysteine S-methyltransferase
p-SMAD3	phosphorylated SMAD family member 3
URB1	URB1 ribosome biogenesis homolog
BMP4	bone morphogenetic protein 4
GATA6	GATA binding protein 6
SMAD3	SMAD family member 3
PSMB3	proteasome 20S subunit beta 3
CXCR4	C-X-C motif chemokine receptor 4
AOP	adverse outcome pathway
MIE	molecular initiating event
KE	key event
TKTD	toxicokinetic-toxicodynamic models

Chapter 1. General Introduction

1.1 Rationale

As one of the most susceptible periods, prenatal exposures to environmental chemicals have been recognized to affect fetal development, leading to adverse pregnancy outcomes, and posing risks to health concerns later in life [1-6]. Due to the rising awareness, a growing body of studies has been looking at the toxic effects of environmental chemicals on developing embryos with both *in vivo* and *in vitro* models, with most existing studies focusing on the effects of single chemicals. However, pregnant women are simultaneously exposed to various contaminants daily through multiple routes. Though studies on single chemicals can provide valuable information on understanding the developmental toxicity of individual chemicals, the interactions among different chemicals may need to be addressed [7]. More importantly, it seems not reliable to assess the effects of chemical mixtures by only considering the "safe levels" of each component within a chemical mixture or by simple addition of their effects [8], which could misestimate the potential risks associated with the chemical mixture [9] as the recent literature has suggested that the effects of chemical mixtures can be synergistic [9-12]. As such, the developmental effects of prenatal chemical mixture exposures are raising growing attention by both toxicological epidemiologists and bench researchers. In addition, most existing publications studying the effects of chemical mixtures were looking at the developing organs in post-implantation stages, and despite several studies looking at the effects of prenatal exposure to chemical mixtures and some animal studies examining the toxicity of chemical mixtures on preimplantation embryos [13, 14], the research focused on the toxicity of chemical mixtures on human early embryo developmental stages, such as blastocyst and implantation stages, are still lacking. Based on these research gaps, the main goal of this thesis is to investigate the effects of a chemical mixture

on human early-stage embryo development. The chemicals and human cell models used will be introduced in detail in the following text.

1.2 Nunavik Contaminant Mixture (NCM)

Due to the unique geological location, long-range transportation of toxic compounds and diets which rely on the marine food web, Indigenous populations residing in Arctic Canada are considered to be exposed to relatively high levels of environmental contaminants including persistent organic pollutants (POPs) such as polychlorinated biphenyls (PCBs), organochlorines (OCs), perfluoroalkyl substance (PFASs) and metals and metalloids such as MeHg and lead [15-17] compared to the populations who are living in the urban areas. There is an urgent need to understand the potential associations between exposure to these chemicals and the increasing health concerns of Indigenous people.

We prepared a chemical mixture that consists of 23 individual environmental chemicals called “Nunavik Contaminant Mixture (NCM)” based on human maternal profiles and levels of these chemicals detected from the blood samples of Nunavik pregnant women [18]. See Table 3.1 for the list of the chemicals included. Many components of NCM have been reported to be toxic to the developing embryos or fetus, leading to adverse pregnancy outcomes and long-lasting developmental failures. For example, prenatal exposure to low concentrations of PCBs was found to be inversely associated with human fetal growth [19] and intelligence (IQ) performance in childhood [20]. Gestational and lactational exposure to a PCB and OC pesticides mixture was reported to disrupt thyroid function and neurobehavioral development in rodents [21]. Animal studies also showed that co-exposure to some components of NCM impaired pancreatic function [22], suppressed growth, reduced weights of spleen and thymic, raised serum cholesterol levels [23], and even decreased progeny survival [24]. However, the effects of

chemical mixtures could not be accurately estimated by separately administering its individual or subgroup components as distinct alterations caused by a chemical mixture and its individual components have been found by gene and protein expression analysis [25, 26]. Thus, it is critical to study the embryonic and developmental effects of NCM as a complete mixture with the relevant dose and relative proportion of each chemical. In addition, since the majority of existing experimental evidence of the effects of these chemicals was concluded from animal studies, there are uncertainties when extrapolating to humans due to the differences among species in their response to chemical exposures [27]. Therefore, it is important to investigate the embryonic and developmental effects of NCM with models originating from humans.

1.3 Methylmercury (MeHg) and its developmental toxicity

Mercury (Hg) is a ubiquitous environmental pollutant that is harmful to both human health and the ecosystem [28]. Humans are exposed to Hg as its organic form, methylmercury (MeHg), which is one of the main constituents of NCM, mainly through the consumption of fish, marine mammals and rice [29, 30]. Among Hg species, MeHg is considered to be the most toxic, with the highest bioaccumulation factor [31]. Once consumed, MeHg forms a complex with cysteine and homocysteine and is well transported across the blood-brain barrier [31] and the placental barrier [32] by amino acid carriers. Although exposure levels of MeHg to the general populations are generally considered to be low, it may still produce subtle health effects, especially among sensitive populations, such as infants and children and Indigenous populations [33, 34]. Adverse developmental outcomes in infants and young children have been shown to be associated with MeHg exposure through maternal fish consumption during fetal development [35]. There is a latency period from months to years between MeHg exposure, and the manifestation of clinical symptoms and the effects are not reversible [36]. Thus, detecting the effects of MeHg at the

lowest level and at the earliest developmental stage is critical for predicting its "late onset" effects in individuals' later life.

As a well-known neurotoxicant, prenatal MeHg exposure has been reported to be associated with cognitive deficits in victims during their childhood, youth and even adulthood by birth cohort studies conducted on the Faroe Islands [37-39]. Both *in vivo* and *in vitro* studies showed that neural stem and progenitor cells were highly susceptible to MeHg, which caused apoptosis and inhibited neuronal differentiation at low concentrations, and even resulted in transgenerational effects [40-43]. Exposure of MeHg before and/or during gestation has also been found to reduce monoamine oxidase activity which plays a critical role in regulating the levels of dopamine and serotonin in the neural system, causing irreversible neurodevelopment damages in the rat brain [44]. In addition, prenatal exposure to MeHg has been shown to decrease parasympathetic activity and increase blood pressure in children [45-47], though these findings are still controversial [48]. Despite these studies looking at the effects of prenatal MeHg exposure on the developing cardiovascular system, most of the existing studies on the developmental toxicity of MeHg have been focusing on its neurological effects. Thus, more research focused on the toxicity of MeHg on the development of non-neuronal organs and systems, especially during their early formation and differentiation is still needed.

MeHg has long been recognized as one of the most hazardous environmental contaminants [49] and is usually employed as a positive control or model toxicant when studying the health effects of other chemicals or establishing novel test systems [49-51]. In addition to MeHg's developmental toxicity, as one of the main components of NCM, MeHg could interact with other components present within NCM when co-exposed, causing health effects on the developing fetus distinct from that of single chemical exposures. For example, combined exposure of PCBs

and MeHg could synergistically reduce dopamine content in rat brains compared to PCB exposure only [12]. For example, the PCB-related permanent auditory deficits resulting from developmental PCB exposure appeared to be diminished by co-exposure to MeHg [52]. Simultaneous exposure to PFOS and MeHg in pregnant rats can also induce additive effects such as delaying behavioural responses and decreasing weight gain in the newborn offspring but showed a chemical antagonism in the neurodevelopmental effects in juveniles due to potential differences in the combined toxicity of the binary chemical mixture at different developmental stages [7, 53].

Therefore, in this thesis, I chose MeHg as the main toxicant to establish procedures for testing of developmental toxicity using a stem cell model (see below) and a set of markers related to cell fate decisions and explored the feasibility of using this model to verify this model for investigating the embryonic and developmental toxicity of the NCM.

1.4 Human Embryonic Stem Cells (hESCs)

The embryonic stem cell test (EST), based on permanent cell lines differentiated from mouse embryonic stem cells (mESCs), has been proven to be a good model to assess embryonic or developmental toxicity *in vitro* due to the advantage of providing good predictions of embryonic or developmental toxicity of the tested chemicals without the need of embryonic tissues from pregnant animals [54, 55]. It also has the advantage of being less time-consuming and more affordable than *in vivo* models. However, the original mESC models failed to accurately classify some neurodevelopmental toxicants, including MeHg [56]. Although subsequent studies incorporated neuronal differentiation into the original mESC models had correctly classified MeHg as embryotoxic, potential false-negatives may still exist due to the species-specific differences [56, 57]. Therefore, the interest in EST has subsided. Recently, human embryonic

stem cells (hESCs), which were primarily separated from the inner cell mass (ICM) of human blastocysts generated from *in vitro* fertilization for clinical purposes [58], have emerged as a promising model for embryonic and developmental toxicity studies [59, 60].

As undifferentiated immature cells, hESCs have the capacity to self-renewal and the potency of differentiate [58]. Commonly, healthy hESCs have the potential to proliferate and differentiate into three primary germ layers, which then give rise to lineage progenitors and precursors, and finally develop into cells of different organs and systems in the body [58, 61]. But when exposed to environmental stressors, such as environmental chemicals, the cell fates of hESCs could be affected by inducing both genetic and epigenetic alterations, reflecting potential health risks on the developing embryos similar to those observed *in vivo*. For instance, a low dose of 2,3,7,8-tetrachlorodibenzo-p-dioxin (TCDD) exposure to hESCs impaired the potency towards early pancreatic lineage differentiation through inducing global DNA methylation pattern, which indicated potential alterations in pancreatogenesis and increased risk of type 2 diabetes [62]. Exposure to Ochratoxin A (OTA) at concentrations lower than that reported in maternal blood was shown to induce oxidative stress, decrease cell viability and induce apoptosis in hESCs [63], which suggested potential adverse pregnancy outcomes caused by prenatal exposure to OTA *in vivo*. However, most studies using hESCs as experimental models focus on clinical therapy and pharmaceutical screening; studies on the embryonic or developmental toxicity tests of environmental chemicals, especially of chemical mixtures, are limited. Moreover, the existing studies looking at the developmental effects of environmental chemicals have been mostly focused on their effects on differentiation or post-differentiation stem cells, with studies on the embryonic or developmental toxicity of environmental chemicals on undifferentiated hESCs, which reflects the initial blastocyst stage *in vivo*, being limited as well.

1.5 Definitive Endoderm (DE)

To further extend the utility of hESCs in examining developmental and embryonic toxicity, I tested the ability of this model to examine the mechanisms of MeHg toxicity. MeHg but not NCM, was chosen as the testing chemical to conduct further mechanistic research due to the accumulative experience of MeHg research in our lab and the inherent complexity and the questionable utility of examining the mechanisms of a contaminant mixture. As mentioned above, since fetal development is one of the most sensitive windows to MeHg toxicity and MeHg is known to be neurotoxic, *in vitro* studies have mainly looked at the effects of MeHg on neural cell development. Some of these studies examined the effects of MeHg on ectoderm differentiation as neural cells are ectoderm derived, using embryonic stem cells as a model [64, 65]. However, in addition to neurotoxicity, exposure to MeHg has also been shown to be associated with hypertension and cardiovascular diseases [66], increased risks of diabetes [67], delayed pancreas development [68], as well as the disruption of gut microbial communities [69] in epidemiological studies and/or animal models. Yet, there are no *in vitro* studies investigating the effects of MeHg on other germ layers that give rise to these organs or systems.

Definitive endoderm (DE), which would typically give rise to the liver, pancreas, lung, and gut *in vivo*, is one of the three primary germ layers generated from the pluripotent epiblast during gastrulation [70] and is considered to be formed prior to the other two germ layers, mesoderm and ectoderm [71], which are also emerging as promising models for developmental toxicity testing [72]. Multiple methodologies [72] have been established to induce hESCs into DE cells with Wnt, Nodal/Activin, and BMPs are three main types of signals that have been shown to regulate DE differentiation [73-77]. Thus, here I studied the effects of MeHg exposure during the

formation of DE cells from hESCs, hypothesizing it effects through these three signaling pathways, as a starting point to elucidate the possible underlying mechanisms.

1.6 Research questions, objectives, and outline of this thesis

Prenatal exposure to multiple types of individual environmental chemicals have been shown to be embryotoxic or developmental toxic, causing various adverse pregnancy or developmental outcomes. However, there is still a general lack of studies on the embryotoxicity and developmental toxicity of environmental chemical mixtures. In addition, many symptoms resulting from exposure of environmental chemicals are "late onset", which to some degree could affect or determine the later development of individuals, appearing months to years after exposure. Thus, investigating the potential effects of these chemicals during early stages of embryo development is important for predicting their developmental toxicities on individuals' later-stage development. However, most studies on the developmental toxicity of environmental chemicals have been focusing on the developing fetus at later *in utero* developmental stages or young children. Therefore, it is important to study the effects of environmental chemicals on early-stage developing embryos, such as blastocyst and implantation stages.

My first research question is whether exposure of MeHg could affect definitive endoderm development and how these effects would potentially impact subsequent embryo development? Also, what are the underlying mechanisms of MeHg toxicity on DE differentiation?

My second research question is whether exposure of environmental chemical mixtures could affect human early embryo development, and how these effects could affect the development in later life-stages? Also, I wanted to see if the no observable effect levels for the chemical mixture are comparable to those observed for individual chemicals.

To answer these research questions and fill in the knowledge gaps, my thesis is organized into three data chapters. To mimic the *in vivo* early embryo developmental stages, including blastocyst, pre-, during-, and early post-implantation stages, undifferentiated human embryonic stem cells (hESCs) were employed as the experimental cell model. Culture conditions were optimized before dosing and endpoint detection.

In the first data chapter (Chapter 2), MeHg was used as the testing chemical to verify the feasibility of chemical toxicity measurement using undifferentiated hESCs. Chapter 3 characterized the effects of prenatal NCM exposure on human early developing embryos, using cultured undifferentiated hESCs as an *in vitro* model, comparing the similarity and differences in the results of single MeHg exposure to that of NCM and inferred the possible reasons. These two chapters screened multiple cell fate related endpoints, including markers of viability, cell cycle, oxidative stress response, apoptosis, autophagy, cytoskeleton, and self-renewal and lineage differentiation potency, and suggested that cultured undifferentiated hESCs could be a useful *in vitro* model in chemical embryotoxicity testing. Moreover, these two chapters provide information in better understanding the adverse pregnancy and developmental outcomes associated with MeHg and NCM exposure, and more importantly make aware of the potential interactions which might be ignored in assessing risks of chemical mixtures' embryotoxicity.

In Chapter 4, I investigated the possible mechanisms of the effects of MeHg exposure during definitive endoderm formation on human embryonic development using hESC-derived DE cells. I exposed the hESC-derived DE cells to population-relevant concentrations of MeHg and measured the effects using a transcriptomics approach. The changes in selected markers were verified on both the gene and protein levels. I explored the potential mechanisms using multiple bioinformatic analyses. The objective of this chapter is to provide insights into the effects of

MeHg exposure on the differentiating definitive endoderm and subsequent embryo development. It offers a research direction which can enrich the understanding of MeHg toxicity in the early generation and development of other organs or systems, not limiting to developing neurons.

All data chapters were written as standalone manuscripts. A final chapter, Chapter 5, is included to summarize highlights or results and discuss the main contributions, limitations and future directions of this thesis. Although I have been trying to avoid repetitions, some repetitions, particularly in the introduction sections, may still exist, as this thesis is composed partly of published or under-review manuscripts.

1.7 Author contribution statement

B. Li, X. Jin and H.M. Chan designed this study. B. Li conducted the experiments and prepared the drafts for all the three papers. C. Qiao and Y. Pan conducted the statistical analysis of Scorecard data for Chapter 2 and 3, respectively. B. Li carried out the data analysis of Chapter 4 and the rest of Chapters 2 and 3. All authors provided comments to the manuscripts. X. Jin and H.M. Chan critically reviewed and edited to the final version of the manuscripts. H.M. Chan finalized and submitted the manuscripts.

1.8 Reference

1. Palanza, P., et al., Prenatal exposure to endocrine disrupting chemicals: effects on behavioral development. Neuroscience & Biobehavioral Reviews, 1999. **23**(7): p. 1011-1027.

2. Perera, F. and J. Herbstman, Prenatal environmental exposures, epigenetics, and disease. Reproductive toxicology, 2011. **31**(3): p. 363-373.
3. Bellinger, D.C., Prenatal exposures to environmental chemicals and children's neurodevelopment: an update. Safety and health at work, 2013. **4**(1): p. 1-11.
4. Rager, J.E., et al., Review of the environmental prenatal exposome and its relationship to maternal and fetal health. Reproductive toxicology, 2020. **98**: p. 1-12.
5. Ha, E., et al., Current progress on understanding the impact of mercury on human health. Environmental research, 2017. **152**: p. 419-433.
6. Doherty, B.T., et al., Periconceptional and prenatal exposure to metal mixtures in relation to behavioral development at 3 years of age. Environmental Epidemiology, 2020. **4**(4).
7. Reardon, A., et al. A Developmental Toxicology Model of Perfluorooctane Sulfonate and Methylmercury Co-Exposure. in ISEE Conference Abstracts. 2018.
8. Stavenes Andersen, I., et al., Effects of methyl mercury in combination with polychlorinated biphenyls and brominated flame retardants on the uptake of glutamate in rat brain synaptosomes: a mathematical approach for the study of mixtures. Toxicological sciences, 2009. **112**(1): p. 175-184.
9. Kortenkamp, A. and M. Faust, Regulate to reduce chemical mixture risk. Science, 2018. **361**(6399): p. 224-226.
10. Cedergreen, N., Quantifying synergy: a systematic review of mixture toxicity studies within environmental toxicology. PloS one, 2014. **9**(5): p. e96580.
11. Kortenkamp, A., Low dose mixture effects of endocrine disrupters and their implications for regulatory thresholds in chemical risk assessment. Current opinion in pharmacology, 2014. **19**: p. 105-111.

12. Bemis, J.C. and R.F. Seegal, Polychlorinated biphenyls and methylmercury act synergistically to reduce rat brain dopamine content *in vitro*. Environmental health perspectives, 1999. **107**(11): p. 879-885.

13. Fabro, S., J. McLachlan, and N. Dames, Chemical exposure of embryos during the preimplantation stages of pregnancy: mortality rate and intrauterine development. American journal of obstetrics and gynecology, 1984. **148**(7): p. 929-938.

14. Greenlee, A.R., T.M. Ellis, and R.L. Berg, Low-dose agrochemicals and lawn-care pesticides induce developmental toxicity in murine preimplantation embryos. Environmental health perspectives, 2004. **112**(6): p. 703-709.

15. Muckle, G., et al., Prenatal exposure of the northern Québec Inuit infants to environmental contaminants. Environmental health perspectives, 2001. **109**(12): p. 1291-1299.

16. Kuhnlein, H.V. and H.M. Chan, Environment and contaminants in traditional food systems of northern indigenous peoples. Annual review of nutrition, 2000. **20**: p. 595.

17. Boucher, O., et al., Prenatal exposure to methylmercury and PCBs affects distinct stages of information processing: an event-related potential study with Inuit children. Neurotoxicology, 2010. **31**(4): p. 373-384.

18. Furgal, C., et al., Exposure to food chain contaminants in Nunavik: Evaluating spatial and time trends among pregnant women & implementing effective health communication for healthy pregnancies and children (Year 2 of 3).

19. Govarts, E., et al., Birth weight and prenatal exposure to polychlorinated biphenyls (PCBs) and dichlorodiphenyldichloroethylene (DDE): a meta-analysis within 12 European Birth Cohorts. Environmental health perspectives, 2012. **120**(2): p. 162-170.

20. Stewart, P.W., et al., The relationship between prenatal PCB exposure and intelligence (IQ) in 9-year-old children. Environmental health perspectives, 2008. **116**(10): p. 1416-1422.

21. Bowers, W.J., et al., Early developmental neurotoxicity of a PCB/organochlorine mixture in rodents after gestational and lactational exposure. Toxicological Sciences, 2004. **77**(1): p. 51-62.

22. Mailloux, R., et al., A Northern contaminant mixture impairs pancreas function in obese and lean JCR rats and inhibits insulin secretion in MIN6 cells. Toxicology, 2015. **334**: p. 81-93.

23. Chu, I., et al., Toxicological effects of *in utero* and lactational exposure of rats to a mixture of environmental contaminants detected in Canadian Arctic human populations. Journal of Toxicology and Environmental Health, Part A, 2008. **71**(2): p. 93-108.

24. Beyrouty, P. and H.M. Chan, Co-consumption of selenium and vitamin E altered the reproductive and developmental toxicity of methylmercury in rats. Neurotoxicology and Teratology, 2006. **28**(1): p. 49-58.

25. Pelletier, G., et al., Contribution of methylmercury, polychlorinated biphenyls and organochlorine pesticides to the toxicity of a contaminant mixture based on Canadian Arctic population blood profiles. Toxicology letters, 2009. **184**(3): p. 176-185.

26. Padhi, B., et al., Gene expression profiling in rat cerebellum following *in utero* and lactational exposure to mixtures of methylmercury, polychlorinated biphenyls and organochlorine pesticides. Toxicology letters, 2008. **176**(2): p. 93-103.

27. Burgess-Herbert, S.L. and S.Y. Euling, Use of comparative genomics approaches to characterize interspecies differences in response to environmental chemicals: challenges,

opportunities, and research needs. Toxicology and applied pharmacology, 2013. **271**(3): p. 372-385.

28. Chan, H.M., Advances in methylmercury toxicology and risk assessment. 2019, MDPI. p. 20.

29. Chan, H.M. and O. Receveur, Mercury in the traditional diet of indigenous peoples in Canada. Environmental Pollution, 2000. **110**(1): p. 1-2.

30. Li, P., et al., Mercury bioaccumulation and its toxic effects in rats fed with methylmercury polluted rice. Science of the Total Environment, 2018. **633**: p. 93-99.

31. Leopold, K., M. Foulkes, and P.J. Worsfold, Preconcentration techniques for the determination of mercury species in natural waters. TrAC Trends in Analytical Chemistry, 2009. **28**(4): p. 426-435.

32. Cernichiari, E., et al., The biological monitoring of prenatal exposure to methylmercury. Neurotoxicology, 2007. **28**(5): p. 1015-1022.

33. Aremu, D.A., M.S. Madejczyk, and N. Ballatori, N-acetylcysteine as a potential antidote and biomonitoring agent of methylmercury exposure. Environmental Health Perspectives, 2008. **116**(1): p. 26-31.

34. Chapman, L. and H.M. Chan, The influence of nutrition on methyl mercury intoxication. Environmental health perspectives, 2000. **108**(suppl 1): p. 29-56.

35. Driscoll, C.T., et al., Mercury as a global pollutant: sources, pathways, and effects. Environmental science & technology, 2013. **47**(10): p. 4967-4983.

36. Clarkson, T.W., The toxicology of mercury. Critical reviews in clinical laboratory sciences, 1997. **34**(4): p. 369-403.

37. Grandjean, P., et al., Cognitive deficit in 7-year-old children with prenatal exposure to methylmercury. Neurotoxicology and teratology, 1997. **19**(6): p. 417-428.

38. Debes, F., et al., Impact of prenatal methylmercury exposure on neurobehavioral function at age 14 years. Neurotoxicology and teratology, 2006. **28**(5): p. 536-547.

39. Debes, F., P. Weihe, and P. Grandjean, Cognitive deficits at age 22 years associated with prenatal exposure to methylmercury. Cortex, 2016. **74**: p. 358-369.

40. Bose, R., et al., Inherited effects of low-dose exposure to methylmercury in neural stem cells. Toxicological Sciences, 2012. **130**(2): p. 383-390.

41. Tamm, C., et al., High susceptibility of neural stem cells to methylmercury toxicity: effects on cell survival and neuronal differentiation. Journal of neurochemistry, 2006. **97**(1): p. 69-78.

42. Tamm, C., et al., Methylmercury inhibits differentiation of rat neural stem cells via Notch signalling. Neuroreport, 2008. **19**(3): p. 339-343.

43. Edoff, K., et al., Gestational age and sex influence the susceptibility of human neural progenitor cells to low levels of MeHg. Neurotoxicity research, 2017. **32**(4): p. 683-693.

44. Beyrouty, P., et al., Effects of prenatal methylmercury exposure on brain monoamine oxidase activity and neurobehaviour of rats. Neurotoxicology and teratology, 2006. **28**(2): p. 251-259.

45. Murata, K., et al., Subclinical effects of prenatal methylmercury exposure on cardiac autonomic function in Japanese children. International archives of occupational and environmental health, 2006. **79**(5): p. 379-386.

46. Chan, P.H.Y., et al., Prenatal methylmercury exposure is associated with decrease heart rate variability in children. Environmental Research, 2021. **200**: p. 111744.

47. Sørensen, N., et al., Prenatal methylmercury exposure as a cardiovascular risk factor at seven years of age. Epidemiology, 1999: p. 370-375.

48. Thurston, S.W., et al., Does prenatal methylmercury exposure from fish consumption affect blood pressure in childhood? Neurotoxicology, 2007. **28**(5): p. 924-930.

49. Watanabe, C. and H. Satoh, Evolution of our understanding of methylmercury as a health threat. Environmental Health Perspectives, 1996. **104**(suppl 2): p. 367-379.

50. Myhre, O. and F. Fonnum, The effect of aliphatic, naphthenic, and aromatic hydrocarbons on production of reactive oxygen species and reactive nitrogen species in rat brain synaptosome fraction: the involvement of calcium, nitric oxide synthase, mitochondria, and phospholipase A. Biochemical pharmacology, 2001. **62**(1): p. 119-128.

51. Krug, A.K., et al., Human embryonic stem cell-derived test systems for developmental neurotoxicity: a transcriptomics approach. Archives of toxicology, 2013. **87**(1): p. 123-143.

52. Powers, B.E., et al., Developmental exposure to PCBs, MeHg, or both: long-term effects on auditory function. Environmental health perspectives, 2009. **117**(7): p. 1101-1107.

53. Reardon, A.J.F., Developmental Toxicity from Perfluoroalkyl Acid and Mercury Co-Exposure in Experimental and Epidemiological Models. 2019.

54. Seiler, A.E. and H. Spielmann, The validated embryonic stem cell test to predict embryotoxicity *in vitro*. Nature protocols, 2011. **6**(7): p. 961-978.

55. van Oostrom, C.T., W. Slob, and L.T. van der Ven, Defining embryonic developmental effects of chemical mixtures using the embryonic stem cell test. Food and Chemical Toxicology, 2020. **140**: p. 111284.

56. Luz, A.L. and E.J. Tokar, Pluripotent stem cells in developmental toxicity testing: a review of methodological advances. Toxicological Sciences, 2018. **165**(1): p. 31-39.

57. Adler, S., et al., First steps in establishing a developmental toxicity test method based on human embryonic stem cells. Toxicology *in vitro*, 2008. **22**(1): p. 200-211.

58. Thomson, J.A., et al., Embryonic stem cell lines derived from human blastocysts. science, 1998. **282**(5391): p. 1145-1147.

59. Yamane, J., et al., Prediction of developmental chemical toxicity based on gene networks of human embryonic stem cells. Nucleic acids research, 2016. **44**(12): p. 5515-5528.

60. Jung, E.M., et al., Evaluation of developmental toxicity using undifferentiated human embryonic stem cells. Journal of Applied Toxicology, 2015. **35**(2): p. 205-218.

61. Fu, Z. and X. Chris, Studying developmental neurotoxic effects of bisphenol A (BPA) using embryonic stem cells. 环境科学学报: 英文版, 2015(10): p. 173-177.

62. Kubi, J.A., et al., Effects of 2, 3, 7, 8-tetrachlorodibenzo-p-dioxin (TCDD) on the differentiation of embryonic stem cells towards pancreatic lineage and pancreatic beta cell function. Environment international, 2019. **130**: p. 104885.

63. Erceg, S., et al., Assessment of Toxic Effects of Ochratoxin A in Human Embryonic Stem Cells. Toxins, 2019. **11**.

64. Kang, S.-J., et al., Toxic effects of methylmercury, arsanilic acid and danofloxacin on the differentiation of mouse embryonic stem cells into neural cells. Journal of Veterinary Science, 2014. **15**(1): p. 61-71.

65. He, X., et al., Effects of methylmercury exposure on neuronal differentiation of mouse and human embryonic stem cells. Toxicology letters, 2012. **212**(1): p. 1-10.

66. Hu, X.F., K. Singh, and H.M. Chan, Mercury exposure, blood pressure, and hypertension: A systematic review and dose–response meta-analysis. Environmental health perspectives, 2018. **126**(07): p. 076002.

67. Tsai, T.-L., et al., Type 2 diabetes occurrence and mercury exposure–From the National Nutrition and Health Survey in Taiwan. Environment international, 2019. **126**: p. 260-267.

68. Mendes F, G.E., et al., Effects of low-dose exposure of rat fetuses pancreas to methylmercury: morphometric and stereologic studies. Rev. chil. anat, 1998: p. 177-83.

69. Lin, X., et al., Acute oral methylmercury exposure perturbs the gut microbiome and alters gut-brain axis related metabolites in rats. Ecotoxicology and environmental safety, 2020. **190**: p. 110130.

70. D'Amour, K.A., et al., Efficient differentiation of human embryonic stem cells to definitive endoderm. Nature biotechnology, 2005. **23**(12): p. 1534-1541.

71. Muhr, J. and K.M. Ackerman, Embryology, gastrulation. 2020.

72. Mennen, R., M. Oldenburger, and A. Piersma, Endoderm and mesoderm derivatives in embryonic stem cell differentiation and their use in developmental toxicity testing. Reproductive Toxicology, 2022. **107**: p. 44-59.

73. Teo, A.K., et al., Activin and BMP4 synergistically promote formation of definitive endoderm in human embryonic stem cells. Stem Cells, 2012. **30**(4): p. 631-642.

74. McLean, A.B., et al., Activin a efficiently specifies definitive endoderm from human embryonic stem cells only when phosphatidylinositol 3-kinase signaling is suppressed. Stem cells, 2007. **25**(1): p. 29-38.

75. Teo, A.K.K., et al., Pluripotency factors regulate definitive endoderm specification through eomesodermin. Genes & development, 2011. **25**(3): p. 238-250.

76. Kim, S.W., et al., Chromatin and transcriptional signatures for Nodal signaling during endoderm formation in hESCs. Developmental biology, 2011. **357**(2): p. 492-504.

77. Funa, N.S., et al., β-Catenin regulates primitive streak induction through collaborative interactions with SMAD2/SMAD3 and OCT4. Cell stem cell, 2015. **16**(6): p. 639-652.

Chapter 2: Characterizing the low dose effects of methylmercury on the early stages of embryo development using cultured human embryonic stem cells

Bai Li[1], Cunye Qiao[2], Xiaolei Jin[3*], Hing Man Chan[1*]

[1] Department of Biology, University of Ottawa. Ottawa, Ontario, Canada

[2] Biostatistics and Modeling Division, Bureau of Food Surveillance and Science Integration, Food Directorate, HPFB, Health Canada, Ottawa, Ontario, Canada

[3] Regulatory Toxicology Research Division, Bureau of Chemical Safety, Food Directorate, Health Canada, Ottawa, Ontario, Canada

This chapter has been published as:

Li, B., Qiao, C., Jin, X. and Chan, H.M., 2021. Characterizing the Low-Dose Effects of Methylmercury on the Early Stages of Embryo Development Using Cultured Human Embryonic Stem Cells. *Environmental Health Perspectives, 129(7), p.077007*.

https://ehp.niehs.nih.gov/doi/full/10.1289/EHP7349

Abstract

Global concerns of methylmercury (MeHg) exposure have been raised, especially on its effects on pregnant women. Recent epidemiological studies revealed associations between maternal blood/hair MeHg concentrations, adverse pregnancy outcomes, and developmental deficits. However, the underlying mechanisms remain unclear. In this study, we characterized the effects of MeHg exposure on undifferentiated human embryonic stem cells (hESCs) and extrapolated the effects to human embryonic development. hESCs were exposed to 0, 1, 5, 10, 50, 100 and 200 nM MeHg for 24 h or 6 days. Cell adherence and colony formation and expansion were examined under the microscope. Cell attachment, viability/proliferation, apoptosis, stress response, cell cycle, autophagy, and expression of cell lineage marker genes and proteins were measured at the end of exposures. Our results indicated that exposure to nanomolar concentrations of MeHg was associated with: 1) higher levels of ROS and HO-1 suggesting increased stress and adaptive response; 2) lower cellular adhesion, viability/proliferation, and colony formation and expansion; 3) higher apoptosis reflected by higher cleaved caspase-3 expression and Annexin V binding; 4) higher level of cytoskeleton protein α-tubulin expression; 5) higher rate of G1/S phase cell cycle arrest, and; 6) autophagy inhibition as shown by lower LC3BII/LC3BI ratio, and accumulation of SQSTM1 (P62). These outcomes were accompanied by higher expressions of self-renewal genes and/or proteins, including OCT4, SOX2, NANOG, cytokine receptor IL6ST, and pluripotency and cell fate regulator cyclin D1. These results revealed that under the selection pressure of exposure to low doses of MeHg, some hESCs underwent apoptosis, while others adapted and survived with enhanced self-renewal gene expression and specific morphological phenotypes. Findings from this study provided *in vitro* evidence that low doses of MeHg adversely

affected hESCs when exposed during a period of time that modeled embryonic pre-, during, and early post-implantation stages.

2.1 Introduction

It is increasingly recognized that early embryonic development is susceptible to environmental stressors like chemical contaminants. Exposure to chemicals can alter cellular programming and differentiation, not only shaping the phenotype of health and disease later in life but also influencing the vulnerability of subsequent generations [1, 2]. Therefore, understanding the effects of chemical exposure at early developmental stages is essential for the assessment and mitigation of the health risks associated with prenatal chemical exposure. Mercury is a ubiquitous environmental contaminant [3]. Humans are exposed to mercury as methylmercury (MeHg) mainly through fish and marine mammal consumption [4-6]. Once consumed, MeHg forms a complex with cysteine and homocysteine and is transported by amino acid transporters across the blood-brain barrier, the placenta and throughout the body [7].

Most studies on the developmental toxicity of mercury have focused on its neurological effects [8-12]. Several studies have shown that mammalian neuroprogenitor cells (NPCs) are highly sensitive to MeHg, which induced apoptosis at nanomolar concentrations [13-15]. Birth cohort studies on populations of the Faroe Islands revealed associations between cognitive deficits and prenatal MeHg exposure predominantly via the consumption of marine mammals (pilot whale meat), which remained detectable at age 7 [16], 14 [17] and 22 [16-18]. Prenatal exposure to mercury has been reported to be associated with neurodevelopmental deficits in motor skill, attention [17], language skill, memory function [19], visual function [20], and general intelligence [18] in infants [21], children [22], and/or youth [17-24]. However, the effects of prenatal exposure to MeHg on the development of other organs and systems remain uncertain [20].

Human embryonic stem cells (hESCs) are undifferentiated immature cells with the capacity of self-renewal and the potential to differentiate into all specific cell types in the human body [25].

The majority of primary hESC lines were separated from the inner cell mass (ICM) of blastocysts that are cultured from the cleavage stage human embryos generated from *in vitro* fertilization (IVF) for clinical purposes [25]. The health and fate of hESCs determine their capability and the potential to proliferate or differentiate into endoderm, ectoderm, and mesoderm lineage cells. Each of these lineages then further differentiates into cells of different organs and systems; examples of this differentiation include the endoderm forming gut epithelial cells, pancreas and hepatocytes; the ectoderm forming neural epithelium, embryonic ganglia and stratified squamous epithelium; and the mesoderm forming cartilage, bone, smooth and striated muscles [25, 26]. Genetic or epigenetic alterations in hESCs induced by environmental stressors, if occurred *in vivo*, may affect the fate and development of the embryo and the health status later in life [27]. MeHg exposures have been associated with a higher number of abnormal blastocysts [28] and blastocyst degeneration [29] in mice. However, there is a lack of in-depth studies of the effects of MeHg on early embryo developmental processes, such as during the blastocyst stage, which spans from day 5 to day 12 after fertilization [30].

Thus, the main objective of this study was to investigate the effects of MeHg in hESCs as a model to extrapolate to human embryonic development. We hypothesized that exposure of hESCs to low concentrations of MeHg might affect the fate and health status of blastocysts, which, if it occurs *in vivo*, would disrupt early embryo development and result in adverse pregnancy outcomes. To test this hypothesis, we examined the impact of MeHg on a number of parameters, including colony formation, viability/proliferation, apoptosis, stress response, cell cycle, autophagy, cytoskeleton protein expression, and cell lineage marker gene and protein expression in hESCs under culture conditions for 24 h or 6 days of MeHg exposure, modelling the *in vivo* acute exposure and continuous exposure of MeHg throughout the pre-, during, and early post-implantation stages.

2.2 Materials and Methods

2.2.1 Ethics Review and Approval

This project was reviewed and approved by the Health Canada and Public Health Agency of Canada's Research Ethics Board (File No. REB 2016-027H) and by the Office of Research Ethics and Integrity of the University of Ottawa (File No. H-05-19-4084).

2.2.2 Cell Maintenance and Expansion

Human embryonic stem cells (H9, Passage 23) were purchased from WiCell Research Institute (Madison, WI, USA), adapted and expanded in Matrigel (Cat # 354230, BD Biosciences, SanJose, CA, USA) pre-coated 6-well plates containing Essential 8™ Flex Medium (Cat # A2858501, Thermo Fisher Scientific, Ottawa, ON, Canada) under 37°C, 4% O_2 and 10% CO_2 in a tri-gas incubator (Thermo Fisher Scientific, Ottawa, ON, Canada). Culture conditions were optimized to allow high viability and attachment upon plating and maintain pluripotency without any visible differentiation during 7 days of culturing (Figure S2.1). Ten µM Rho-associated kinase inhibitor (Cat # 72304, StemCell Technologies, Vancouver, BC, Canada) was added to the medium, which was changed daily. For passaging, cells were lifted using Gibco™ Versene Solution (Cat # 15040066, Thermo Fisher Scientific, Ottawa, ON, Canada). Cells at 85% confluence were either frozen in mFreSR™ (Cat # 05855, StemCell Technologies, Vancouver, BC, Canada) or used for dosing experiments. Only the hESCs under passage 38 (within 15 passages from purchase) were used to avoid genetic instability with prolonged passaging.

On the 7th day of continuous culture, expression of pluripotency markers, OCT4 and Tra-1-81 were determined by immunocytochemical staining (Figure S2.2). Briefly, the medium was disposed and the cells were washed twice with PBS, fixed in 4% paraformaldehyde (Santa Cruz

Biotechnology, Santa Cruz, CA, USA) for 10 min, and then blocked with 5% bovine serum albumin (BSA) diluted in PBS containing 0.3% Triton X-100 (Sigma-Aldrich, Oakville, ON, Canada). The cells were then incubated with rabbit anti-human OCT4 antibody (Cat # C30A3, Cell Signaling, Tech. Danvers, MA, USA) and mouse anti-human Tra-1-81 antibody (Cat # 4745, Cell Signaling, Tech. Danvers, MA, USA) diluted at 1:200 in 5% BSA in PBS, at 4 ^{o}C overnight. After washing three times with PBS, the cells were incubated with Alexa Fluor 488 goat anti-rabbit IgG (Cat # A11008, Thermo Fisher Scientific, Ottawa, ON, Canada) and Alexa Fluor 594 goat anti-mouse IgG (Cat #A11005, Thermo Fisher Scientific, Ottawa, ON, Canada) diluted at 1:500 in 5% BSA in PBS at room temperature for 1 h. After washing three times with PBS, the Prolong® Gold anti-fade reagent containing DAPI (Cat # S36939, Thermo Fisher Scientific, Ottawa, ON, Canada) was added. The immunofluorescent images were acquired on a Zeiss LSM 880 confocal microscope (Carl Zeiss Canada Ltd., Toronto, Canada) with ZEN imaging software.

2.2.3 Chemical Preparation and Exposure

Methylmercury (MeHg) chloride (purity: 99.9%) was obtained from Sigma-Aldrich (Oakville, ON, Canada) and dissolved in 5 mM Na_2CO_3 to obtain 100x stock solutions (i.e. 0.1, 0.5, 1, 5, 10, 20, and 50 µM). The hESCs were seeded in 6- or 24-well culture dishes at a density of 1 x 10^4 cells/ml and allowed to attach for 24 h. Then the cells were exposed to 0 (0.05 mM Na_2CO_3 as vehicle control), 1, 5, 10, 50, 100, 200, and/or 500 nM MeHg by 100x dilution of the stock solutions in culture dishes, which were incubated at 37 ^{o}C, 4% O_2, and 10% CO_2 for 24 h or 6 days with daily change of medium and dosing to mimic acute exposure and continuous exposure of MeHg throughout the *in vivo* pre-, during, and early post-implantation processes. The measurements of all endpoints were repeated at least three times using samples from at least three different passages. Depending on the endpoints, one or two technical replicates were used.

2.2.4 Cell Attachment and Colony Formation

hESCs were treated with MeHg for 6 days, as described above. Vehicle- and MeHg-treated hESCs were observed and imaged daily under a 10x objective on a Zeiss Axiovert 40CFL inverted microscope (Carl Zeiss Microscopy, LLC) with a SPOT RT3 digital camera and SPOT basic software (Diagnostic Instrument Inc., Sterling Heights, MI, USA).

2.2.5 Cell Viability and Proliferation

hESCs were exposed to MeHg in 24-well plates for 6 days as described above. WST-1 assays were performed to determine the effects of MeHg on cell viability and proliferation using a WST-1 assay kit (Cat # ab155902, Abcam Inc. Toronto, ON. Canada) according to the manufacturer's instructions. WST-1 assay measures the cleavage of the tetrazolium salt WST-1 to formazan by cellular mitochondrial dehydrogenases. The higher amount of formazan dye indicates a larger amount and/or higher activity of cellular mitochondrial dehydrogenases, indicating higher cell numbers and/or viability. Briefly, 20 µl of WST-1 solution per well was added into the culture in 24-well plate, followed by shaking for 10 s. Absorbance at 420-480 nm wavelength was measured on a BioTek™ Cytation™ 3 Cell Imaging Multi-Mode Reader (Fisher Scientific, Ottawa, ON, Canada) after a 1.5 h incubation at 37 ^{o}C.

2.2.6 Intracellular Total Hg Content

Intracellular mercury content was measured after 24 h and 6 days of exposure. At the corresponding time points, the culture medium was first collected. Cells were rinsed twice with 500 µl PBS each time, and the PBS was collected after both rinses. The cells were then collected using a scraper and suspended in 140 µl (for cells after 24 h of MeHg exposure) and 500 µl (for cells after 6 days of MeHg exposure) of clean PBS. Ten µl of cell suspension was taken from each sample, and cell densities were counted using a Countess™ Automated Cell Counter (Invitrogen,

Thermo Fisher Scientific, Ottawa, ON, Canada) after 1:1 dilution of cell suspension in Trypan blue solution (Cat. T10282, ThermoFisher Scientific). Total Hg contents in medium, PBS and cells were measured using a mercury analyzer (MA 3000, Nippon Instruments Corp., Japan) according to the manual. Intracellular total Hg was normalized to cell number and reported as pmol/10^4 cells.

The following endpoints, except for measurements of ROS and Cyclin D1, were measured only in the 0, 10, 50, and 200 nM treatment groups.

2.2.7 Cell Apoptosis

The Annexin V-FITC Early Apoptosis Detection Kit (Cat # 6592S, Cell Signalling Tech., Danvers, MA, USA) was used according to the manufacturer's instruction to detect the effects of MeHg on early apoptosis. Briefly, hESCs were exposed to MeHg as described above for 24 h or 6 days. Cells were detached using Accutase (Cat # A11105-01, Thermo Fisher Scientific, Ottawa, ON, Canada), resuspended in Annexin V binding buffer, and aliquoted at 96 µl/tube. Then, 1 µl of Annexin V conjugate and 12.5 µl of Propidium Iodide (PI) were added to each tube and incubated in the dark for 10 min. The cell suspension was then diluted to a final volume of 250 µl using Annexin V binding buffer before analysis. All the steps were conducted on ice. The fluorescent labelling of apoptotic cells was counted on a BD LSR II Flow Cytometer (Becton Dickinson, Mississauga, ON, Canada) using 505LP (long pass), 525/50BP (band pass) on the Blue (488nm) laser for detection of the early apoptosis marker Annexin-V, while 570LP, 582/15BP on the Yellow/Green (561nm) laser allowed detection of the necrosis marker (PI). The detached cells were collected by centrifuging the supernatant and stained with Trypan blue. The cell number was then counted with a Countess™ Automated Cell Counter.

After hESCs were exposed to MeHg in Matrigel pre-coated chamber slides (Cat # 0030742010, Eppendorf) for 24 h, the effects of MeHg on intermediate and late apoptosis was

determined by measuring the expression of cleaved caspase-3 (CC3), which is an active form of caspase 3 [31], with immunocytochemical staining as previously described using rabbit anti-human CC3 antibody (Cat # 9661S, Cell Signaling, Tech. Danvers, MA, USA) at 1: 200 dilution. The immunofluorescent images were taken with a Nikon A1RsiMP confocal microscope (Nikon Instruments Inc. Canada) with Nikon's Imaging Software NIS-Elements. CC3-positive cells were counted using ImageJ (https://imagej.nih.gov/ij/index.html), and the percentage of CC3-positive cells was calculated against total counts (DAPI-stained). The higher percentage of CC3-positive cells indicates higher levels of apoptosis. The expression of CC3 of hESCs after 6 days of MeHg exposure was measured by Western blot. Briefly, after exposure of hESCs to MeHg in 6-well plate for 6 days, the medium was removed, cells were washed with PBS, lysed in Pierce RIPA buffer (Thermo Fisher Scientific, Ottawa, ON, Canada) containing the proteinase and phosphatase inhibitor cocktails (Cat # 5872S, Cell Signaling, Tech. Danvers, MA, USA) on ice, and homogenized by sonication using a Microson Ultrasonic Cell Disruptor XL2000 (Misonix Inc. New York, USA). The protein concentrations of the lysates were quantified using a Pierce™ BCA Protein Assay kit (Thermo Fisher Scientific, Ottawa, ON, Canada). Cell lysates were mixed with 4X Laemmli sample buffer (Bio-Rad Laboratories Ltd, Montreal, Quebec, Canada) and denatured by heating at 100°C for 4 min. Cell lysates were separated on a Stain-Free gel made with TGX Stain-Free™ FastCast™ acrylamide solutions (Cat # 161-0185, Bio-Rad Laboratories Ltd, Montreal, Quebec, Canada). For each batch, the same amount of protein was loaded, and the amount of total protein loaded ranged from 25-30 μg between different batches. After electrophoresis, gels were activated under UV-light using the ChemiDoc XRS+ imaging system (Bio-Rad Laboratories Ltd, Montreal, Quebec, Canada). Proteins were electro-transferred from gels to PVDF membranes with the Mini Trans-Blot® Cell (Cat # 1703930, Bio-Rad Laboratories

Ltd, Montreal, Quebec, Canada). Membranes were then blocked with 5% Non-fat dry milk (NFDM, Cat # 1706404, Bio-Rad Laboratories Ltd, Montreal, Quebec, Canada) for 1 h at room temperature and incubated with rabbit anti-human CC3 antibody (Cat # 9661S, Cell Signaling, Tech. Danvers, MA, USA) (1:1000 diluted in blocking buffer) at 4 ^{o}C overnight. After membranes were washed three times in TBST on a shaker for 5 min, they were incubated with HRP-linked goat anti-rabbit secondary antibody (G-21234, Thermo Fisher Scientific, Ottawa, ON, Canada) for 1 h at room temperature. All membranes were then incubated with the ECL substrate (Cat # 1705062, Bio-Rad Laboratories Ltd, Montreal, Quebec, Canada) in the dark and imaged using the ChemiDoc XRS+ imaging system. The band intensity was quantified and normalized against total protein band intensity using Image Lab software (Bio-Rad Laboratories Ltd, Montreal, Quebec, Canada). Since our previous observation suggested that MeHg treatment can influence the expression of some loading control proteins, we used Stain-free gels in all Western blot assays to obtain total protein bands for normalization of target proteins. All secondary antibodies used in Western blot were diluted at 1:5000 in the corresponding blocking buffer.

2.2.8 Cytoskeleton Protein Expression

To determine the effects of MeHg on cytoskeleton protein expression, we used Western blot to examine β-actin and α-tubulin expression. The protein extracts were obtained and the electrophoresis was conducted as described above after culture and exposure of MeHg for 6 days. Proteins were electro-transferred from gels to PVDF membranes with the Trans-Blot Turbo Transfer System (Bio-Rad Laboratories Ltd, Montreal, Quebec, Canada). Membranes were then blocked with 3% BSA for 1 h at room temperature and incubated with mouse anti-human α-tubulin antibody (Cat # ab4074) (1:1000 in 3% BSA) and rabbit anti-human β-actin antibody (Cat # ab8227, Abcam Inc. Toronto, ON. Canada) (1:1000 in 3% BSA) at 4 ^{o}C overnight. After

membranes were washed three times in TBST on a shaker for 5 min, they were incubated with HRP-linked goat anti-mouse (Cat # P0447, Dako) or HRP-linked goat anti-rabbit secondary antibody (Cat # A16110, Thermo Fisher Scientific, Ottawa, ON, Canada) for 1 h at room temperature.

2.2.9 Assays for Oxidative Stress

To quantify MeHg-induced stress and adaptive response in hESCs, we measured the production of reactive oxygen species (ROS) and protein expression of hemeoxygenase-1 (HO-1). To determine the ROS production, CellROX® deep red reagent (Cat # C10422, Thermo Fisher Scientific, Ottawa, ON, Canada) was added into the culture at a final concentration of 5 µM and incubated for 30 min at 37 ºC. After removing the medium, the cells were washed three times in PBS for 5 min, and the nuclei were stained with DAPI. Images were viewed and acquired using Zeiss Axiovert 40 CFL inverted microscope (Carl Zeiss Microscopy, LLC, Carl Zeiss Canada Ltd, North York, ON, Canada) with a SPOT RT3 digital camera and SPOT basic software (Diagnostic Instrument Inc., Sterling Heights, MI, USA) and quantified by ImageJ (https://imagej.nih.gov/ij/index.html). To quantify HO-1 protein expression, we conducted Western blot assays, as described above, using anti-human HO-1 as the primary antibody (Cat # ab13248, Abcam Inc. Toronto, ON. Canada) (1:1000 3% BSA).

2.2.10 Cell Cycle

To determine if MeHg affects the cell cycle, we examined cyclin A2, cyclin D1, and cyclin E1 protein expression and measured cell cycle phases. hESCs were exposed to MeHg for 6 days, and protein extracts were obtained as described above. Western blot analysis was performed as above using antibodies against human cyclin A2 (Cat # ab181591) (1:1000 in 3% BSA), cyclin D1 (Cat # ab134175) (1:1000 in 3% BSA), and cyclin E1 (Cat # ab133266, Abcam Inc. Toronto,

ON. Canada) (1:1000 in 3% BSA) and goat anti-rabbit secondary antibody (G-21234, Thermo Fisher Scientific, Ottawa, ON, Canada; 1:5000). Band intensities were quantified and normalized as described above.

For cell cycle assay, hESCs were exposed to MeHg for 6 days, washed with cold PBS, detached by Accutase, centrifuged, and resuspended and stained in Nuclear green CCS1 solution provided in a Cell Cycle Assay kit (Cat # ab112116, Abcam Inc. Toronto, ON. Canada). After incubating for 40 min at 37 ^{o}C, fluorescent intensity was quantified using a BD LSR II Flow Cytometer (Becton Dickinson, Mississauga, ON, Canada) with 505LP (long pass), 525/50BP (band pass) on the Blue (488nm).

2.2.11 Cellular Autophagy

To determine the effects of MeHg on autophagy, we measured the protein expression of microtubule-associated proteins 1A/1B light chain 3B (LC3BI), LC3BII and SQSTM1 (P62) using Western blot. Once hESCs were exposed to MeHg for 6 days, cells were lysed in Pierce RIPA buffer containing the proteinase and phosphatase inhibitor cocktails (Cat # 5872S, Cell Signaling, Tech. Danvers, MA, USA) on ice, and cell lysates were collected and measured for total protein and protein LC3BI, LC3BII and SQSTM1 (P62) using the Western blot with 4-20% MP TGX Stain-Free gels (Cat # 4568094, Bio-Rad Laboratories Ltd, Montreal, Quebec, Canada) and stain-free technique as described previously. Membranes were immunoblotted with rabbit polyclonal anti-human LC3B antibody (Cat # 2775) (1:1000 in 5% NFDM) from Cell Signalling Technology or mouse monoclonal anti-human p62 antibody (Cat. # ab56416) (1:1000 in 5% NFDM) from Abcam. Band intensities were quantified as described before.

2.2.12 Cell Lineage Marker Gene Expression

The TaqMan ® hPSC Scorecard Assay (Cat # A15871, Thermo Fisher Scientific, Ottawa, ON, Canada) was used to determine the effects of MeHg on cell lineage marker gene expression. hESCs were exposed to MeHg in 6-well dishes for 6 days as described before. To isolate total RNA, cells were washed with PBS and lysed in 1 ml of Invitrogen TRIzol (Thermo Fisher Scientific, Ottawa, ON, Canada) for 5 min. Cell lysates were pipetted up and down several times, mixed with 200 µl chloroform (Sigma-Aldrich Canada Ltd, Oakville, ON, Canada), hand-shaken vigorously, and incubated for 3 min. Supernatants were transferred to new tubes after centrifugation at 4 ^{o}C and 12000 g for 15 min. Isopropanol (0.5 ml/tube) was added, mixed well, and incubated for 10 min. Supernatants were removed after centrifugation at 4 ^{o}C and 12000 g for 10 min. The isolated total RNA was washed with 75% DEPC-treated ethanol, air-dried and dissolved in Ambion™ RNase free water (Thermo Fisher Scientific, Ottawa, ON, Canada). The concentration and quality of RNA were measured by NanoDrop 1000 (Thermo Fisher Scientific, Ottawa, ON, Canada). RNA samples were purified using the Ambion® DNA-free™ kit (Life Technology, Thermo Fisher Scientific, Ottawa, ON, Canada). Then RNA samples were reverse-transcribed with the Applied Biosciences High-capacity cDNA Reverse Transcription kit with RNase inhibitor (Thermo Fisher Scientific, Ottawa, ON, Canada) following the manufacturer's instructions. Briefly, RNA samples were mixed with the master mix solution and aliquoted into 8-strip PCR tubes. Then the RT reaction cycles were run following the manufacturer's instruction. The cDNA was then diluted, mixed with TaqMan® Fast Advanced Master Mix (Thermo Fisher Scientific, Ottawa, ON, Canada), and loaded on the pre-coated Scorecard plates, which were then sealed and centrifuged at 600 g for 2 min. The RT-PCR cycles were run with the fast 96-well template on a QuantStudio™ 7 Flex Real-Time PCR System (Life Technologies Inc., Burlington,

ON, Canada). qRT-PCR array analysis was conducted on five batches of experimental samples from five different cell passages.

2.2.13 Cell Lineage Marker Protein Expression

To confirm if the effects of MeHg on gene expression also occur at protein levels, we measured protein expression using Western blot and ELISA. hESCs were exposed to MeHg in 6-well plates for 6 days, and protein extracts were obtained as described previously. Immunoblotting of PVDF membranes was conducted using primary antibodies (1:1000 in 3% BSA, except for NPPB, PRDM1, PAX3 and PDGFRA) against human OCT4 (Cat # C30A3), SOX2 (Cat # D6D9), NANOG (Cat # D73G4, Cell Signalling Tech., Danvers, MA, USA), NPPB (Cat # MBS9607555, MyBiosource, San Diego, USA) (1:500 in 5% NFDM), PAX3 (Cat # SAB2107888, Sigma-Aldrich, Oakville, ON, Canada) (1:1000 in 5% NFDM), PDGFRA (Cat # PA5-16571) (1:500 in 5% NFDM) and PRDM1 (Cat # MA5-14879, Thermo Fisher Scientific, Ottawa, ON, Canada) (1:500 in 5% NFDM), FOXA2 (Cat # ab108422), GATA4 (Cat # ab134057), KLF5 (Cat # ab137676), TRPM8 (Cat # ab3243, Abcam Inc. Toronto, ON. Canada), SOX17 (Cat # AF1924) and c-MYC (Cat # MAB3696, R&D systems, MA, USA) and HRP-linked goat anti-mouse (Cat # P0447, Dako), HRP-linked rabbit anti-goat (P0160, Dako), or HRP-linked goat anti-rabbit (Cat # G-21234, Thermo Fisher Scientific, Ottawa, ON, Canada) secondary antibody (1:5000 in corresponding blocking buffer). The band intensities were quantified and normalized as described above. Because of logistics reasons, protein expression of RGS4, DRD4 and IL6ST were measured using ELISA with commercial kits from AVIVA Systems Biology, San Diego, CA, USA (for RGS4, Cat # OKEI00172), and Life Span Biosciences, Seattle, WA, USA (for DRD4, Cat # LS-F39474 and IL6ST, Cat # LS-F3388) according to manufacturer's instructions. Samples were

diluted before analysis to ensure all sample absorbance values fall in the linear part of standard curves.

2.2.14 Statistical analysis

All data were expressed as the mean plus or minus the standard error of the mean (Mean ±SEM) and were tested for statistical significance with one-way ANOVA, followed by Dunnett's post hoc test. The differences were considered significant if $p < 0.05$. Except for TaqMan Scorecard assay analysis, all statistical analyses were performed using GraphPad Prism 8 (La Jolla, CA, USA).

For Scorecard analysis, CT values of target genes were subtracted by the CT values of the reference genes (ACTB, CTCF, EP300, SMAD1) to obtain ΔCT values. A cluster analysis was performed on the ΔCT values using the heatmap function in R [32]. This cluster analysis revealed that most samples within a batch were clustered together. Thus, a statistical model including the dose and batch factors on ΔCT (ΔCT = Dose + Batch) was applied using SAS Enterprise Guide 7.1 according to the method of Yuan et al. [33]. Using this model, each batch effect estimate was obtained. The ΔCT for each gene was subtracted by the batch effect estimate to give a derived ΔCT value for the gene. The same model (ΔCT = Dose + Batch) was used to estimate the gene expression difference between all MeHg dose groups and the control group based on ΔCT values. The level of probability of statistical significance was $p < 0.05$, where p was adjusted by the Dunnett method for the multiple comparisons of 10 nM vs 0 nM, 50 nM vs 0 nM and 200 nM vs 0 nM. Fold change was estimated using the function of 2^(-least square mean for MeHg dose group) /2^(-least square mean for control).

2.3 Results

2.3.1 Cell adhesion and colony formation in hESCs exposed to MeHg for 6 days

Cell adhesion to the extracellular matrix is essential for hESCs to maintain intercellular communication, migration, viability and proliferation. In this study, we found that after 24 h of exposure to 200 nM MeHg, some hESCs lifted off the Matrigel, and those exposed to 500 nM entirely became floating (Figure 2.1A-H). After 3 days of exposure, the colony size and number in the 200 nM MeHg treatment group were much smaller than those in the vehicle control group (Figure 2.1I-N). After 5 days of exposure, the same phenomenon was seen in all three of the 50, 100, and 200 nM MeHg dose groups (Figure 2.1O-T). After 6 days of exposure, colonies in the 200 nM MeHg treatment group formed a multilayer structure with an evident peripheral membrane, a morphology markedly different from that of vehicle control colonies (Figure 2.1U-W). The abnormal morphology was observed after 6 days of exposure at around 80% frequency, though the number of abnormal colonies in each batch was different. Another two batches of morphological images are provided in Figure S2.3.

2.3.2 Cell viability and proliferation in hESCs exposed to MeHg for 6 days

After 24 h of exposure, cell viability in the hESCs treated with 200 nM MeHg was significantly lower than the vehicle control cells (Figure 2.2). This effect of 200 nM MeHg became more evident with the increasing duration of exposure from 24 h to 5 days (Figure 2.2). Significantly lower levels of cell viability were also detected in 10, 50, 100 and 200 nM MeHg treated cells after 6 days of exposure compared to the control. The viability of the cells treated with 200 nM was the lowest at around 10% of control.

2.3.3 Intracellular total Hg content in hESCs exposed to MeHg for 24 hours and 6 days

We observed higher levels of intracellular total Hg content in hESCs after 24 h and 6 days of MeHg exposure that appeared to be dose-dependent in nature (Figure 2.3), although the average

amount of total Hg per cell was higher after 24 h than 6 days of exposure in the 50, 100, and 200 nM dose groups.

2.3.4 Measurement of apoptosis in hESCs exposed to MeHg for 24 hours and 6 days

After 24 h of exposure, the percentages of CC3-positive cells were significantly higher in 10, 50, 200 nM MeHg-treated than vehicle control cells (Figure 2.4A), while no significant differences in the percentages of Annexin V-positive cells were observed between MeHg treatment and the control group (Figure 2.4B). Some floating cells were observed in the culture media of all treatment groups, including the control group, every day before the medium change. The number of floating cells was significantly higher in 200 nM MeHg than the control groups after 24 h of exposure (Figure S2.4). There were no significant differences in the expression of CC3 among treatment groups (Figure 2.4C) after 6 days of exposure, while the percentages of Annexin V-positive cells in all MeHg treatment groups were significantly higher than the control group (Figure 2.4D).

2.3.5 Expression of cytoskeletal proteins in hESCs exposed to MeHg for 6 days

We detected significantly higher protein expression of α-tubulin, but not β-actin, in hESCs exposed to 200 nM MeHg than the vehicle for 6 days (Figure 2.5A and 5B).

2.3.6 ROS presence and HO-1 expression in hESCs exposed to MeHg for 24 hours or 6 days

We detected significantly higher levels of ROS in hESCs exposed to 200 nM MeHg versus vehicle for 24 h (Figure 2.6A). We observed higher HO-1 protein expression after 6 days of exposure in the same dose groups (Figure 2.6B) as exhibited higher ROS at 24 h. A trend of higher ROS level and HO-1 expression was also observed in lower MeHg dose groups (Figure 2.6A and 6B). However, none reached a statistically significant level.

2.3.7 Measurement of cell cycle in hESCs exposed to MeHg for 6 days

After 6 days of exposure, cells treated with 10, 50 and 200 nM MeHg showed significantly higher levels in the proportion of cells in the G1/S phase and lower levels in the proportion of cells in the G2 phase, compared to the cells treated with vehicle (Figure 2.7A). These changes were associated with significantly higher protein levels of cyclin D1 (Figure 2.7B), but not cyclin A2 and E1 (Figure S2.5A and B), in the 200 nM MeHg versus the vehicle treated cells.

2.3.8 Measurement of autophagy markers in hESCs exposed to MeHg for 6 days

Lower LC3BII/LC3BI ratio (Figure 2.8A), accompanied by higher expression of SQSTM1 (P62) (Figure 2.8B), was found in hESCs treated with 200 nM MeHg than the vehicle for 6 days. Pictures of the entire blot of LC3B with ladder is provided in Figure S2.6.

2.3.9 Expression of cell lineage markers in hESCs exposed to MeHg for 6 days

We used Scorecard to examine the effects of MeHg on the expression of 82 cell lineage marker genes after 6 days of exposure. Our data revealed that the gene expression profile in the 200 nM MeHg treated hESCs clustered away from the profile of all other dose groups (Figure 2.9A). In addition, the self-renewal genes clustered together, while other cell lineage marker genes were distributed in other clusters with no obvious cell lineage separation. Cells treated with each of the three doses (10, 50, and 200 nM) of MeHg exhibited significant differences in the expression of one or more cell lineage marker genes; cells treated with 10 nM exhibited 1 differentially expressed gene, cells treated with 50 nM exhibited 3 differentially expressed genes and cells treated with 200 nM exhibited 9 differentially expressed genes (Figure 2.9B-9G). The expression of IL6ST, a mesoderm gene, was significantly higher in all three MeHg dose groups than in the control. The expression of PAX3, an ectoderm gene, and KLF5, an endoderm gene, was significantly lower in the 50 nM MeHg group than in the control group. The expression of MYO3B, an ectoderm gene, FOXA2, an endoderm gene, PDGFRA, a mesoderm gene, and POU5F1 (OCT4),

a self-renewal gene, were significantly higher in the 200 nM MeHg group than in the control group. In contrast, the expressions of KLF5, and PRDM1, an endoderm gene, NPPB, a mesendoderm gene, and MYC, a non-cell lineage-related gene, were significantly lower in the 200 nM MeHg group than in the control group. The expressions of SOX2, CXCL5, and DNMT3B, all self-renewal genes, were also higher in the 200 nM MeHg group than in the control group but did not reach statistically significant levels.

At the protein level, we found higher levels of OCT4 (Figure 2.10A) in the 50 nM and 200 nM MeHg groups after 6 days of exposure. Five other proteins, including two self-renewal proteins, NANOG (Figure 2.10B) and SOX2 (Figure 2.10C), two endoderm proteins, GATA4 (Figure 2.10D) and PRDM1 (Figure 2.10E), and a mesoderm protein IL6ST (Figure 2.10F) were all higher in the 200 nM MeHg treated cells only. We found no significant difference in the protein expression of FOXA2, KLF5, PAX3, TRPM8, c-MYC, SOX17, PDGFRA, NPPB, RGS4, and DRD4 in the hESCs treated with MeHg compared to the control group (Figure S2.7). Therefore, only OCT4, PRDM1, and IL6ST showed significant differences at both gene and protein levels in the 200 nM MeHg cells compared to control cells. Besides, the protein expressions of another two self-renewal makers, SOX2 (Figure 2.10C) and NANOG (Figure 2.10B) were also significantly higher in 200 nM MeHg treated cells, even though no significant difference was detected in the gene expression levels of these two markers (Figure 2.9B).

2.4 Discussion

Previous studies looking at the effects of MeHg on embryo development focused mostly on the neural system. Little is known about the effects of MeHg on the physiology of undifferentiated hESCs. In humans, the implantation starts from about day 7~8 and basically

completes at around day 12 after fertilization [30, 34]. Since many pregnancies are unplanned, it is important to understand the effects of MeHg at this early stage of embryo development, particularly for the risk assessment for the fish consumption populations. Our observed low dose effects of MeHg in undifferentiated hESCs cultured under physiologically relevant oxygen condition after 24 h or 6 days of exposure to mimic the acute (24 h exposure) and continuous *in vivo* MeHg exposure throughout the pre-, during, and early post-implantation stages of embryo development (6 days exposure) (Figure 2.11). Our results showed dose-response effects of nanomolar concentrations of MeHg on the hESCs colony morphology, cell viability and proliferation, apoptosis, stress response, cytoskeleton protein expression, autophagy, cell cycle, and the expression of various cell lineage marker genes/proteins. The significance of this observation in the physiopathology of spontaneous abortions warrants further study.

Conducting toxicology experiments using undifferentiated hESCs presented many challenges in both the methodology and the interpretations of results. hESCs were isolated from the inner cell mass (ICM) of human blastocysts. ICM cells have relatively high natural apoptotic rates as the result of an eliminative process that helps trim the embryonic cell lineages of surplus or dysfunctional stem cells [35, 36]. Undifferentiated hESCs have a primed death machinery with Bax already active, which rapidly translocate from Golgi to mitochondria upon DNA damage, where it exerts apoptosis in hours [37]. In this study, we observed floating cells every day, even in the control group before the daily medium change, and the number of floating cells was higher wells with cells that had been treated with MeHg. This effect of MeHg treatment on cell adhesion had also been reported previously [38]. The reduced cell adhesion may be caused by lower cell viability and/or by a change in cellular adherent molecules such as integrins, cadherins and selectins, which lead to a re-arrangement of cell skeleton structures [39] and disruption of cell

junctions. Therefore, all the results reported are on the "survived" cells that may have developed selective resistance mechanisms.

The viability of cultured hESCs decreased with time and MeHg concentrations (Figure 2.2). On day 6, the cell viability was around 90% at 10nM, 80% at 50nM, and 10% at 200 nM relative to the control. These results suggest that undifferentiated hESCs are as vulnerable to MeHg toxicity as the neural stem cells. For example, exposure to MeHg at 50 nM caused a 50% reduction in cell viability and proliferation in human embryonic neural progenitor cells after 20 h of exposure accompanied by an increase in ROS production and apoptosis [40] and MeHg at ≥50 nM significantly decreased cell viability in hESCs after 12 days of exposure [41]. We measured cell viability using the WST assay similar to the previous studies, which measured the formation of formazan from tetrazolium salt (WST-1) and required the action of mitochondrial dehydrogenase present in the metabolically active cells, thus reflecting cell viability and proliferation. As MeHg acts on sulfhydryl groups and may decrease the mitochondrial dehydrogenase activity by directly binding to SH- in proteins or indirectly by ROS-induced oxidation of SH-, the WST values may reflect the combined effects of MeHg on cell viability, cell proliferation, and mitochondrial dehydrogenase. Therefore, the estimate of cell death, particularly at 200 nM may be over-estimated. Nevertheless, the increase of ROS and HO-1showed that those cells were under stress, and the MeHg treatment clearly decreased proliferation. After 6 days of exposure, cells treated with 10, 50 and 200 nM MeHg all showed a higher proportion of cells in G1/S phase and less in G2 phase, and showed higher levels of cyclin D1 (Figure 2.7). Similar observations were reported by Burke et al. [42] and Xu et al. [43] in cortical progenitor cells. This could be a result of an increase in ROS-induced DNA damage, leading to activation of checkpoint and DNA repair processes in the G1/S phase, preventing the transition of cells from G1/S to G2 phase. The higher level of α-tubulin

expression in 200 nM MeHg treated cells is also consistent with the changes in cell cycle dynamics observed in these cells. It has been demonstrated that the cell cycle machinery is directly involved in the transcriptional initiation of developmental genes controlling primary germ layer specification [44]. While hESCs in the early G1 phase can only initiate differentiation into endoderm, hESCs in late G1 were limited to neuroectoderm differentiation [45].

MeHg was reported to increase apoptosis in mouse neural progenitor cells after 3 h of exposure at 100 nM [14]. Our results also showed that apoptosis was important in MeHg mediated cell death in hESCs, and it also played a significant role in the selection of resistant hESCs. There appear to be inconsistencies in our results for apoptosis measured by two different markers, CC3 and Annexin V, in the hESCS at 24 h and day 6. CC3 showed MeHg treatment effects at 24 h but not at day 6, while Annexin V showed MeHg treatment effects at day 6 but not at 24 h (Figure 2.4). This could be due to a number of factors. First, the percentage of CC3 positive cells for 24 h exposure were measured by immunocytochemical staining and by Western blot at day 6 because the cells grew into multiple layers after 6 days of exposure. Second, the higher rate of apoptosis (indicated by CC3) in the 200 nM MeHg group after 24 h than 6 days of exposure could be explained as A) the survived cells at day 6 were more resistant to MeHg; B) as the cell density increased from $1x10^4$ cells/ml at 24 h to (5-20) $x10^4$ cells/ml at day 6, the effective dose of MeHg that each cell was exposed were lower at 24 h than day 6 (the measured total Hg per cell was higher at 24 h than at day 6); and C) the cells that could show high expression of CC3 had been removed with medium change (Figure S2.4), and the cells survived 6 days were protected from MeHg exposure by forming more compact, multilayered, and smaller colonies. Third, at 24 h, the cells could be at the middle/late stage of apoptosis, and that could be shown by the CC3 but not the Annexin V, which stained for an earlier stage of apoptosis. At day 6, the surviving cells were more

resistant and did not undergo further middle/late apoptosis, and hence showed more positive staining for Annexin V. The cells survived 6 days of MeHg treatment also had higher expression of self-renewal genes and/or proteins OCT4, SOX2, and NANOG. It remains to be determined if these cells would be able to implant and develop further *in vivo*.

Even though the underlying molecular mechanisms for MeHg toxicity are not completely understood, much evidence indicates MeHg toxicity is mediated by its pro-oxidative properties [46]. We observed a higher level of ROS after 24 h of 200 nM MeHg exposure, similar to that reported in human embryonic neural progenitor cells [40], which could be attributed to the induction of the uncoupling of mitochondrial electron transport chain or depletion of GSH [47, 48]. As the hESCs were maintained at physiologically relevant oxygen level (4%) in this study, they had not adapted to atmosphere oxygen environment (~20%), and thus were prone to ROS damage induced by MeHg, resulting in increased apoptosis. The conjugation of sulfhydryl groups with MeHg could also contribute to cell death by inhibiting enzymatic activity related to DNA replication, carbohydrate and lipid metabolism, and heme synthesis [49]. Another possible mechanism is the modulation of autophagy and apoptosis. We observed that MeHg casued a decrease in autophagy as indicated by a lower LC3BII/LC3BI ratio and higher protein expression of P62 with the increase in apoptosis as reported in the anterior pituitary of rats [50]. Therefore, the MeHg treatment effect may be mediated through a similar mechanism of causing a blockage of autophagy that augmented the apoptotic profile that led to the release of pro-apoptotic cell mediators, increasing mitochondrial membrane permeability and promoting cell death. The most recent advances in the comprehension of the functions of autophagy pathways suggested that autophagy is a ‘‘decision-maker’’ between quiescence, self-renewal and differentiation in physiological versus pathological conditions [51]. mTOR, a negative regulator of autophagy [52],

supported long-term self-renewal and suppressed mesoderm and endoderm differentiation in hESCs [53]. Spontaneous and induced differentiation promoted autophagy in hESC cell line HES3 LC3-GFP [54]. Chaperone-mediated autophagy (CMA) was up-regulated during differentiation of mouse ESCs [55], while pluripotency factors OCT4 and SOX2 suppressed CMA [55]. These observations also support our findings that the cells that survived 6 days of MeHg treatment had decreased autophagy measured as the decreased ratio of LC3BII/LC3BI [56] and the increased protein expression of SQSTM1 (P62) [57], which paralleled with increased expression of self-renewal genes and/or proteins. Normally, GATA4 is degraded by autophagy, so the observed increase in GATA4 in the 200 nM treated hESCs may be caused by the autophagy inhibition observed, and may lead to a possible initiation of the senescence-associated secretory phenotype [58].

It is important to note that the uniqueness of this study is to investigate the properties of the "undifferentiated" cell population in the cell culture system. The hESCs were grown in Essential 8^{TM} Flex Medium that was formulated to support and maintain pluripotency, and lacking factors required for germ layer differentiation. Therefore, the levels of lineage gene expression will be small and very minor shifts in the cell population can result in very large changes in marker gene expression. Nevertheless, our results in cell lineage markers at both gene and protein expression levels provide preliminary evidence on the mechanisms of MeHg toxicity. For example, we found that hESCs exposed to 200 nM MeHg had markedly higher cyclin D1 expression, which is consistent with the higher expression of self-renewal genes and proteins observed under the same condition. Cyclin D1, which is highly expressed in the late G1 phase, recruits transcriptional corepressors to endoderm genes, thereby blocking the induction of the corresponding germ layers [59]. There is evidence demonstrating that a proper level of Cyclin D is necessary for maintaining

the pluripotent state of ESCs, while its overexpression may induce reprogramming of epidermal cells into stem-like cells with higher expression of OCT4 [60, 61]. These changes may prevent the hESCs from germ layer lineage commitment, which, if it occurs *in vivo*, would result in miscarriage. Varum et al. found inhibition of mitochondrial respiratory chain enhanced pluripotency measured by OCT4 expression in hESCs [62]. Therefore, our observed higher expression of OCT4 at both the gene and protein level in the 200 nM MeHg treated cells could also be caused by a similar disruption of the mitochondria respiratory chain by MeHg. OCT4 is a transcription factor vital for maintaining ESC pluripotency and plays a coordinating role in the G1/S phase transition by regulating the expression of cyclin D and cyclin E [60]. Therefore, OCT4 may also play a key role in the observed increased expression of cyclin D and cell cycle arrest at the G1/S phase in the hESCs. The SOX2 expression may also relate to the higher expression of cyclin D1 and cell cycle arrest, as suggested by others [63, 64]. Our finding of the higher expression of OCT4, SOX2 and PRDM1 in the 200 nM treated hESCs is interesting as the development from pluripotent stem cells to primordial germ cells is driven by switching partners with OCT4 from SOX2 to PAX5, resulting in the upregulation of PRDM1 [65]. As the dysregulation of genetic pathways during human germ cell development can lead to infertility, the effects of MeHg on the core transcriptional network of PAX5–OCT4–PRDM1 proteins that activates germline and represses somatic programmes during human germ cell differentiation should be further investigated. Both IL6ST and NANOG are known to play an important role in the maintenance of self-renewal of ESCs *in vitro* [66, 67]. The fact that cell exposed to MeHg had a simultaneously higher expression of IL6ST and 3 self-renewal genes and/or proteins (OCT4, SOX2, NANOG) shows that exposure of hESCs to MeHg at the blastocyst stages could inhibit or delay the differentiation of three germ layers and increase the risk of early developmental disorders

in vivo. This enhanced expression of self-renewal genes could be due to the selection of a population of pluripotent cells for their ability to survive the MeHg ROS damage because of the higher level of antioxidant capabilities. Increased ROS has been shown to prime stem cells for differentiation under intermediate levels [68]. Thus, hESCs with lower antioxidant capabilities began to differentiate and became more prone to oxidative damage [69], resulting in the death under prolonged MeHg exposure. The remaining cells would then be those that were not primed to differentiate and thus show higher levels of self-renewal gene expression.

It is known that the well-being of early embryo development in the oviduct and uterus is critical for successful implantation and positive pregnancy outcome, but that about 70% of human implantation sites are defective and, thus, prone to resorption [70]. Spontaneous resorption is a major problem in assisted reproduction in humans [71]. Findings from this study suggest that exposure of blastocysts to nanomolar concentrations (10-200 nM) of MeHg, if it occurs *in vivo*, could disrupt early embryo development, implantation, and post-implantation development, outcomes that could explain the positive association between urinary mercury concentrations, oxidative stress, and spontaneous abortion in pregnant dental staff in Egypt [72]. Monitoring blood and hair mercury concentrations during the preconception period to minimize the risk of adverse pregnancy outcomes has been practiced in the Hospital for Sick Children in Toronto, Canada [73].

hESC-H9, the cell line used in this study, can maintain normal XX karyotype for more than 6 months in continuous culture as described by J.A. Thomson et al. [25]. However, all findings in the current study were obtained from only one hESC line that was derived from an embryo of one donor. Therefore, the characteristics of this cell line may only represent the population that the donor represents. Other hESCs with different genetic and gender backgrounds should be tested for the effects of MeHg. A caution on the interpretation of the cell viability result is that WST

measured the activities of mitochondrial dehydrogenase as indicators for cell viability and cell proliferation. Since we could not exclude the possibility that MeHg dosing can affect the protein levels or activities of mitochondrial dehydrogenase, the WST values may reflect the combined effects of MeHg on cell viability, cell proliferation, and mitochondrial dehydrogenase. In addition, even though a significant dose-response relationship between MeHg treatments and many measured endpoints was observed, the significant changes were mostly found in the 200 nM MeHg treatment group, which was also associated with lower cell viability and higher stress after continuous dosing. Due to technical difficulties, we could not use the same method to assess apoptosis at different exposure times. New methodologies for measuring apoptosis in various stages of hESCs need to be established and applied in future studies.

In summary, our study confirmed that the reported cytotoxic effects of MeHg previously observed in fetal brain cells could also occur in undifferentiated hESC at similar or even lower concentrations (Figure 2.11). Our results suggest that the undifferentiated hESC shows merit for further validation as an *in vitro* model to screen chemicals for early developmental toxicities. Findings from this study provided *in vitro* evidence that nanomolar concentrations of MeHg adversely affected the growth and health of hESCs, which suggests that *in vivo* exposure to MeHg can potentially result in adverse pregnancy and developmental outcomes, such as implantation failure, spontaneous abortion, and/or developmental deficit.

Despite the risk of MeHg exposure, fish is an important source of nutrients beneficial to cardiovascular and neurological development [4]. With embryos and fetuses as the most sensitive stages of human development, it has become a delicate issue to balance the risks and benefits of fish consumption. Findings from this study enriched the understanding of the potential pregnant

and developmental outcomes associated with MeHg exposure and thus help vulnerable populations to minimize the risk of MeHg exposure through fish consumption.

2.5 Acknowledgements

This study was supported by an internal project funding provided to Dr. Jin in the Bureau of Chemical Safety, Food Directorate, Health Products and Food Branch, Health Canada, and a Discovery Grant from the Natural Sciences and Engineering Research Council of Canada and a Canada Research Chair to H.M. Chan. We are thankful to Andrew Stalker, Regulatory Research Division, Center for Biologics Evaluation, Biologic and Radiopharmaceutical Drugs Directorate, Health Products and Food Branch, Health Canada for technical support in flow cytometry and Emmanuel Yumvihoze, Department of Biology, University of Ottawa, for technical support in MeHg concentration measurements. We thank Yihang Pan for reading through the manuscript and providing comments. We also thank the two editors and 4 reviewers for their positive comments and constructive suggestions that have significantly improved the manuscript from the initial submission.

2.6 References

1. Hanson, M.A. and M.K. Skinner, Developmental origins of epigenetic transgenerational inheritance. Environmental epigenetics, 2016. **2**(1).
2. Heindel, J.J., The developmental basis of disease: Update on environmental exposures and animal models. Basic & clinical pharmacology & toxicology, 2019. **125**: p. 5-13.
3. Driscoll, C.T., et al., Mercury as a global pollutant: sources, pathways, and effects. Environmental science & technology, 2013. **47**(10): p. 4967-4983.

4. Mahaffey, K.R., et al., Balancing the benefits of n-3 polyunsaturated fatty acids and the risks of methylmercury exposure from fish consumption. Nutrition reviews, 2011. **69**(9): p. 493-508.
5. Chan, H.M. and O. Receveur, Mercury in the traditional diet of indigenous peoples in Canada. Environmental Pollution, 2000. **110**(1): p. 1-2.
6. Canuel, R., et al., New evidence on variations of human body burden of methylmercury from fish consumption. Environmental health perspectives, 2006. **114**(2): p. 302-306.
7. Kerper, L.E., N. Ballatori, and T.W. Clarkson, Methylmercury transport across the blood-brain barrier by an amino acid carrier. American Journal of Physiology-Regulatory, Integrative and Comparative Physiology, 1992. **262**(5): p. R761-R765.
8. dos Santos, A.A., et al., Methylmercury and brain development: A review of recent literature. Journal of trace elements in medicine and biology, 2016. **38**: p. 99-107.
9. Sheehan, M.C., et al., Global methylmercury exposure from seafood consumption and risk of developmental neurotoxicity: a systematic review. Bulletin of the World Health Organization, 2014. **92**: p. 254-269F.
10. Grandjean, P. and K.T. Herz, Methylmercury and brain development: imprecision and underestimation of developmental neurotoxicity in humans. Mount Sinai Journal of Medicine: A Journal of Translational and Personalized Medicine, 2011. **78**(1): p. 107-118.
11. Ceccatelli, S., E. Daré, and M. Moors, Methylmercury-induced neurotoxicity and apoptosis. Chemico-biological interactions, 2010. **188**(2): p. 301-308.

12. Shao, Y., et al., Methylmercury can induce Parkinson's-like neurotoxicity similar to 1-methyl-4-phenylpyridinium: a genomic and proteomic analysis on MN9D dopaminergic neuron cells. The Journal of toxicological sciences, 2015. **40**(6): p. 817-828.
13. Edoff, K., et al., Gestational age and sex influence the susceptibility of human neural progenitor cells to low levels of MeHg. Neurotoxicity research, 2017. **32**(4): p. 683-693.
14. Watanabe, J., et al., Low dose of methylmercury (MeHg) exposure induces caspase mediated-apoptosis in cultured neural progenitor cells. The Journal of toxicological sciences, 2013. **38**(6): p. 931-935.
15. Tamm, C., et al., High susceptibility of neural stem cells to methylmercury toxicity: effects on cell survival and neuronal differentiation. Journal of neurochemistry, 2006. **97**(1): p. 69-78.
16. Grandjean, P., et al., Cognitive deficit in 7-year-old children with prenatal exposure to methylmercury. Neurotoxicology and teratology, 1997. **19**(6): p. 417-428.
17. Debes, F., et al., Impact of prenatal methylmercury exposure on neurobehavioral function at age 14 years. Neurotoxicology and teratology, 2006. **28**(5): p. 536-547.
18. Debes, F., P. Weihe, and P. Grandjean, Cognitive deficits at age 22 years associated with prenatal exposure to methylmercury. Cortex, 2016. **74**: p. 358-369.
19. Choi, A.L., et al., Negative confounding by essential fatty acids in methylmercury neurotoxicity associations. Neurotoxicology and teratology, 2014. **42**: p. 85-92.
20. Karagas, M.R., et al., Evidence on the human health effects of low-level methylmercury exposure. Environmental health perspectives, 2012. **120**(6): p. 799-806.
21. Oken, E., et al., Maternal fish consumption, hair mercury, and infant cognition in a US cohort. Environmental health perspectives, 2005. **113**(10): p. 1376-1380.

22. Prpić, I., et al., Prenatal exposure to low-level methylmercury alters the child's fine motor skills at the age of 18 months. Environmental research, 2017. **152**: p. 369-374.

23. Julvez, J., et al., Sensitivity of continuous performance test (CPT) at age 14 years to developmental methylmercury exposure. Neurotoxicology and teratology, 2010. **32**(6): p. 627-632.

24. Ha, E., et al., Current progress on understanding the impact of mercury on human health. Environmental Research, 2017. **152**: p. 419-433.

25. Thomson, J.A., et al., Embryonic stem cell lines derived from human blastocysts. science, 1998. **282**(5391): p. 1145-1147.

26. Li, J., et al., Studying developmental neurotoxic effects of bisphenol A (BPA) using embryonic stem cells. J. Environ. Sci, 2015. **36**: p. 173-177.

27. Worley, J.R. and G.C. Parker, Effects of environmental stressors on stem cells. World Journal of Stem Cells, 2019. **11**(9): p. 565.

28. Kajiwara, Y. and M. Inouye, Effects of methylmercury and mercuric chloride on preimplantation mouse embryos *in vivo*. Teratology, 1986. **33**(2): p. 231-237.

29. Spindle, A. and N. Matsumoto, Enhancement of methylmercury toxicity by L-cystine in cultured mouse blastocysts. Reproductive Toxicology, 1987. **1**(4): p. 279-284.

30. Lopata, A., Implantation of the human embryo. Human reproduction, 1996. **11**(Supplement_5): p. 175-184.

31. Konstantinidou, A., et al., Caspase-3 immunohistochemical expression is a marker of apoptosis, increased grade and early recurrence in intracranial meningiomas. Apoptosis, 2007. **12**(4): p. 695-705.

32. Team, R., R: A language and environment for statistical computing. Vienna, Austria: R Foundation for Statistical Computing; 2011. URL https://www. R-project. org, 2019.
33. Yuan, J.S., et al., Statistical analysis of real-time PCR data. BMC bioinformatics, 2006. **7**(1): p. 85.
34. Lenton, E.A., L.M. Neal, and R. Sulaiman, Plasma concentrations of human chorionic gonadotropin from the time of implantation until the second week of pregnancy. Fertility and sterility, 1982. **37**(6): p. 773-778.
35. Pampfer, S. and I. Donnay, Apoptosis at the time of embryo implantation in mouse and rat. Cell Death & Differentiation, 1999. **6**(6): p. 533-545.
36. Huppertz, B. and A. Herrler, Regulation of proliferation and apoptosis during development of the preimplantation embryo and the placenta. Birth Defects Research Part C: Embryo Today: Reviews, 2005. **75**(4): p. 249-261.
37. Dumitru, R., et al., Human embryonic stem cells have constitutively active Bax at the Golgi and are primed to undergo rapid apoptosis. Molecular cell, 2012. **46**(5): p. 573-583.
38. Jayashankar, S., et al., Cerebral gene expression in response to single or combined gestational exposure to methylmercury and selenium through the maternal diet. Cell biology and toxicology, 2011. **27**(3): p. 181-197.
39. Coleman, M. and M. Olson, Rho GTPase signalling pathways in the morphological changes associated with apoptosis. Cell Death & Differentiation, 2002. **9**(5): p. 493-504.
40. Wang, X., et al., Low-dose methylmercury-induced apoptosis and mitochondrial DNA mutation in human embryonic neural progenitor cells. Oxidative medicine and cellular longevity, 2016. **2016**.

41. Stummann, T.C., L. Hareng, and S. Bremer, Hazard assessment of methylmercury toxicity to neuronal induction in embryogenesis using human embryonic stem cells. Toxicology, 2009. **257**(3): p. 117-126.

42. Burke, K., et al., Methylmercury elicits rapid inhibition of cell proliferation in the developing brain and decreases cell cycle regulator, cyclin E. Neurotoxicology, 2006. **27**(6): p. 970-981.

43. Xu, M., et al., Effects of low level of methylmercury on proliferation of cortical progenitor cells. Brain research, 2010. **1359**: p. 272-280.

44. Pauklin, S. and L. Vallier, Activin/Nodal signalling in stem cells. Development, 2015. **142**(4): p. 607-619.

45. Pauklin, S. and L. Vallier, The cell-cycle state of stem cells determines cell fate propensity. Cell, 2013. **155**(1): p. 135-147.

46. Farina, M. and M. Aschner, Methylmercury-induced neurotoxicity: focus on pro-oxidative events and related consequences, in Neurotoxicity of Metals. 2017, Springer. p. 267-286.

47. Mori, N., et al., Methylmercury inhibits electron transport chain activity and induces cytochrome c release in cerebellum mitochondria. The Journal of toxicological sciences, 2011. **36**(3): p. 253-259.

48. Gatti, R., et al., Methylmercury cytotoxicity in PC12 cells is mediated by primary glutathione depletion independent of excess reactive oxygen species generation. Toxicology, 2004. **204**(2-3): p. 175-185.

49. Ajsuvakova, O.P., et al., Sulfhydryl groups as targets of mercury toxicity. Coordination chemistry reviews, 2020. **417**: p. 213343.

50. El Asar, H.M., et al., Selenium protection against mercury neurotoxicity: modulation of apoptosis and autophagy in the anterior pituitary. Life sciences, 2019. **231**: p. 116578.

51. Rodolfo, C., S. Di Bartolomeo, and F. Cecconi, Autophagy in stem and progenitor cells. Cellular and molecular life sciences, 2016. **73**(3): p. 475-496.

52. Wang, Y. and H. Zhang, Regulation of autophagy by mTOR signaling pathway. Autophagy: Biology and Diseases, 2019: p. 67-83.

53. Zhou, J., et al., mTOR supports long-term self-renewal and suppresses mesoderm and endoderm activities of human embryonic stem cells. Proceedings of the national academy of sciences, 2009. **106**(19): p. 7840-7845.

54. Tra, T., et al., Autophagy in human embryonic stem cells. PloS one, 2011. **6**(11): p. e27485.

55. Xu, Y., et al., Chaperone-mediated autophagy regulates the pluripotency of embryonic stem cells. Science, 2020. **369**(6502): p. 397-403.

56. Yuntao, F., et al., Role of autophagy in methylmercury-induced neurotoxicity in rat primary astrocytes. Archives of toxicology, 2016. **90**(2): p. 333-345.

57. Rusten, T.E. and H. Stenmark, p62, an autophagy hero or culprit? Nature cell biology, 2010. **12**(3): p. 207-209.

58. Kang, C., et al., The DNA damage response induces inflammation and senescence by inhibiting autophagy of GATA4. Science, 2015. **349**(6255).

59. Pauklin, S., et al., Initiation of stem cell differentiation involves cell cycle-dependent regulation of developmental genes by Cyclin D. Genes & development, 2016. **30**(4): p. 421-433.

60. She, S., et al., Cell cycle and pluripotency: Convergence on octamer-binding transcription factor 4. Molecular medicine reports, 2017. **16**(5): p. 6459-6466.

61. Zhao, A., et al., Overexpression of cyclin D1 induces the reprogramming of differentiated epidermal cells into stem cell-like cells. Cell Cycle, 2016. **15**(5): p. 644-653.

62. Varum, S., et al., Enhancement of human embryonic stem cell pluripotency through inhibition of the mitochondrial respiratory chain. Stem cell research, 2009. **3**(2-3): p. 142-156.

63. Card, D.A.G., et al., Oct4/Sox2-regulated miR-302 targets cyclin D1 in human embryonic stem cells. Molecular and cellular biology, 2008. **28**(20): p. 6426-6438.

64. Li, C., et al., Sex-Determining Region Y-box 2 Promotes Growth of Lung Squamous Cell Carcinoma and Directly Targets Cyclin D1. DNA and Cell Biology, 2017. **36**(4): p. 264-272.

65. Fang, F., et al., A PAX5–OCT4–PRDM1 developmental switch specifies human primordial germ cells. Nature cell biology, 2018. **20**(6): p. 655-665.

66. Hu, G., et al., A genome-wide RNAi screen identifies a new transcriptional module required for self-renewal. Genes & development, 2009. **23**(7): p. 837-848.

67. Saunders, A., F. Faiola, and J. Wang, Concise review: pursuing self-renewal and pluripotency with the stem cell factor Nanog. Stem cells, 2013. **31**(7): p. 1227-1236.

68. Bigarella, C.L., R. Liang, and S. Ghaffari, Stem cells and the impact of ROS signaling. Development, 2014. **141**(22): p. 4206-4218.

69. Guo, Y.-L., et al., Effects of oxidative stress on mouse embryonic stem cell proliferation, apoptosis, senescence, and self-renewal. Stem cells and development, 2010. **19**(9): p. 1321-1331.

70. Hertig, A.T., The evolution of a research program. American Journal of Obstetrics & Gynecology, 1958. **76**(2): p. 252-270.

71. Drews, B., et al., Spontaneous embryo resorption in the mouse is triggered by embryonic apoptosis followed by rapid removal via maternal sterile purulent inflammation. BMC developmental biology, 2020. **20**(1): p. 1-18.

72. El-Badry, A., M. Rezk, and H. El-Sayed, Mercury-induced oxidative stress may adversely affect pregnancy outcome among dental staff: a cohort study. The international journal of occupational and environmental medicine, 2018. **9**(3): p. 113.

73. Neuman, G., J. Gareri, and G. Koren, Preconceptional monitoring of mercury levels in hair and blood as a tool for minimizing associated reproductive risks. Therapeutic drug monitoring, 2014. **36**(6): p. 696-698.

2.7 Tables and Figures

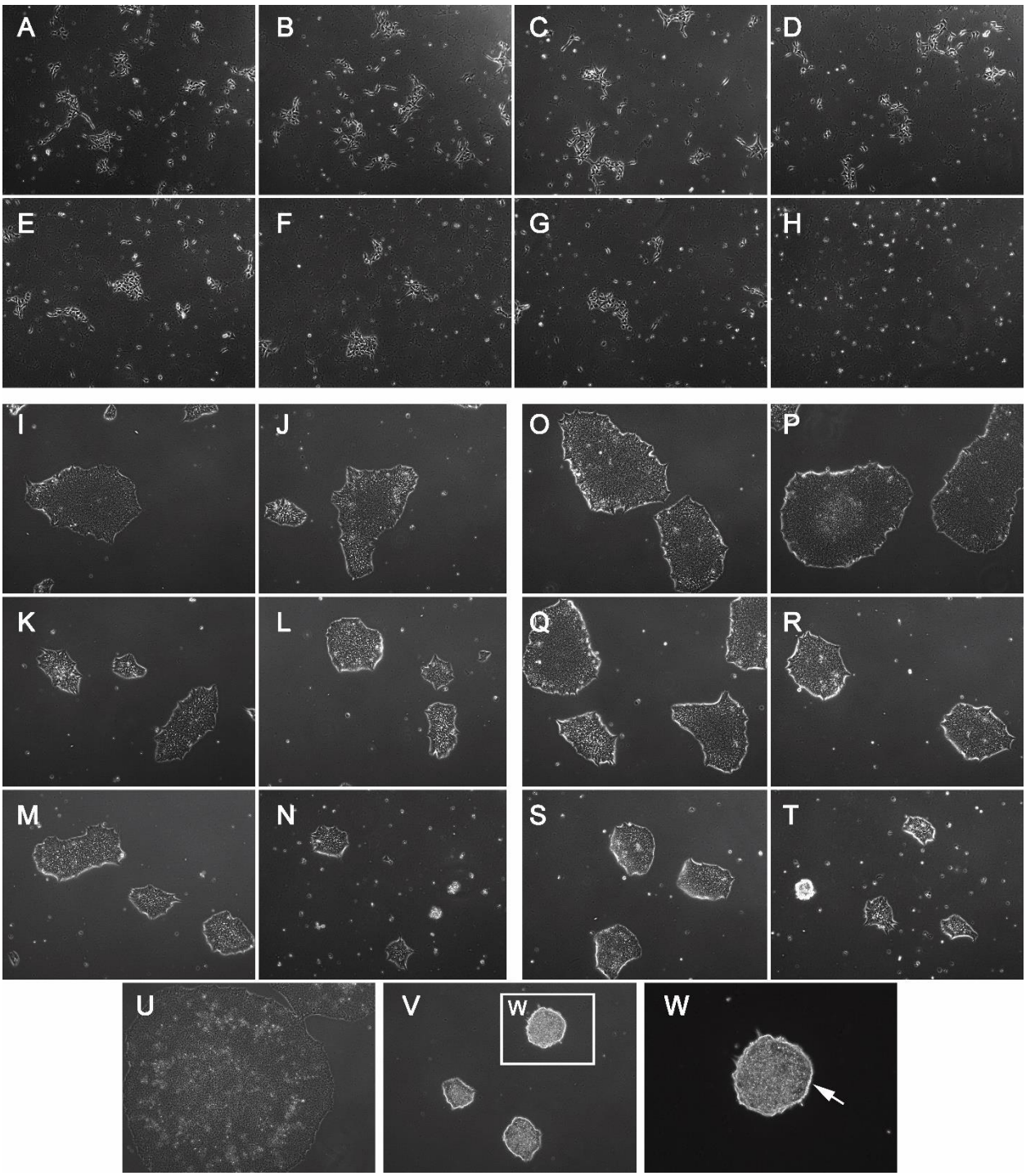

Figure 2.1. The effect of MeHg exposure on the cell attachment, colony formation, and morphology of hESCs. Representative images showing cellular attachment and colony formation of hESCs after 24 h of exposure to (A) 0, (B) 1, (C) 5, (D) 10, (E) 50, (F) 100, (G) 200, and (H)

500 nM MeHg, and colony size or morphology of hESCs after 3 d of exposure to (I) 0, (J) 5, (K) 10, (L) 50, (M) 100, and (N) 200 nM MeHg, after 5 d of exposure to (O) 0, (P) 5, (Q) 10, (R) 50, (S) 100, and (T) 200 nM MeHg, or after 6 d of exposure to (U) 0 and (V and W) 200 nM MeHg. (A–V) were taken under a 10 × objective. (W) is the Zoom-in of (V) and which was taken under a 20 × objective. At least five wells with at least five fields were observed, and at least three images were taken for each treatment group. The arrow indicates the peripheral membrane of the multilayer structure. Note: hESC, human embryonic stem cell; MeHg, methylmercury.

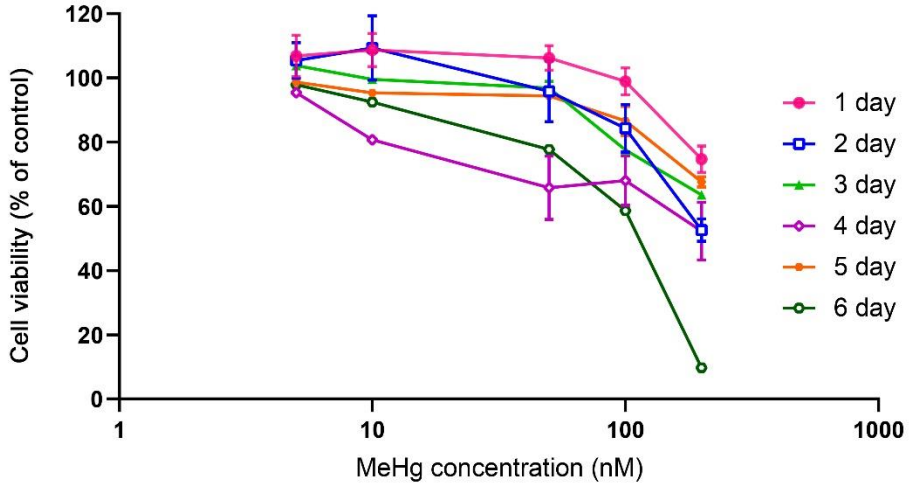

Figure 2.2. Effects on cell viability of hESCs exposed to MeHg for 24 h to 6 d. Cell viability of each dose at each time point was adjusted to the respective sodium carbonate vehicle control. One-way ANOVA was used at each time point to compare between the different doses and the dose response of the treatment effects was significant. Dunnett's post hoc test was then used to compare the treatments to the vehicle control. Significance was set at $p < 0.05$. Data are presented as means ± SEMs with n= 4 for each group. Five-nanomolar MeHg showed significantly higher cell viability on Day 3; 10 nM MeHg showed significantly lower cell viability on Day 6; 50 nM MeHg showed significantly lower cell viability on Days 4 and 6; 100 nM MeHg showed significantly lower cell viability on Days 3–6; and 200 nM MeHg showed significantly lower cell viability at all time points. Note: ANOVA, analysis of variance; hESC, human embryonic stem cell; MeHg, methylmercury; SEM, standard error of the mean.

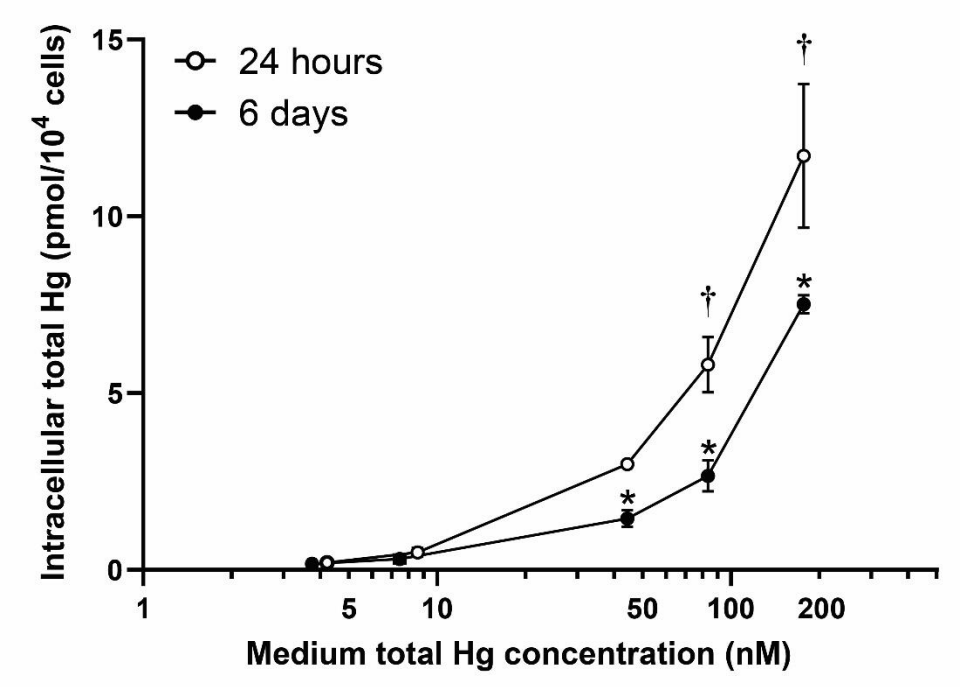

Figure 2.3. Intracellular total mercury content in hESCs exposed to MeHg for 24 h and 6 d. One-way ANOVA was used at each time point to compare between the different doses, and the dose response of the treatment effects was significant. Dunnett's post hoc test was then used to compare the treatments to the sodium carbonate vehicle control. Significance was set at $p < 0.05$. Data are presented as means ± SEMs with N = 3 for each group. The values <0 were regarded as 0. †, $p < 0.05$ within 24 h. *, $p < 0.05$ within 6 d. Values on the x-axis represent actual total mercury concentrations measured in culture medium dosed with 5, 10, 50, 100, and 200 nM MeHg for 24 h or 6 d, respectively. The doses shown in the figure were the measured concentrations in the media. Note: ANOVA, analysis of variance; hESC, human embryonic stem cell; Hg, mercury; MeHg, methylmercury; SEM, standard error of the mean.

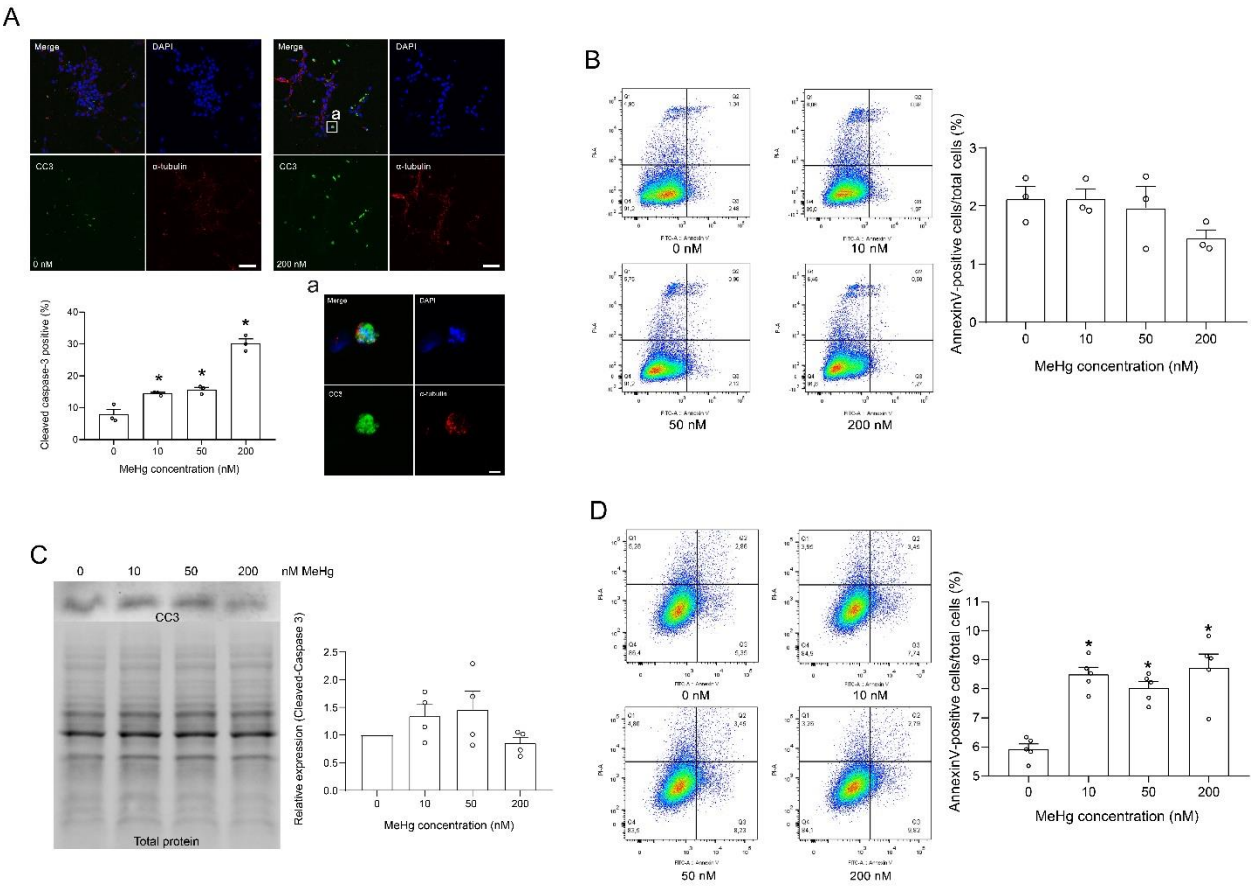

Figure 2.4. Measures of apoptosis in hESCs exposed to MeHg for 24 h and 6 d. (A) Representative image of positive staining of cleaved caspase-3 (CC3) (green), nuclei (DAPI, blue) and α-tubulin (red) and quantification of CC3-positive cells (as a percentage of nuclei) in hESCs exposed to 0 and 200 nM MeHg for 24 h. Scale bar: 100 μm; scale bar in the Zoom-in of (A): 10 μm. (B) Flow cytometry analysis of cell population (percentage) positively stained for Annexin V-FITC and propidium iodide (PI) as measures of early apoptosis and necrosis after 24 h of MeHg treatment, respectively. (C) Expression of CC3 protein after 6 d of MeHg exposure. Each batch was first normalized to its sodium carbonate vehicle control (0 nM) before comparison. Thus, there is no error bar in the 0 nM MeHg group. (D) Flow cytometry analysis of cell population (percentage) positively stained for Annexin V-FITC and PI as measures of early apoptosis and necrosis after 6 d of MeHg treatment, respectively. Data are presented as means ± SEMs with N = 3 for

immunostaining and flow cytometry (24 h), N = 4 for Western blot, and N = 5 for flow cytometry (6 d). The small circle symbols represent individual values of each experiment. One-way ANOVA was used at each time point to compare between the different doses, and the dose response of the treatment effects was significant for (A) CC3 expression at 24 h and (D) Annexin V-positive cells at 6 d. Dunnett's post hoc test was then used to compare the treatments to the vehicle control. Significance (*) was set at $p < 0.05$. Note: ANOVA, analysis of variance; DAPI, 40 ,6-diamidino-2-phenylindole; FITC, fluorescein-5-isothiocyanate; hESC, human embryonic stem cell; MeHg, methylmercury; SEM, standard error of the mean.

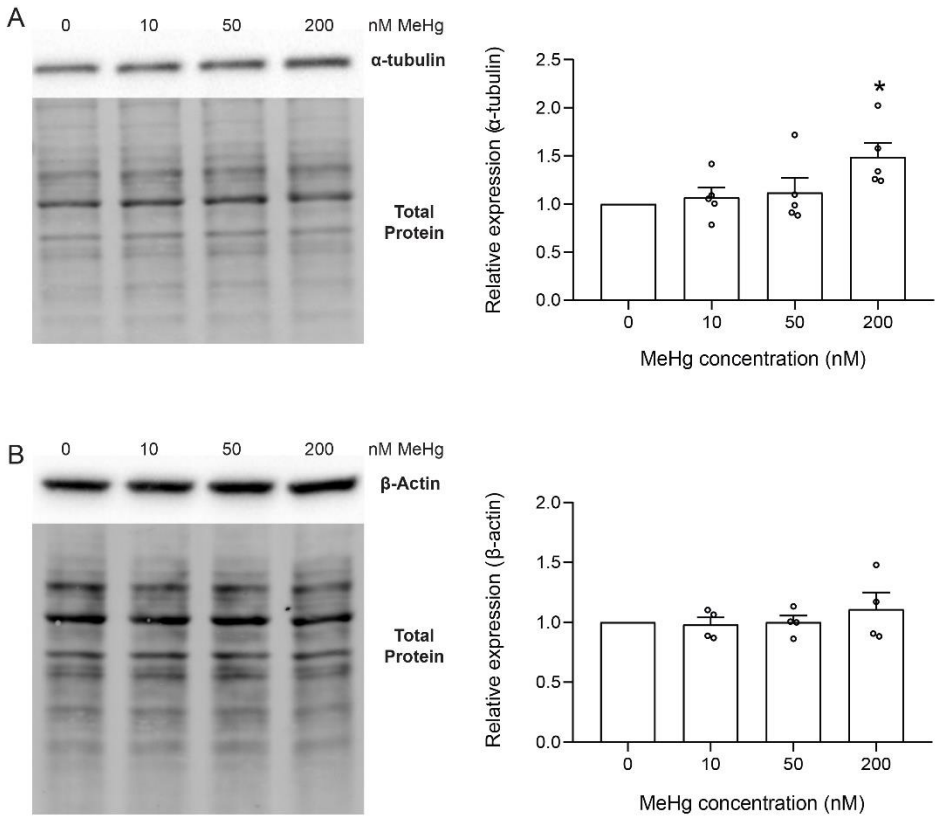

Figure 2.5. Expressions of (A) α-tubulin and (B) β-actin proteins in hESCs exposed to 0, 10, 50, and 200 nM MeHg for 6 d. Data are presented as means ± SEMs with N = 5 for α-tubulin and N = 4 for β-actin. Each batch was first normalized to its sodium carbonate control (0 nM) before comparison. Thus, there are no error bars in the 0 nM MeHg groups. The small circle symbols represent individual values of each experiment. One-way ANOVA was used at each time point to compare between the different doses, and the dose response of the treatment effects was significant for (A) expression of a-tubulin. Dunnett's post hoc test was then used to compare the treatments to the vehicle control. Significance (*) was set at $p < 0.05$. Note: ANOVA, analysis of variance; hESC, human embryonic stem cell; MeHg, methylmercury; SEM, standard error of the mean.

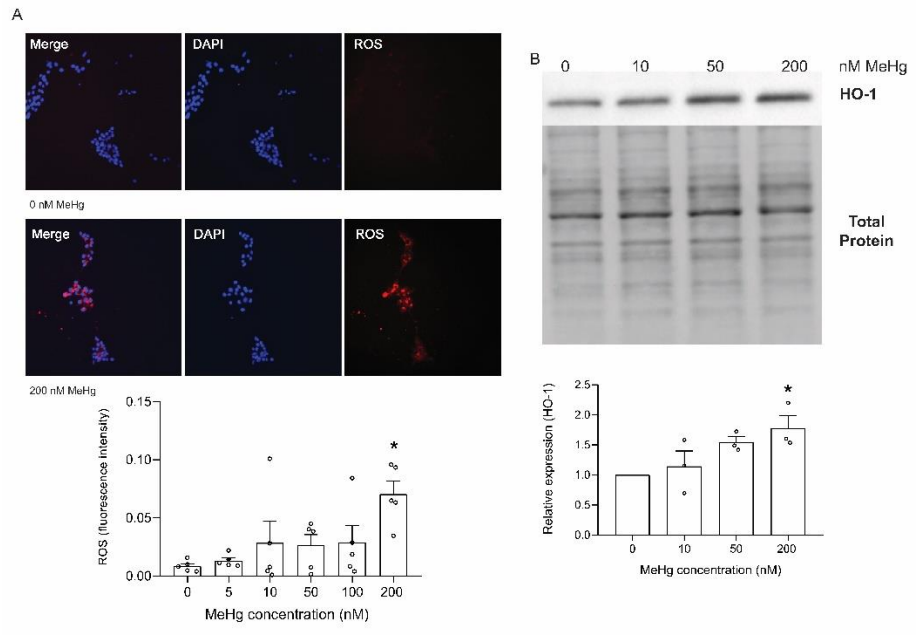

Figure 2.6. Presence of (A) reactive oxygen species (ROS) and (B) protein expression of HO-1 in hESCs exposed to MeHg for 24 h and 6 d, respectively. Microscopic images are DAPI staining of nuclei (blue) and CellRox staining of ROS (red). Data are presented as means ± SEMs with N = 5 for ROS fluorescence intensity and N = 3 for HO-1 Western blots. For Western blots, each batch was first normalized to its sodium carbonate vehicle control (0 nM) before comparison. Thus, there are no error bars in the 0 nM MeHg groups. The small circle symbols represent individual values of each experiment. One-way ANOVA was used at each time point to compare between the different doses, and the dose response of the treatment effects was significant. Dunnett's post hoc test was then used to compare the treatments to the vehicle control. Significance (*) was set at $p < 0.05$. Note: ANOVA, analysis of variance; DAPI, 40 ,6-diamidino-2-phenylindole; hESC, human embryonic stem cell; HO-1, hemeoxygenase-1; MeHg, methylmercury; SEM, standard error of the mean.

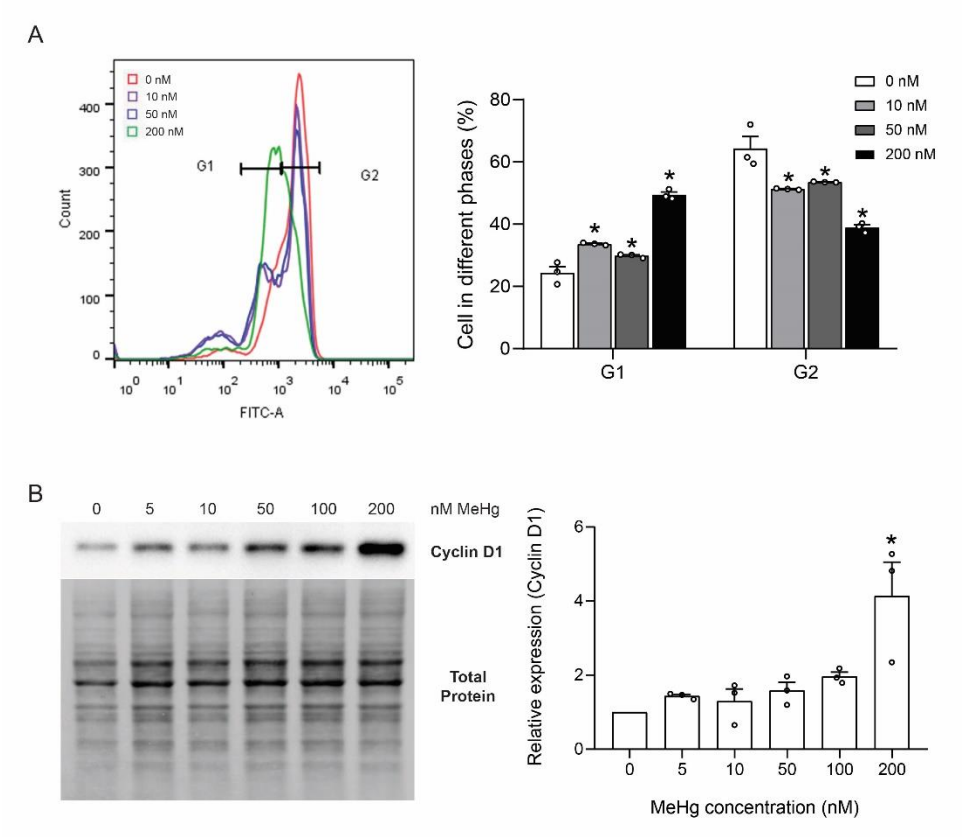

Figure 2.7. Analysis of the cell cycle of hESCs after 6 d of exposure to MeHg. (A) Flow cytometry analysis of cell cycle phases, with a histogram showing the peak for FITC-staining of DNA content as identifications of cell phases and bar graph showing the percentage of cells in different cell cycle phases of hESCs after 6 d of exposure to 0, 10, 50, and 200 nM MeHg. (B) Protein expression of cyclin D1 was measured in hESCs after 6 d of exposure to 0, 5, 10, 50, 100, and 200 nM MeHg. Data are presented as means ± SEMs with N = 3 for each group. For Western blots, each batch was first normalized to its sodium carbonate vehicle control (0 nM) before comparison. Thus, there is no error bar in the 0 nM MeHg group. The small circle symbols represent individual values of each experiment. One-way ANOVA was used at each time point to compare between the different doses, and the dose response of the treatment effects was significant. Dunnett's post hoc test was then used to compare the treatments to the vehicle control. Significance (*) was set at $p < 0.05$.

Note: ANOVA, analysis of variance; FITC, fluorescein-5-isothiocyanate; hESC, human embryonic stem cell; MeHg, methylmercury; SEM, standard error of the mean.

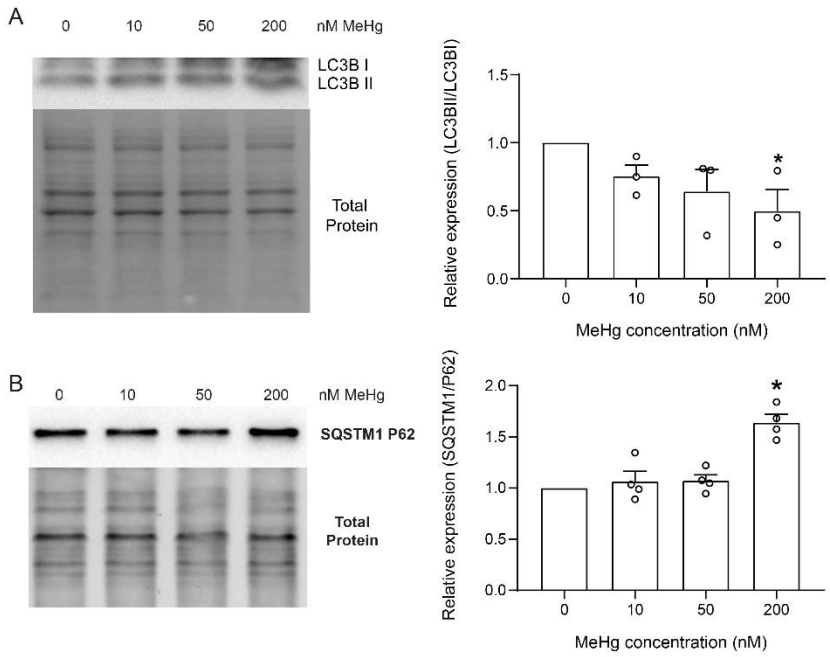

Figure 2.8. Protein expressions of LC3B (LC3BI and LC3BII) and SQSTM1 (p62) were measured in hESCs after 6 d of exposure to 0, 10, 50, and 200 nM MeHg. Data are presented as means ± SEMs with N = 3 for LC3B and N = 4 for SQSTM1 (p62). For LC3B, the ratio of LC3BII/LC3BI was calculated first before comparison. Each batch was first normalized to its sodium carbonate vehicle control (0 nM) before comparison. Thus, there are no error bars in the 0 nM MeHg groups. The small circle symbols represent individual values of each experiment. One-way ANOVA was used at each time point to compare between the different doses, and the dose response of the treatment effects was significant. Dunnett's post hoc test was then used to compare the treatments to the vehicle control. Significance (*) was set at $p < 0.05$. Note: ANOVA, analysis of variance; hESC, human embryonic stem cell; LC3B, microtubule associated proteins 1A/1B light chain 3B; MeHg, methylmercury; SEM, standard error of the mean; SQSTM1 (p62), sequestosome 1.

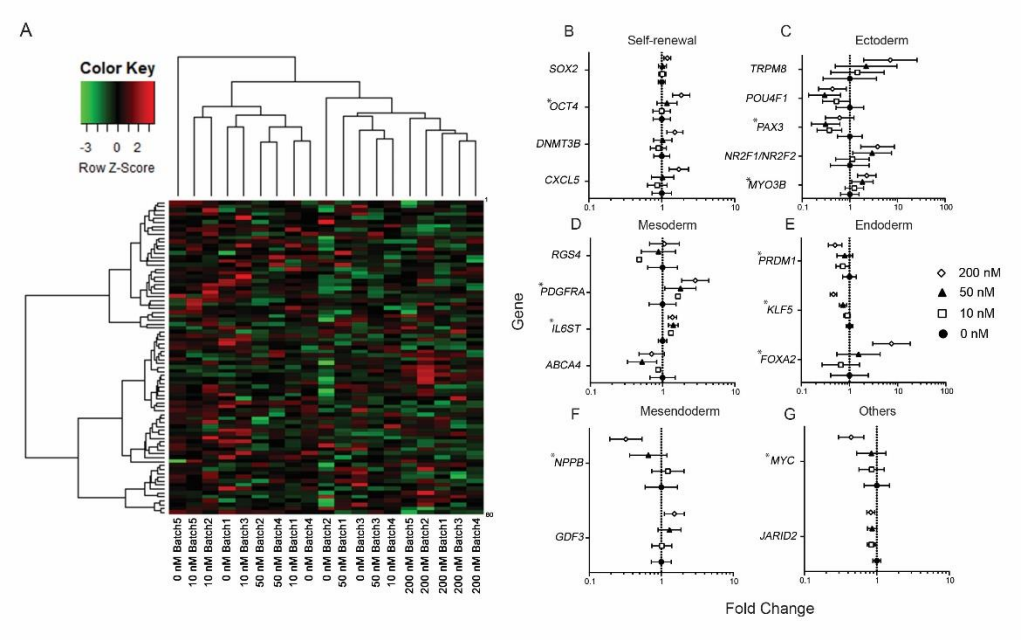

Figure 2.9. Hierarchical cluster analysis and fold change estimates of cell lineage marker gene expression data. (A) A cluster analysis was carried out using the heatmap function in R for the derived △CT values, as described in the "Materials and Methods" section. Rows represent genes, and columns represent samples. Red and green blocks respectively represent high and low expression relative to the reference gene, whereas black blocks indicate equal expression. (B–G) The expression of genes with significant difference between the MeHg-treatment groups and the control group. Fold change was estimated using the function of $2^{(-\text{least square mean for MeHg dose group})}/2^{(-\text{least square mean for control})}$. Data are presented as mean fold change ± 95% CI with N = 5 for each group. The dashed line in each panel represents the line of no fold change. An asterisk indicates genes that remain significant (adjusted $p < 0.05$) after controlling for batch effect using a statistical model (△CT = dose + batch), as described in the "Materials and Methods" section. Note: ABAC4, ATP Binding Cassette, Subfamily A, Member 4; CI, confidence interval; CXCL5, C-X-C Motif Chemokine Ligand 5; DNMT3B, DNA Methyltransferase 3 Beta; FOXA2, forkhead box A2; GDF3, Growth Differentiation Factor 3; IL6ST, interleukin 6 cytokine

family signal transducer; JARID, Jumonji/ARID domain-containing protein 2; KLF5, Kruppel-like factor 5; MeHg, methylmercury; MYC, Myc proto-oncogene protein; MYO3B, myosin IIIB; NPPB, natriuretic peptide B; NR2F1/NR2F2, Nuclear receptor subfamily 2, group F, member 2/member 1; OCT4, octamer-binding transcription factor 4; PAX3, paired box 3; PRDM1, PR domain-containing protein 1; PDGFRA, platelet-derived growth factor receptor-alpha; POU4F1, POU domain, class 4, transcription factor 1; RGS4, protein expression of regulator of G protein signaling 4; SOX2, SRY-box transcription factor 2; TRPM8, transient receptor potential cation channel subfamily M member 8.

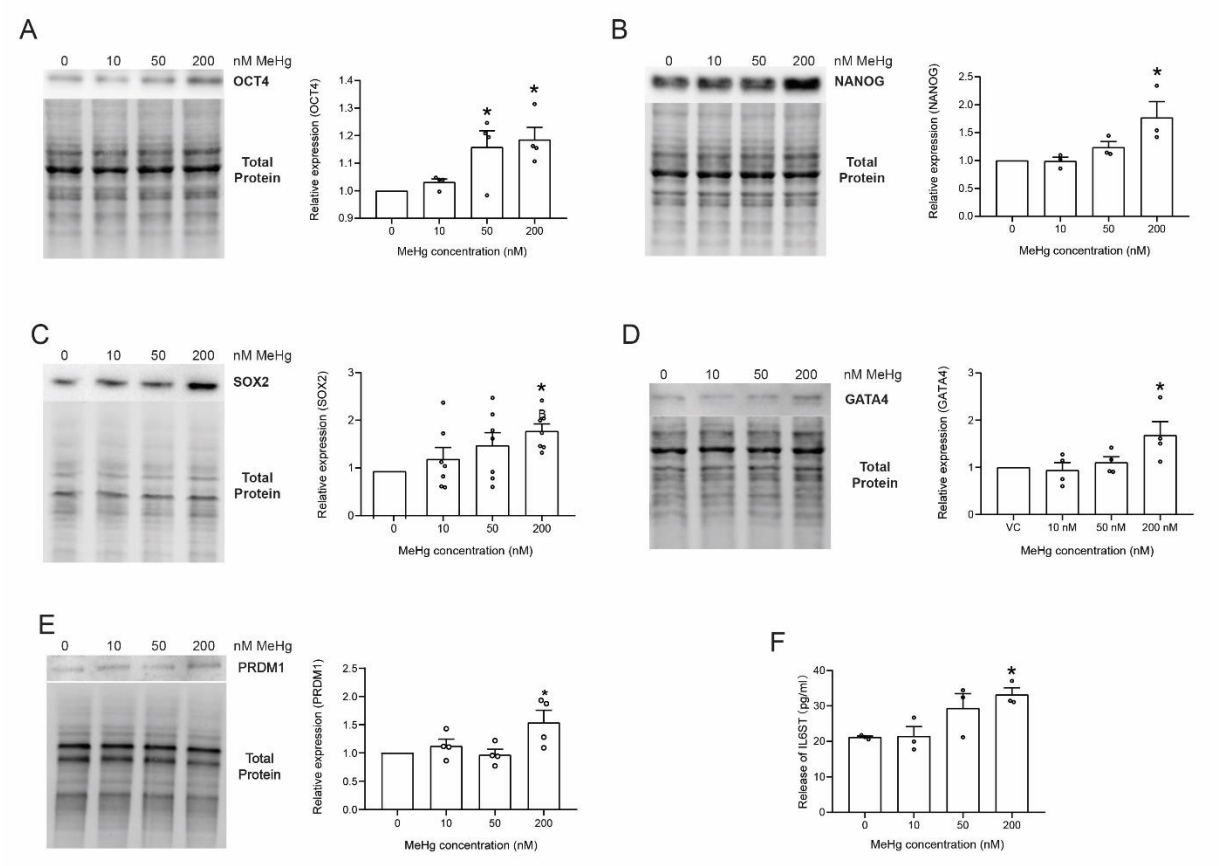

Figure 2.10. Expressions of selected cell lineage marker proteins, (A) OCT4, (B) NANOG, (C) SOX2, (D) GATA4, and (E) PRDM1 as measured using Western blots, and (F) IL6ST as measured using ELISAs in hESCs after 6 d of exposure to 0, 10, 50, 200 nM MeHg. Data are presented as means ± SEMs with N = 3 for NANOG and IL6ST; N = 4 for OCT4, GATA4, and PRDM1; and N = 7 for SOX2. For Western blots, each batch was first normalized to its sodium carbonate vehicle control (0 nM) before comparison. Thus, there are no error bars in the 0 nM MeHg groups for (A–E). The small circle symbols represent individual values of each experiment. One-way ANOVA was used at each time point to compare between the different doses, and the dose response of the treatment effects was significant. Dunnett's post hoc test was then used to compare the treatments to the vehicle control. Significance (*) was set at $p < 0.05$. Note: ANOVA, analysis of variance; ELISA, enzyme-linked immunosorbent assay; GATA4, GATA binding protein 4; hESC, human

embryonic stem cell; IL6ST, interleukin 6 cytokine family signal transducer; MeHg, methylmercury; NANOG, Nanog homeobox; OCT4, octamer-binding transcription factor 4 [also known as POU5F1 (POU domain, class 5, transcription factor 1)]; PRDM1, PR domain-containing protein 1; SEM, standard error of the mean; SOX2, SRY-box transcription factor 2.

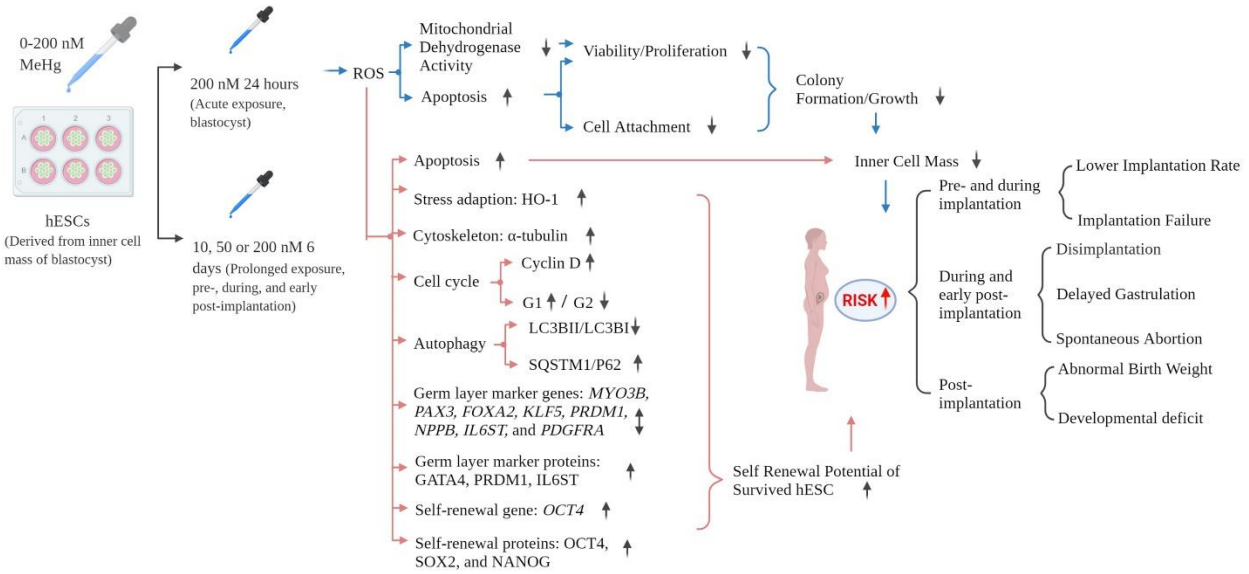

Figure 2.11. A schematic summary of the present study. Note: FOXA2, forkhead box A2; GATA4, GATA binding protein 4; hESC, human embryonic stem cell; HO-1, hemeoxygenase-1; IL6ST, interleukin 6 cytokine family signal transducer; KLF5, Kruppel-like factor 5; LC3B, microtubule-associated proteins 1A/1B light chain 3B; MYO3B, myosin IIIB; NANOG, Nanog homeobox; NPPB, natriuretic peptide B; OCT4, octamer-binding transcription factor 4 [also known as POU5F1 (POU domain, class 5, transcription factor 1)]; PAX3, paired box 3; PDGFRA, platelet-derived growth factor receptor-alpha; PRDM1, PR domain-containing protein 1; ROS, reactive oxygen species; SOX2, SRY-box transcription factor 2.

2.8 Supplemental Tables and Figures

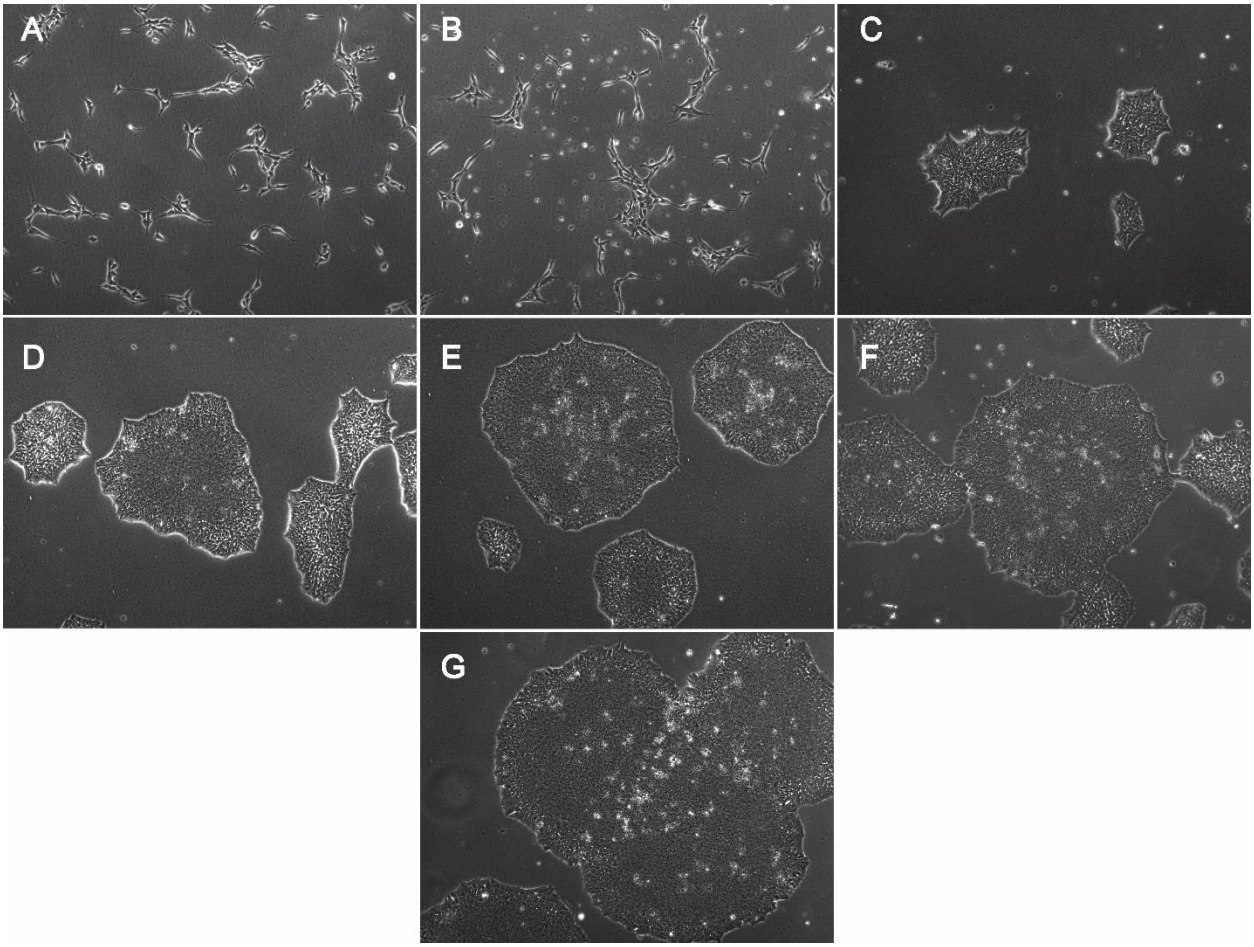

Figure S2.1. Images of hESCs cultured from day 0 to day 6. Cells were grown on Matrigel-coated 6 well plates. (A) Day 0 (24 h after thaw or passage); (B) Day 1; (C) Day 2; (D) Day 3; (E) Day 4; (F) Day 5; (G) Day 6.

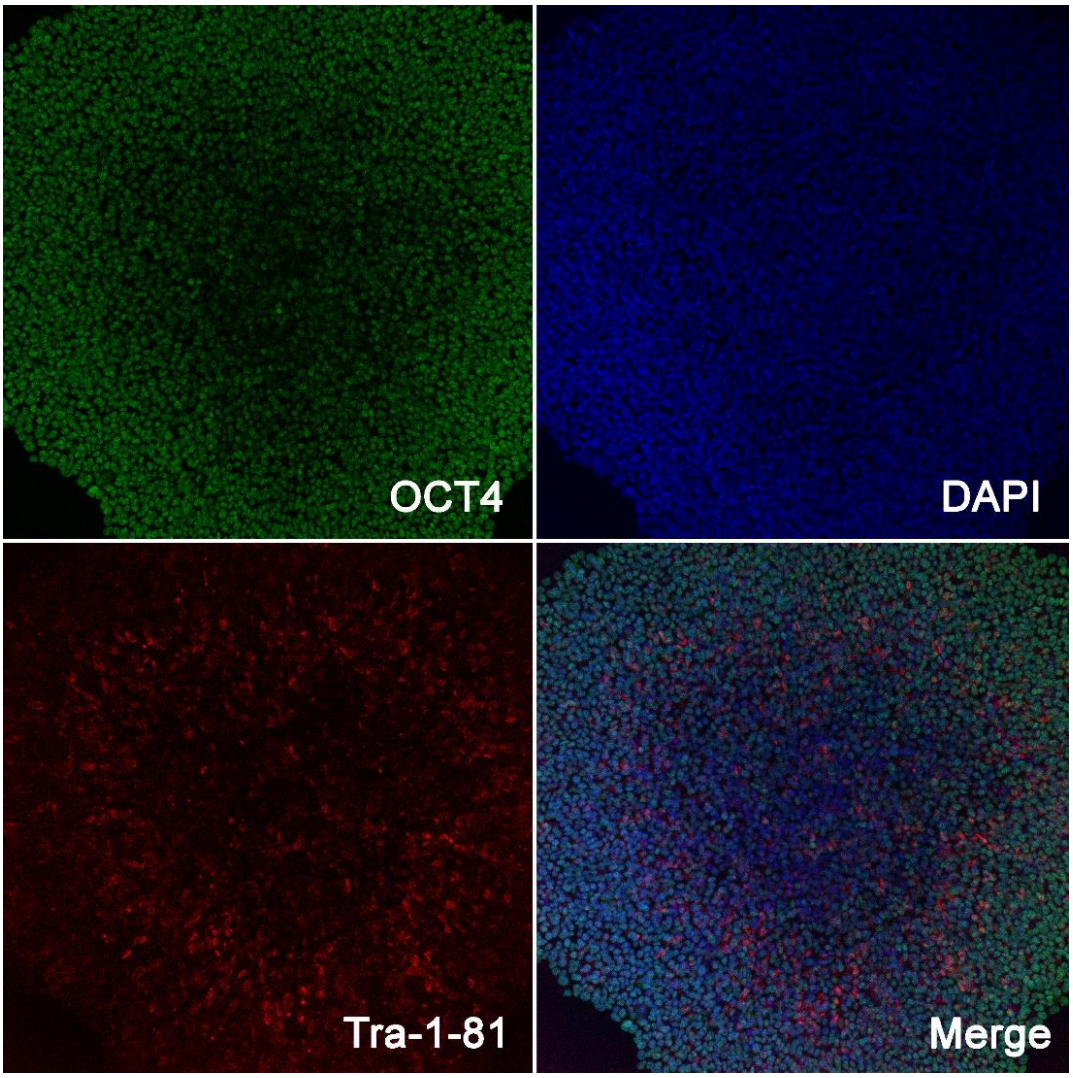

Figure S2.2. Confirmation of pluripotency of hESCs before conducting experiments. hESCs were plated on Matrigel-coated 6 well plates and grown from day 0 to day 6, after which they were immunostained for markers (OCT4, a transcriptional factor; Tra-1-81, a surface marker) of pluripotency. Green indicates positive staining of OCT4. Red indicates positive staining of Tra-1-81. Blue indicates positive staining of nuclei using DAPI.

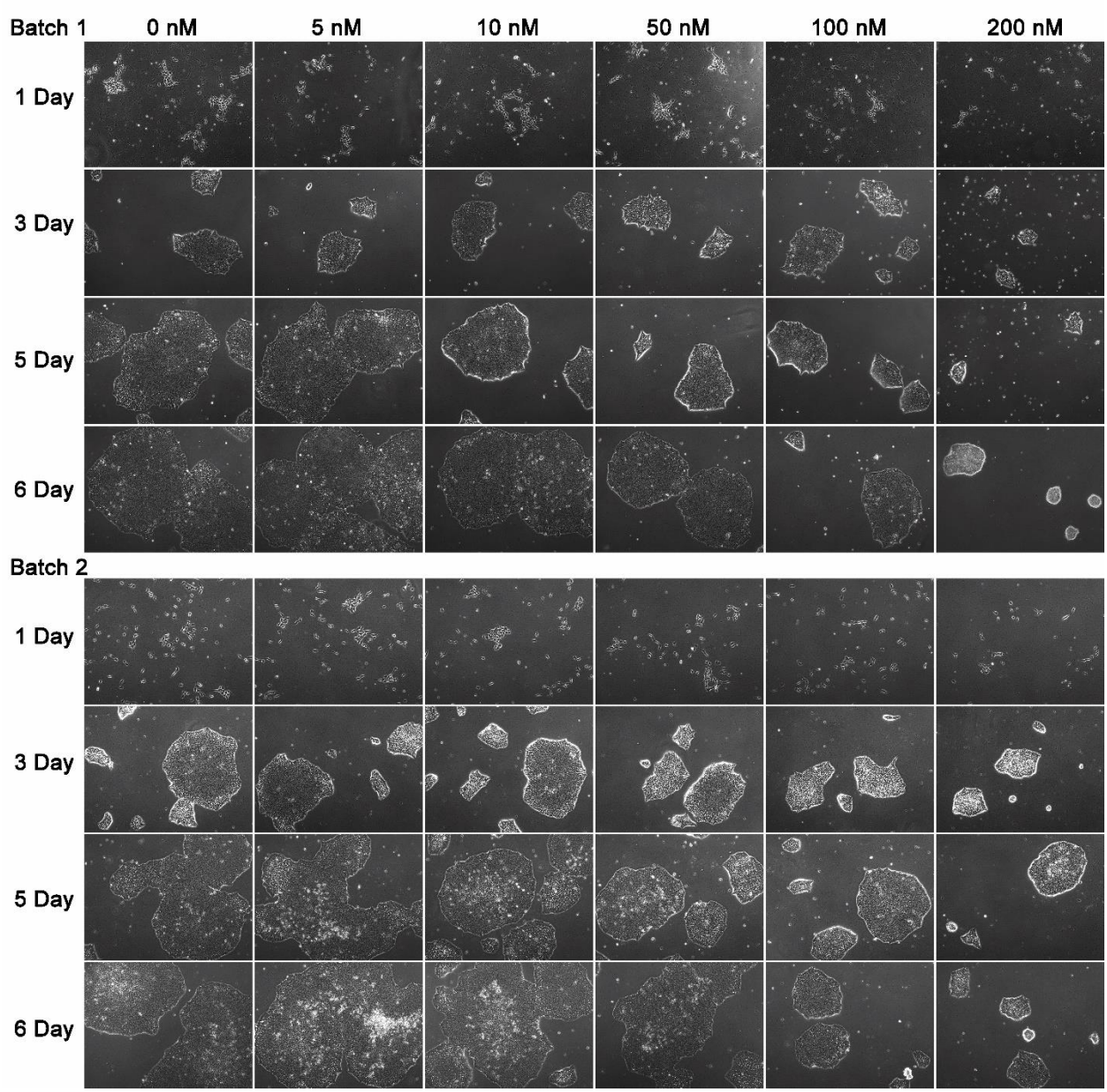

Figure S2.3. The effect of MeHg exposure on the cell attachment, colony formation and morphology of hESCs. Images taken under 10x objective.

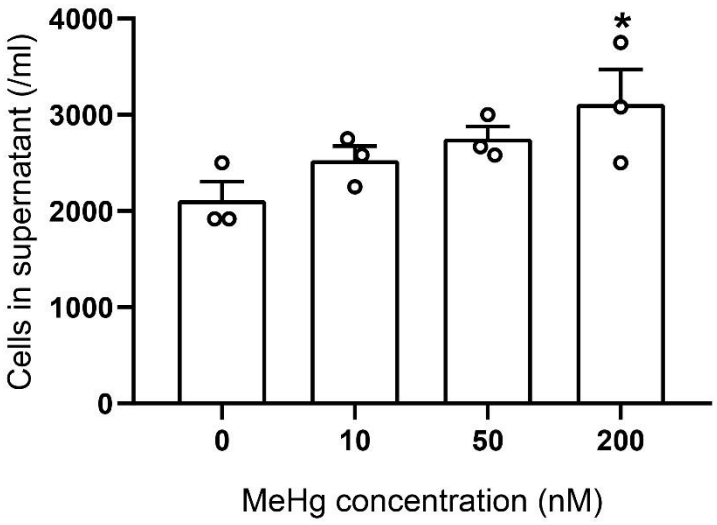

Figure S2.4. Cells in supernatant after 24 h of MeHg exposure as measured by Trypan blue staining. Data is presented as Mean ± SEM with N=3 for each group. The small circle symbols represent individual values of each experiment. One-way ANOVA was used at each time point to compare between the different doses followed by Dunnett's post hoc test comparing to the vehicle control. Significance (*) was set at $p < 0.05$.

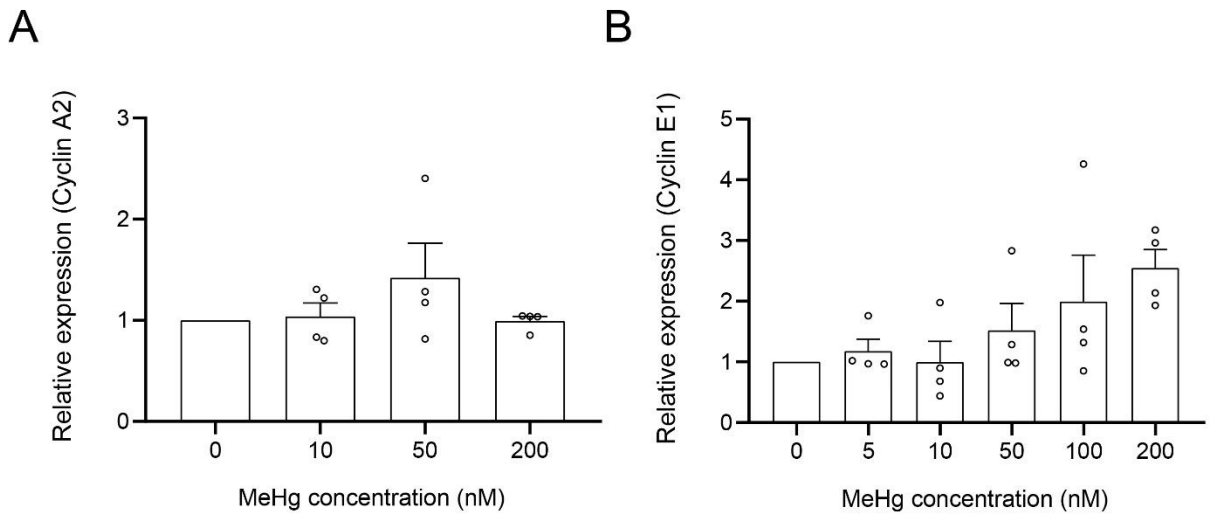

Figure S2.5. Protein expression of cyclin A2 and cyclin E1 after 6 days of MeHg exposure as measured by Western blot. Data is presented as Mean ± SEM with N=4 for each group. Each batch was first normalized to its vehicle control (0 nM) before comparison. Thus, there are no errors in 0 nM groups. The small circle symbols represent individual values of each experiment. One-way ANOVA was used at each time point to compare between the different doses followed by Dunnett's post hoc test comparing to the vehicle control. Significance (*) was set at $p < 0.05$.

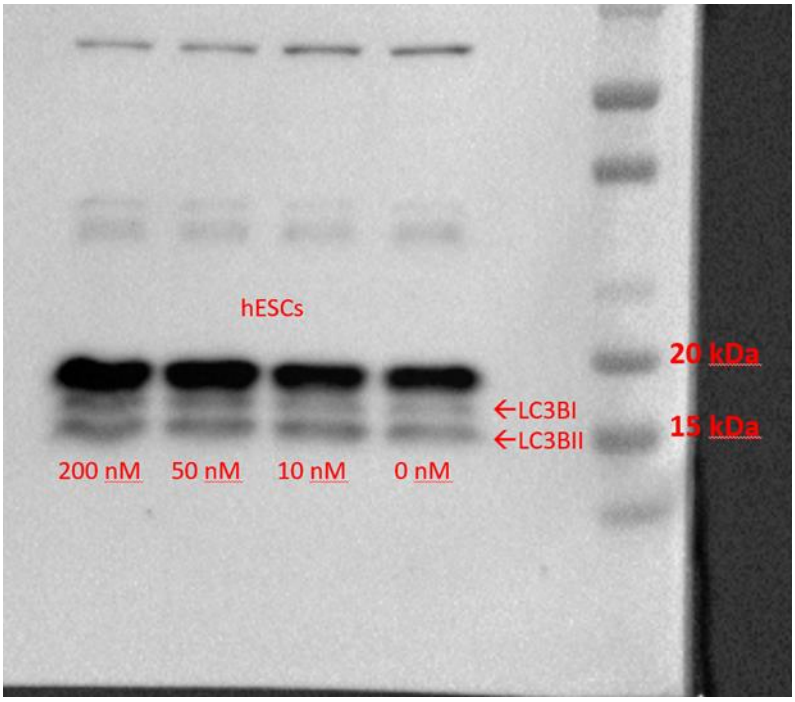

Figure S2.6. LC3B Western blot with ladder. The excepted band of LC3BI and LC3BII should be around 16kDa and 14kDa, respectively. The dark band (around 20kDa) above LC3BI may be a phosphorylation event as this antibody may also recognize a region of the LCB3 sequence which encompasses a single phosphorylation site at Thr6.

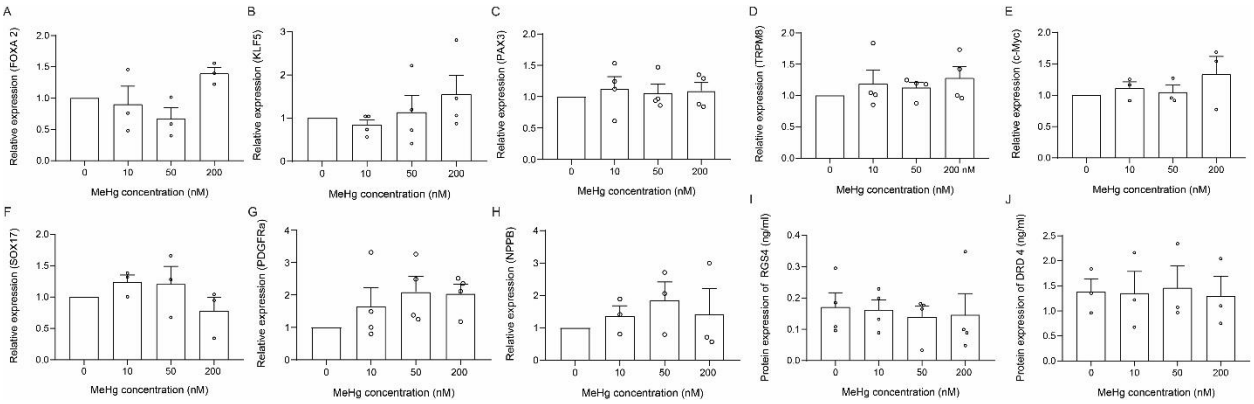

Figure S2.7. Expression of selected cell lineage marker proteins, (A) FOXA2, (B) KLF5, (C) PAX3, (D) TRPM8, (E) c-MYC, (F) SOX17, (G) PDGFRA, (H) NPPB, (I) RGS4, and (J) DRD4 in hESCs after 6 days of exposure to 0, 10, 50, 200 nM MeHg via Western blot (FOXA2, KLF5, PAX3, TRPM8, c-MYC, SOX17, PDGFRA, NPPB) or ELISA (RGS4, DRD4) assay. Data is presented as Mean ± SEM with N=3 for FOXA2, c-MYC, SOX17, NPPB and DRD4, N=4 for KLF5, PAX3, TRPM8, PDGFRA and RGS4. For Western blot, each batch was first normalized to its vehicle control (0 nM) before comparison. Thus, there are no errors in 0 nM groups. The small circle symbols represent individual values of each experiment. One-way ANOVA was used at each time point to compare between the different doses followed by Dunnett's post hoc test comparing to the vehicle control. Significance (*) was set at $p < 0.05$.

Chapter 3: Using cultured human embryonic stem cells to study the effects of an environmental chemical mixture on early-stage embryo development

Bai Li[1], Yihang Kevin Pan[1], Xiaolei Jin[2*], and Hing Man Chan[1*]

[1]Department of Biology, University of Ottawa, Ottawa, Ontario, Canada

[2]Regulatory Toxicology Research Division, Bureau of Chemical Safety, Food Directorate, HPFB, Health Canada, Ottawa, Ontario, Canada

Abstract

Prenatal exposure to many environmental chemicals, such as metals and persistent organic chemicals, are known risk factor for adverse pregnancy and developmental outcomes. However, only some studies have studied the combined effects of co-exposure to environmentally relevant chemical mixtures. This study investigated the effects of an environmentally relevant chemical mixture containing 23 chemicals reported in the maternal blood samples of Nunavik pregnant women in northern Canada, termed the Nunavik Chemical Mixture (NCM), on early-stage embryo development using human embryonic stem cells (hESCs). hESCs were exposed to 0X (vehicle control), and 0.16X-100X doses of NCM (X is the sum of the geometric mean maternal concentrations of individual components of NCM) for 24 h and 6 d to mimic the acute and prolonged exposure that covered pre-, during, and early post-implantation stages *in vivo*. Cell viability and morphology, apoptosis, stress response, cell cycle, cytoskeleton, autophagy, and expression of cell lineage marker genes and proteins were measured at the end of exposures. NCM exposure adversely affected cell viability and adhesion, induced apoptosis, disrupted the cell cycle, altered the expression of cytoskeleton and autophagy proteins, and changed the levels of lineage marker gene and protein expressions at a dose-dependent manner. These results suggested that early-stage prenatal exposure to human-relevant concentrations of NCM could affect embryo development, leading to potential adverse pregnancy outcomes if it occurs *in vivo*. Moreover, the combined effects caused by NCM exposures, especially on the expression levels of lineage marker genes and proteins, were different from that caused by the same doses of MeHg exposure alone that we previously found, indicating potential interactions among different chemicals within the mixture. Thus, our results highlight the importance of considering the combined effects of chemical mixtures when

characterizing the risk of embryotoxicity and developmental effects in populations that are exposed to elevated levels of multiple environmental chemicals.

3.1 Introduction

Fetal development is one of the most sensitive windows to the toxic effects of environmental chemicals, as prenatal exposure impacts embryo development and leads to long-lasting health effects [1-5]. In some cases, even transgenerational effects are observed following prenatal chemical exposure [6-8]. Numerous *in vivo* and *in vitro* studies have examined the effects of environmental chemicals on developing embryos, but most studies look at the effects of individual chemicals. However, on a daily basis, pregnant women are simultaneously exposed to a mix of chemicals through ingestion, inhalation, dermal absorption and other routes [4, 9]. The traditional risk assessment approach was to ensure that the levels of every single chemicals within a mixture were below the "no observed adverse effect level (NOAEL) [10]. However, there is increasing evidence that the effects of chemical mixtures can be additive or even synergistic [10-12]. This growing awareness of the potential risk of chemical mixtures is also reflected in the increase in studies examining the effects of prenatal exposure to chemical mixtures. Epidemiological studies revealed associations between prenatal exposure to various chemical mixtures and increased risk of preterm birth [13, 14], reduced birth weights of newborns [15-18] and impaired neurobehavioral development in later life [19-25]. Animal and *in vitro* studies showed that prenatal chemical mixture exposures could cause reproductive disruptions in F1 generations [26-29], and impact organ differentiation or development [30-32]. However, there is a lack of research on the effects of chemical mixtures representing human exposure profiles and levels at early human embryo developmental stages, such as the blastocyst and implantation stages.

The embryonic stem cell test (EST), which examines the effects of chemicals on the differentiation of mouse embryonic stem cells, has been shown to be a good model for assessing

embryotoxicity *in vitro* [33, 34]. EST has the advantage of using permanent cell lines and not utilizing embryonic tissues from pregnant animals while still providing good predictions of embryotoxicity of the tested chemicals in animals [33-36]. However, EST results may not be extrapolated to human embryotoxicity due to the potential species differences. In the last decade, human embryonic stem cells (hESCs), i.e., pluripotent cells derived from the inner cell mass of the human blastocyst, have emerged as a promising model for embryotoxicity studies of environmental chemical exposures in humans [5, 37-39]. For instance, methylmercury (MeHg), a well-known developmental neurotoxicant [40-42] was found to increase apoptosis in undifferentiated hESCs and enhance self-renewal gene expression in the survived hESCs at nanomolar concentrations [5]. These findings suggest that environmentally relevant levels of MeHg exposure may adversely affect the growth of the developing embryos and increase the risk of implantation failure and other adverse pregnancy or development outcomes. However, like animal studies, most of the existing *in vitro* studies have also focused on examining the developmental toxicity of individual chemicals. Information on the combined effects, particularly the interactions, such as additive and synergistic effects among multiple chemicals, during the early stages of pregnancy, is still lacking.

Global pollution has caused the accumulation of many environmental contaminants such as metals and metalloids (including MeHg and lead), and persistent organic pollutants (POPs), including polychlorinated biphenyls (PCBs), and perfluoroalkyl substances (PFASs), in the biota of northern and Arctic Canada. Inuit people living in the regions are exposed to higher levels of these contaminants because of subsistence living [43, 44]. The environmental contaminant mixture that was detected in maternal blood samples of pregnant women in Nunavik, Quebec, Canada (termed as Nunavik Contaminant Mixture (NCM) in this study) has received increased

attention due to its potential health concerns of indigenous populations [45-50]. Individual components within NCM, such as POPs [51, 52] and MeHg [5, 40-42, 53] have been shown to be embryotoxic. Moreover, prenatal exposure to NCM was also shown to suppress growth, change organ weights, and induce biochemical and histopathological changes in the liver, thyroid, and spleen [54-56]. In addition, gene and protein expression analyses have shown that changes caused by NCM exposure are different from that caused by administering individual components of the NCM, such as PCBs or MeHg. Thus, the effects of NCM could not be accurately predicted from the effects of its individual components administered separately [55, 57], making it more important to study the embryotoxic effects of the NCM as a chemical mixture. Therefore, the main objective of this study is to use undifferentiated hECSs as a model to characterize the embryotoxic effects of the NCM to predict the potential health risks of *in vivo* prenatal exposure to NCM. The second objective is to compare NCM exposure to one of NCM's individual components – MeHg that we had previously studied using the same cell model under the same culture conditions [5]. Although prenatal exposure to some POPs, such as PFASs, has been shown to be associated with low birth weight, reduced body length and abdominal circumference, and risk of obesity in childhood and adolescents in epidemiological studies [58-60], low doses of POPs are usually not considered to induce cytotoxicity. Instead, they may affect cell fate decisions by disrupting endocrine-related pathways in a non-monotonic manner [59, 61]. In addition, as 24 h of 200 nM of MeHg significantly reduced cell viability [5] while 1.9 μM of lead did not induce any cell death [62] in the same hESC line, we hypothesize that MeHg could be the main driver in causing toxic effects, especially cytotoxicity, of the NCM on hESCs.

3.2 Materials and Methods

3.2.1 Ethics review and approval

This project was reviewed and approved by the Health Canada and Public Health Agency of Canada's Research Ethics Board (File No. REB 2016-027H) and by the Office of Research Ethics and Integrity of the University of Ottawa (File No. H-05-19-4084).

3.2.2 Maintenance of human embryonic stem cells (hESCs)

Human embryonic stem cells were maintained according to previous protocols established in our laboratory [5]. In brief, hESCs (H9; passage 23; WiCell Research Institute) were passaged and expanded in Matrigel (Catalog no. 354230; BD Biosciences)-coated six-well plates using Essential 8 Flex Medium (Catalog no. A2858501; Thermo Fisher Scientific) under 37°C, 4% oxygen (O_2) and 10% carbon dioxide (CO_2) in a tri-gas incubator (Thermo Fisher Scientific). Fresh medium was changed daily, and the medium was supplemented with 10 µM Rho-associated kinase inhibitor (Catalog no. 72304; StemCell Technologies) on the first day of seeding to enhance the survival of the cells. Cells at ~85% confluence were lifted using Gibco StemPro Accutase cell dissociation reagent (Catalog no. A1110501; Thermo Fisher Scientific) and seeded onto new plates for subsequent experiments. Only hESCs under passage 38 (within 15 passages from purchase) were used to avoid genetic instability associated with prolonged passaging.

3.2.3 Nunavik Chemical Mixture (NCM) preparation and exposure

The chemical mixture NCM was prepared based on measured concentrations in the maternal blood samples collected from pregnant women in Nunavik in 2016-2017 [63]. The chemical components of NCM, concentrations, solvents and sources are shown in Table 3.1. The

23 chemicals were individually dissolved in DMSO or double-distilled waster to make highly concentrated stocks (mostly 10^6X or 10^7X the geometric mean of the reported concentrations). To avoid any effects from the solvents, two 2000X working mixture solutions (one in DMSO and one in water) were made from the single chemical stocks for cell dosing. The final concentrations in the cell culture were 0X, 0.2X, 0.8X, 4X, 20X and 100X for cell morphology and cytotoxicity assays. Based on the results from the above two assays and to match MeHg concentrations with our previous study [5], 0X, 0.1X, 0.5X, 2.4X and 4.8X were chosen for the subsequent experiments.

To mimic the acute and the prolonged exposure *in vivo*, hESCs were treated with NCM for 24 h or 6 d, depending on the assays. The NCM working solutions were freshly diluted in the culture medium. The medium was changed daily.

3.2.4 Cell morphology assessment

hESCs were treated with NCM for 6 d, as described above. Vehicle- and NCM-treated hESCs were observed and imaged daily under a 10× objective on a Zeiss Axiovert 40 CFL inverted microscope (Carl Zeiss Microscopy LLC) with a SPOT RT3 digital camera and SPOT basic software (Diagnostic Instruments Inc.).

3.2.5 Intracellular mercury measurements

hESCs were exposed to NCM for 24 h or 6 d, as described above. The cells were rinsed twice with 500 μL PBS each time after collecting the culture medium. After collecting the PBS from each rinse, cells were collected with cell scrapers and suspended in 200 μL (for cells after 24 h of NCM treatment) or 500 μL (for cells after 24 h of NCM treatment) of PBS. Cells were gently mixed by pipetting, and 10 μL of cell suspension was taken from each sample for cell

counting. Total mercury contents in culture medium, PBS and cells were measured individually with a mercury analyzer (MA 3000; Nippon Instruments Corp.), according to the manufacturer's instructions. The intracellular mercury content was then normalized to cell numbers counted by using a Countess Automated Cell Counter (Invitrogen, Thermo Fisher Scientific) after 1:1 dilution of cell suspension in Trypan blue solution (Catalog no. T10282; Thermo Fisher Scientific). The result of intracellular mercury content was reported as picomoles per 10,000 cells.

3.2.6 Fluorescence microplate assays

Fluorescence microplate assays were used to determine the effects of NCM on cell viability and the cellular stress response reflected by ROS production.

Tetrazolium salt (WST-1) assays (Catalog no. ab155902; Abcam Inc.) were performed according to the manufacturer's instructions to determine the effects of NCM on cell viability and proliferation. Briefly, hESCs were exposed to NCM in six-well plates for 1-6 d, as described above. One plate was used for WST-1 assay after each 24 h of exposure. 200 µL of WST-1 solution was added into each well on the culture plate, followed by 10 s of shaking. Absorbance at 450 nm wavelength was measured on a BioTek Cytation 3 Cell Imaging Multi-Mode Reader (Fisher Scientific) after a 1.5-h incubation at 37°C.

The generation of ROS in each dose group was determined by measuring the fluorescence intensity of 2', 7' –dichlorofluorescein (DCF) which is oxidized from DCFDA / H_2DCFDA by intracellular ROS using a cellular ROS assay kit (ab113851, Abcam). hESCs were seeded in a 96-well plate and were allowed to attach overnight. The next day, the culture medium was removed, and each well was rinsed with 100 µL of assay buffer included in the kit, followed

by staining with 100 μL DCFDA working solutions at 37°C for 45 min in the dark. The staining buffer was then removed, and each well was rinsed once with supplemented buffer containing 10% FBS. The cells were then exposed to NCM in 100 μL of the same buffer for 24 h. Fluorescence intensity was read at Ex/Em = 485/535 nm wavelength on a BioTek Cytation 3 Cell Imaging Multi-Mode Reader immediately after treatment without washing. Cells dosed with 50 μM tert-butyl hydroperoxide, a ROS inducer, for 4 h were used as a positive control.

3.2.7 Flow cytometry

Flow cytometry was used to detect the effects of NCM on apoptosis as well as the cell cycle. The Annexin V–fluorescein-5-isothiocyanate (FITC) Early Apoptosis Detection Kit (Catalog no. 6592S; Cell Signaling Technology) was used according to the manufacturer's instructions to detect the effects of NCM on apoptosis. Briefly, hESCs were exposed to NCM as described above for 24 h or 6 d. Cells were detached using StemPro Accutase, resuspended in Annexin V binding buffer, and aliquoted at 96μL/tube. 1 μL of Annexin V conjugate and 12.5 μL of propidium iodide (PI) were then added to each tube and incubated in the dark for 10 min. The cell suspension was then diluted to a final volume of 250 μL using Annexin V binding buffer before analysis. All the steps were conducted on ice. The fluorescent labelling of apoptotic cells was counted on a BD LSR II Flow Cytometer (Becton Dickinson) using 505LP (long pass), 525/50BP (bandpass) on the blue (488-nm) laser for detection of the early apoptosis marker Annexin V, whereas 570LP, 582/15BP on the yellow/green (561nm) laser allowed detection of the necrosis marker (i.e., PI). The detached cells were collected by centrifugation and subsequent staining with Trypan blue. The cell number was then counted with a Countess Automated Cell Counter.

The effects of NCM on the cell cycle were determined using a Cell Cycle Assay kit (Catalog no. ab112116; Abcam Inc.) following the manufacturer's protocol. In brief, hESCs were exposed to NCM for 6 d, washed with cold PBS, detached by StemPro Accutase, centrifuged, resuspended, and stained in the nuclear green CCS1 solution provided in the kit. After 40 min of incubation at 37°C, the fluorescence of cells was quantified using a BD LSR II Flow Cytometer (Becton Dickinson) with 505LP, 525/50BP on the blue (488-nm) laser.

3.2.8 Immunocytochemistry

The fluorescent intensity of cleaved caspase-3 (CC3) and the number of CC3 positive cells was quantified to determine the effects of NCM on intermediate and late apoptosis. After hESCs were exposed to NCM in Matrigel-precoated chamber slides (Catalog no. 0030742010; Eppendorf) for 24 h or 6 d, immunocytochemical staining of CC3 was performed. Briefly, the medium was disposed, and the cells were washed twice with PBS, fixed in 4% paraformaldehyde (Santa Cruz Biotechnology) for 10 min, and then blocked with 5% bovine serum albumin (BSA) diluted in PBS containing 0.3% Triton X-100 (Sigma-Aldrich). The cells were then incubated with rabbit antihuman CC3 antibody (Catalog no. 9661S; Cell Signaling Technology) at 1: 200 dilution and mouse antihuman α-tubulin antibody (Catalog no. ab4074) at 1:1000 dilution in PBS containing 5% BSA, at 4°C overnight. After washing three times with PBS, the cells were incubated with Alexa Fluor 488 goat antirabbit immunoglobulin G (IgG) (Catalog no. A11008; Thermo Fisher Scientific) and Alexa Fluor 594 goat anti-mouse IgG (Catalog no. A11005; Thermo Fisher Scientific) diluted at 1:500 in 5% BSA in PBS at room temperature for 1 h. After washing three times with PBS, the Prolong Gold antifade reagent containing 4′,6-diamidino-2-phenylindole (DAPI; Catalog no. S36939; Thermo Fisher Scientific) was added. The immunofluorescent images were taken with a Nikon A1RsiMP confocal microscope (Nikon

Instruments Inc.) with Nikon's Imaging Software NIS-Elements. Fluorescent intensity of CC3 and CC3-positive cells was measured and counted using ImageJ. The percentage of CC3-positive cells was also calculated against the total number of cells measured by DAPI staining. A higher intensity/percentage of CC3-positive cells indicates a higher level of apoptosis.

3.2.9 Western blotting

Protein expression levels were measured to determine the effects of NCM on the cellular stress response, cytoskeleton, cell cycle, autophagy, as well as protein expression of cell lineage markers.

Protein extraction of NCM-dosed hESCs were conducted by washing the cells with PBS and lysing in Pierce radioimmunoprecipitation assay buffer (RIPA buffer; Thermo Fisher Scientific) containing proteinase and phosphatase inhibitor cocktails (Catalog no. 5872S; Cell Signaling Technology) through sonication on ice using a Microson Ultrasonic Cell Disruptor XL2000 (Misonix Inc.). Protein concentrations of the lysates were quantified using a Pierce Bicinchoninic Acid Protein Assay kit (Catalog no. 23225; Thermo Fisher Scientific). Cell lysates were mixed with 4× Laemmli sample buffer (Bio-Rad) and denatured by heating at 100°C for 4 min.

Western blot was performed by running the cell lysates on a Stain-Free gel made with 7.5% or 12% TGX Stain-Free FastCast acrylamide solutions (Catalog no. 1610181, 1610185; Bio-Rad) depending on the target proteins. For each batch, the same amount of protein was loaded, and the amount of total protein loaded ranged from 25 to 30μg between different batches. After electrophoresis, gels were activated under ultraviolet light using the ChemiDoc XRS+ imaging system (Bio-Rad). Proteins were electro-transferred from gels to polyvinylidene

difluoride (PVDF) membranes with the Mini Trans-Blot Cell (Catalog no. 1703930; Bio-Rad). Membranes were then blocked with 5% non-fat dry milk (NFDM, Catalog no. 1706404; Bio-Rad) for 1 h at room temperature and incubated with the antibody of interest (Table S3.1) at 4°C overnight. After the membranes were washed three times in Tris-buffered saline with 0.1% Tween 20 (TBST) on a shaker for 5 min, they were incubated with 1:5,000 dilution of horseradish peroxidase (HRP)–linked secondary antibodies (Table S3.1) in blocking buffer for 1 h at room temperature. All membranes were then incubated with the enhanced chemiluminescence substrate (Catalog no. 1705062; Bio-Rad) in the dark and imaged using the ChemiDoc XRS+ imaging system. Following imaging, band intensities were quantified and normalized against total protein band intensities using Image Lab software (Bio-Rad).

3.2.10 TaqMan hPSC scorecard assay

The TaqMan hPSC Scorecard Assay (Catalog no. A15871; Thermo Fisher Scientific) was used to determine the effects of NCM on cell lineage marker gene expression. hESCs were exposed to NCM in six-well dishes for 6 d as described above. RNA was isolated using TRIzol (Catalog no. 15596026; Thermo Fisher Scientific) and then reverse-transcribed with the Applied Biosciences High-Capacity complementary DNA Reverse Transcription kit with RNase inhibitor (Catalog no. 4374966; Thermo Fisher Scientific) following the respective manufacturer's protocol. The cDNA was then diluted, mixed with TaqMan Fast Advanced Master Mix (Catalog no. 4444556; Thermo Fisher Scientific), and loaded onto the precoated Scorecard plates, which were then sealed and centrifuged at 600×g for 2 min. The RT-PCR cycles were run with the fast 96-well template on a QuantStudio 7 Flex RT-PCR System (Life Technologies Inc.). Quantitative RT-PCR array analysis was conducted on four batches of experimental samples from four different cell passages.

3.2.11 Statistical analysis

All data were expressed as the means plus or minus the standard errors of the mean (means ± SEMs) and were tested for statistical significance with one-way ANOVA, followed by Dunnett's post hoc tests. The differences were considered significant if $p < 0.05$. Except for TaqMan Scorecard assay analysis, all statistical analyses were performed using GraphPad Prism (version 8; GraphPad).

For Scorecard analyses, CT values of target genes were subtracted by the CT values of the reference genes [Actin Beta (ACTB), CCCTC-binding factor (CTCF), E1A binding protein p300 (EP300), SMAD family member 1 (SMAD1)] to obtain ΔCT values. A cluster analysis was performed on the ΔCT values using the heatmap.2 function within the gplots package in R (R Development Core Team). This cluster analysis revealed that most samples within a batch were clustered together. Thus, a statistical model including the dose and batch factors on ΔCT (ΔCT = dose + batch) was applied using the lsmeans package in R to estimate the gene expression difference between all NCM dose groups and the control group based on ΔCT values. As some of the genes tested in the Scorecard analyses may not be independent, a second statistical model was also run to control for potential interaction between the genes (ΔCT = dose + gene + dose*gene + batch), and results from both statistical models are reported. The level of probability of statistical significance was set at $p < 0.05$. Fold change was estimated using the function of $2^{(-\text{least square mean for NCM dose group})}/2^{(-\text{least square mean for control})}$.

3.3 Results

3.3.1 Morphology and viability of hESCs exposed to NCM

hESCs were dosed with a 5-fold dilution series of NCM (0.2X – 100X) to examine the effects of NCM on hESC morphology and viability. Following 24 h exposure to 20X and 100X NCM, hESCs failed to attach and form visible colonies (Figure 3.1A). Colonies of hESCs that did form following 4X NCM exposure were also visibly smaller after 24 h exposure and remained smaller all the way up to 6 d of exposure (Figure 3.1). This trend was also reflected when measuring cell viability through the WST-1 assay (Figure 3.2). Following 24 h exposure to 20X and 100X NCM, cell viability was close to 0. Cell viability of the 4X NCM dose group was significantly lower than that of the control group beginning at 72 h post-exposure, followed by the 0.8X NCM dose group at 96 h post-exposure and lastly, the 0.2X NCM dose group at 120 h post-exposure. At 6 d (144 h) post-exposure to all doses of NCM, hESCs showed significantly decreased cell viability.

3.3.2 Intracellular mercury concentrations

A dose-dependent increase in intracellular total mercury content was observed following both 24 h and 6 d of exposure to increasing concentrations of NCM in hESCs (Figure 3.3).

3.3.3 Apoptosis and autophagy in hESCs exposed to NCM

A significant increase in both early and late apoptosis was observed following 24 h and 6 d of 4.8X NCM treatment, as shown by the increase in the percentage of annexin V or annexin V and propidium iodide-positive cells (Figure 3.4B, D). CC3 immunocytochemistry also showed a significant increase in fluorescent intensity and CC3 positive cell percentage following 24 h of 4.8X NCM treatment (Figure 3.4A). However, this increase was no longer observed after 6 d of NCM treatment (Figure 3.4C).

In addition to apoptosis, autophagy was also examined in hESCs following NCM treatment by examining the expression of autophagy markers LC3BII/LC3BI ratio and SQSTM1 after 6 d of NCM treatment. LC3BII/LC3BI ratio was significantly decreased in 4.8X NCM-treated hESCs. However, no significant difference was observed for SQSTM1 (Figure 3.5).

3.3.4 Oxidative stress in hESCs exposed to NCM

ROS levels in hESCs increased after 24 h exposure to 2.4X NCM as measured by DCF fluorescent intensity (Figure 3.6A). However, HO-1 protein expression was not altered in hESCs following 6 d of NCM exposure (Figure 3.6B).

3.3.5 Cell cycle of hESCs exposed to NCM

Following 6 d exposure to 4.8X NCM, hESCs in G1 phase significantly increased, whereas hESCs in the G2 phase decreased (Figure 3.7). This was associated with a significantly increased expression of cyclin D1 and E1, but not cyclin A2 or B2 in the 4.8X NCM dose group (Figure 3.8).

3.3.6 Cytoskeletal protein expression in hESCs exposed to NCM

Exposure to 4.8X NCM resulted in a significant upregulation of β-actin protein expression in hESCs. Protein expression of α-tubulin exhibited an increasing trend with increasing doses of NCM, though it was not significant (Figure 3.9).

3.3.7 Lineage marker gene and protein expression in hESCs exposed to NCM

Lineage marker gene expression was examined using the TaqMan hPSC scorecard assay following 6 d of NCM exposure. The gene expression profile of hESC exposed to 4.8X NCM clustered together and away from the other lower dose groups of NCM and the control (Figure

3.10A). When lineage marker gene expression was analyzed ignoring potential interactions between the lineage genes, the mesoderm markers FCN3 and COLEC10 was significantly upregulated in the 4.8X NCM dose group (Figure 3.10B) and the mesoderm markers TM4SF1 and ABCA4 was significantly downregulated in the 4.8X NCM dose group (Figure 3.10B). The endoderm markers LEFTY2 and HNF1B were also upregulated in the 4.8X NCM dosed group (Figure 3.10B). When the lineage marker gene expression was analyzed taking into account of potential interactions between lineage genes, ectoderm marker CDH9 and endoderm markers FOXA2 and EOMES were significantly down regulated in the 4.8X NCM dose group (Figure 3.10C), the mesoderm marker FCN3 and endoderm marker HNF1B were significantly upregulated in the 4.8X NCM dose group (Figure 3.10C), and the mesoderm marker TBX3 was significantly downregulated in the 0.1X NCM dose group (Figure 3.10C). The protein expression of these genes was further examined by Western blot. When hESCs were exposed to NCM, FCN3 showed a dose-dependent increase in protein levels, with FCN3 being significantly upregulated when exposed to 4.8X NCM (Figure 3.11A, B). LEFTY2 showed a significant increase in expression in hESCs exposed to 0.5X but no other doses of NCM (Figure 3.11C, D). In contrast, EOMES showed significant downregulation in hESCs exposed to 4.8X NCM (Figure 3.11E, F). All lineage marker proteins that do not show significance were displayed in Figure S3.1.

3.4 Discussion

The main goal of this study was to characterize the embryotoxicity of the NCM *in vitro* using hESCs as a model. We showed that NCM concentrations that are similar and up to 20 times higher than those found in maternal blood samples in Nunavik pregnant women affected

the cell morphology, cell viability, cellular stress response, cell cycle, apoptosis and autophagy, and cytoskeletal protein expression, with MeHg being the main driver of cellular toxicity within NCM. However, cell lineage gene/protein expression in hESCs exposed to NCM was drastically different compared to MeHg exposure alone. This could be likely due to the influence of the POPs within the NCM. These observed effects may be the underlying toxic mechanisms for adverse pregnancy or development outcomes, such as implantation failure, miscarriage, and delayed organ development *in vivo*.

Our results showed that exposure to NCM concentrations greater than 20X resulted in hESCs failing to attach and an almost complete loss of viability following 48 h of exposure, suggesting that these high concentrations of NCM exposure would prevent embryo implantation *in vivo*. 4X NCM containing 83.94 nM MeHg had similar effects on cell adhesion and colony formation as MeHg at 100 nM alone after 6 days of exposure, whereas NCM concentrations closer to what is observed in maternal blood (1X) containing 20.94 nM MeHg had similar effects on cell adhesion and colony formation as MeHg at 50 nM alone after 6 days of exposure [5]. These results suggest that the effects of MeHg on cell adhesion and colony formation were not drastically affected by the presence of other component chemicals in the NCM at the concentrations used and, in turn, support our hypothesis that MeHg may be the main driver affecting cell viability within the NCM. However, it should be noted that NCM did exert higher levels of cellular toxicity compared to MeHg exposure alone. This is not surprising considering that main components other than MeHg within the mixture have been shown to induce apoptosis and alter cell viability in human cell lines. For example, lead has been shown to induce apoptosis and alter cell viability in human cell lines at concentrations within 10-fold of what is present within NCM [62], and may have synergistical effects with Hg [64]. Even though PCBs [65-67],

organochlorines (OCs) [68, 69], and PFASs [70, 71] may also have cytotoxic effects at micro molar concentrations, these are more than 1,000-fold more concentrated that what is present within the NCM in the current study, and thus are not as likely to have significant contributions to the cytotoxic effects of NCM.

In addition to decreased cell viability, we also observed a disruption of the cell cycle in hESCs following 6 d of 4.8X NCM (containing 100 nM MeHg) exposure, with an increase in the proportion of G1 and a reduction in G2 phase cells, a characteristic of G1/S phase cell cycle arrest. This was accompanied by increased protein expression of cyclin D1. It is interesting that MeHg alone at 200 nM, but not 100 nM, also increased cyclin D1 expression in hESCs under the same experimental conditions [5], which also paralleled with G1/S phase cell cycle arrest. Upregulation of cyclin D1 by MeHg alone and NCM could have mediated this cell cycle arrest, as acute overexpression of cyclin D1 in fibroblasts have been shown to prevent S-phase entry [72, 73]. It is intriguing that 4.8X NCM containing 100 nM MeHg also increased protein expression of cyclin E1, while MeHg alone had no effect on it. It is believed that cyclin E1 drives the transitions from G1 to S phase through the assembly of pre-replication complexes and activating CDK2, leading to the initiation of the DNA synthesis [74]. In hESCs, cyclin E1 expression was found to peak at G1/S boundary, and PD0332991 (PD), a pharmacological inhibitor that arrested cells in the early G1 phase, also increased cyclin E1 expression [74]. It is possible that 4.8X NCM caused cell cycle arrest at the early G1 phase as PD did. Other than cyclins, β-actin also mediates the cell cycle, with its downregulation or depletion associated with the accumulation of G2/M phase cells [75]. In this study, 4.8X NCM increased β-actin protein expression in hESCs after 6 days of exposure, alongside a decreased proportion of G2 phase cells. This suggests that 4.8X NCM disrupted the action of β-actin in cell cycle regulation. Thus,

the data suggest that NCM had similar effects on the cell cycle as MeHg alone, with other compounds within the NCM enhancing the cell cycle disrupting effects caused by MeHg.

Other than the effects on the cell cycle, NCM at 4.8X containing 100 nM MeHg also decreased the ratio of LC3BII/LC3BI after 6 days of exposure, suggesting a decreased autophagy in hESCs. This is consistent with our previous finding that MeHg at 200 nM also decreased autophagy in hESCs under the same experimental conditions [5]. The decreased LC3BII/LC3BI ratio by NCM was not accompanied by the increased accumulation of SQSTM1 (p62) as what was found for MeHg alone. This could be due to the different concentrations (100 nM vs 200 nM) of MeHg used in the two studies, or the presence of other chemicals that altered the effects of MeHg on autophagy.

Thus, even though the cellular effects caused by NCM and MeHg may contain some differences, the general conclusion that can be drawn from our cellular experiment data is that MeHg within NCM is the main driver for cellular toxicity, with other components within the NCM enhancing the cytotoxic effects of MeHg.

In addition to the cellular effects, NCM also altered cell lineage marker gene and protein expressions in hESCs after 6 d of exposure. This includes genes for key transcription factors such as EOMES that functions in trophoblast differentiation and regulates endoderm differentiation later in gastrulation [76, 77]; TBX3 that promotes proliferation and regulates mesendoderm differentiation in hESCs [78, 79]; HNF1B that plays an important role in the regulation of endoderm patterning and directs the differentiation of endodermal cells into pancreatic progenitors [80]; FOXA2 (also named HNF3β) that acts as a pioneer factor to facilitate enhancer activation through H3K4me1 deposition during human pancreatic differentiation [81]; FCN3 that encodes ficolin 3 protein, which is a recognition molecule in the

lectin pathway of the complement system [82] and a marker gene of liver sinusoidal endothelial cells (LSEC) [83]; and LEFTY2 which is critical for the proper differentiation of embryonic stem cells into the three germ layers [84]. The decreased expression of EMOES, FOXA2 and TBX3, and the increased expression of HNF1B, FCN3 and LEFTY2 gene and/or protein in hESCs exposed to NCM imply disruptions in lineage specification during hESC differentiation towards endoderm/mesendodoerm, indicating a potential risk of adverse outcomes in the development of endoderm or mesoderm and their derived organs, such as liver, pancreas, and kidney if such effects of NCM exposure occur *in vivo*. This assumption is based on the fact that gestational and lactational exposure of rats to a similar environmental contaminant mixture found in maternal blood of Canadian Arctic human populations produced adverse effects in the offspring, including growth suppression and damage to multiple organs that are either endoderm or mesoderm derived, including the liver, thyroid, and spleen [54]. Interesting to note that most effects induced by this contaminant mixture on rats were observed at the highest dose, which was 100-fold higher than the levels detected in the human blood [54], whereas our data suggests that NCM can induce embryotoxicity and gene changes at doses (0.1X-4.8X of the human maternal GM concentrations) much closer to that detected in the human blood. This difference could be attributed to the differences between species, *in vivo* versus *in vitro* systems used, different biomarkers determined, and slight variations in mixture compositions between the two studies. This also suggests that hESCs is a sensitive model for assessing the potential embryotoxicity of chemical mixtures on humans.

Despite NCM exposure causing similar cellular effects on hESCs as single MeHg exposure, changes in the expression of lineage genes and proteins caused by NCM were drastically different compared to that of single MeHg exposure. In MeHg-exposed hESCs,

expression of lineage genes of all three germ layers, as well as self-renewal genes, were altered, with the greatest number of altered genes related to ectoderm that gives rise to the central nervous system. Changes at the protein level, however, were mainly confined to self-renewal and endodermal proteins [5], unlike NCM exposure, where most changes were in mesoderm and endoderm genes with no self-renewal genes/proteins being altered. The total number of genes and proteins altered was also significantly less compared to hESCs being exposed to MeHg only. Other components in the NCM may mask the effects of MeHg on the expression of these lineage genes, which has been shown in animal studies. In rats exposed to a similar chemical mixture designed to reflect the blood contaminant profile of Canadian arctic populations, genes and proteins related to nerve cell differentiation, migration, myelination and synaptic transmission that were altered by individual components within the mixture returned to baseline control levels when rats were exposed to the mixture [55, 57]. This masking effect could like be exerted by POPs, as POPs have been shown to act as endocrine disruptors to disrupt the actions of sex steroids that regulate gene expression and are involved directly with organ differentiation [85]. Thus, POPs in the NCM, on one hand, could interact with MeHg to mask some of the gene expression changes caused by MeHg, hence the decreased number of lineage genes altered by NCM compared to MeHg, while on the other hand, disrupt endodermal/mesodermal lineage genes. Like previous studies, our results also show the importance of studying mixtures as a whole, especially at the molecular level, as the effects of mixtures cannot be simply predicted by studying the effects of single chemicals.

In conclusion, our results showed that hESCs is a sensitive *in vitro* model for assessing the early developmental effects of chemical mixtures. The NCM at concentrations detected in human maternal blood samples of highly exposed populations have toxic effects in hESCs,

which could potentially lead to adverse pregnancy outcomes, such as implantation failure and miscarriage, and developmental deficit when exposed *in vivo*. There is epidemiological evidence that the Inuit had higher rates of preterm birth, stillbirth and infant death compared with the rest of Canada and with other rural and northern areas [86]. Although social, economic, nutritional status and lifestyle factors may contribute to the discrepancy, the role of exposure to environmental chemicals may also be a risk factor. In addition, epidemiological studies in Nunavik also showed that prenatal exposure to environmental chemicals was associated with adverse developmental outcomes among infants and children, including attention-deficit/hyperactivity disorder [87, 88] and anxiety [89]. Findings from this study provide insights into the mechanisms associated with embryotoxicity and the potential risks of NCM exposure in human early-stage developing embryos. More importantly, even though some cellular effects caused by the NCM can, to some degree, be predicted by studying the effects of single chemical components like MeHg, the effects caused by sublethal doses of NCM at the molecular level may be unique to the mixture and should be assessed independently. Our study also suggests that regulating these environmental contaminants on a chemical-by-chemical basis might not be sufficient, as mixtures might exert different effects than their individual components. As the main route for NCM exposure is likely through fish and marine mammal consumption, it is important to note that the risk assessment needs to consider the benefits of these foods, including their importance to nutritional health [44]. Findings from the present study will improve the understanding of the embryotoxicity of chemical mixtures and contribute to characterizing the risk of potential adverse pregnancy and developmental outcomes related to NCM exposure during early embryo developmental stages among specific human populations.

3.5 Acknowledgments

B. Li, X. Jin and H.M. Chan designed this study. B. Li conducted the experiments and prepared the draft. Y. Pan conducted the statistical analysis of Scorecard data. X. Jin and H.M. Chan critically reviewed the manuscript. H.M. Chan finalized the manuscript and submitted it. We thank A. Stalker and E. Yumvihoze for providing technical support in flow cytometry and mercury content measurements. This project was supported by an internal project funding provided to X. Jin in the Bureau of Chemical Safety, Food Directorate, Health Products and Food Branch, Health Canada, and a Discovery Grant from the Natural Sciences and Engineering Research Council of Canada and a Canada Research Chair to H.M. Chan.

3.6 References

1. Palanza, P., et al., Prenatal exposure to endocrine disrupting chemicals: effects on behavioral development. Neuroscience & Biobehavioral Reviews, 1999. **23**(7): p. 1011-1027.
2. Perera, F. and J. Herbstman, Prenatal environmental exposures, epigenetics, and disease. Reproductive toxicology, 2011. **31**(3): p. 363-373.
3. Bellinger, D.C., Prenatal exposures to environmental chemicals and children's neurodevelopment: an update. Safety and health at work, 2013. **4**(1): p. 1-11.
4. Rager, J.E., et al., Review of the environmental prenatal exposome and its relationship to maternal and fetal health. Reproductive Toxicology, 2020. **98**: p. 1-12.
5. Li, B., et al., Characterizing the Low-Dose Effects of Methylmercury on the Early Stages of Embryo Development Using Cultured Human Embryonic Stem Cells. Environmental health perspectives, 2021. **129**(7): p. 077007.

6. Janesick, A.S., T. Shioda, and B. Blumberg, Transgenerational inheritance of prenatal obesogen exposure. Molecular and cellular endocrinology, 2014. **398**(1-2): p. 31-35.
7. Brehm, E., et al., Prenatal exposure to di (2-ethylhexyl) phthalate causes long-term transgenerational effects on female reproduction in mice. Endocrinology, 2018. **159**(2): p. 795-809.
8. Shi, M., et al., Prenatal exposure to bisphenol A, E, and S induces transgenerational effects on male reproductive functions in mice. Toxicological Sciences, 2019. **172**(2): p. 303-315.
9. Mitro, S.D., T. Johnson, and A.R. Zota, Cumulative chemical exposures during pregnancy and early development. Current environmental health reports, 2015. **2**(4): p. 367-378.
10. Kortenkamp, A. and M. Faust, Regulate to reduce chemical mixture risk. Science, 2018. **361**(6399): p. 224-226.
11. Cedergreen, N., Quantifying synergy: a systematic review of mixture toxicity studies within environmental toxicology. PloS one, 2014. **9**(5): p. e96580.
12. Kortenkamp, A., Low dose mixture effects of endocrine disrupters and their implications for regulatory thresholds in chemical risk assessment. Current opinion in pharmacology, 2014. **19**: p. 105-111.
13. Liang, J., et al., Prenatal exposure to bisphenols and risk of preterm birth: Findings from Guangxi Zhuang birth cohort in China. Ecotoxicology and Environmental Safety, 2021. **228**: p. 112960.
14. Liu, J., et al., Associations between prenatal multiple metal exposure and preterm birth: Comparison of four statistical models. Chemosphere, 2022. **289**: p. 133015.

15. Govarts, E., et al., Birth weight and prenatal exposure to polychlorinated biphenyls (PCBs) and dichlorodiphenyldichloroethylene (DDE): a meta-analysis within 12 European Birth Cohorts. Environmental health perspectives, 2012. **120**(2): p. 162-170.
16. van den Dries, M.A., et al., Prenatal exposure to nonpersistent chemical mixtures and fetal growth: A population-based study. Environmental health perspectives, 2021. **129**(11): p. 117008.
17. Hu, J.M., et al., Prenatal exposure to endocrine disrupting chemical mixtures and infant birth weight: A Bayesian analysis using kernel machine regression. Environmental Research, 2021. **195**: p. 110749.
18. Chiu, Y.-H., et al., Evaluating effects of prenatal exposure to phthalate mixtures on birth weight: a comparison of three statistical approaches. Environment international, 2018. **113**: p. 231-239.
19. Hernández-Martínez, C., et al., A longitudinal study on the effects of maternal smoking and secondhand smoke exposure during pregnancy on neonatal neurobehavior. Early Human Development, 2012. **88**(6): p. 403-408.
20. Guo, J., et al., Prenatal exposure to mixture of heavy metals, pesticides and phenols and IQ in children at 7 years of age: The SMBCS study. Environment international, 2020. **139**: p. 105692.
21. Oppenheimer, A.V., et al., Prenatal exposure to chemical mixtures and working memory among adolescents. Environmental Research, 2022. **205**: p. 112436.
22. Shah-Kulkarni, S., et al., Prenatal exposure to mixtures of heavy metals and neurodevelopment in infants at 6 months. Environmental research, 2020. **182**: p. 109122.

23. Fruh, V., et al., Prenatal exposure to a mixture of elements and neurobehavioral outcomes in mid-childhood: Results from Project Viva. Environmental Research, 2021. **201**: p. 111540.

24. Valeri, L., et al., The joint effect of prenatal exposure to metal mixtures on neurodevelopmental outcomes at 20–40 months of age: evidence from rural Bangladesh. Environmental health perspectives, 2017. **125**(6): p. 067015.

25. Doherty, B.T., et al., Periconceptional and prenatal exposure to metal mixtures in relation to behavioral development at 3 years of age. Environmental Epidemiology, 2020. **4**(4).

26. Zhou, C., L. Gao, and J.A. Flaws, Prenatal exposure to an environmentally relevant phthalate mixture disrupts reproduction in F1 female mice. Toxicology and applied pharmacology, 2017. **318**: p. 49-57.

27. Barakat, R., et al., Prenatal exposure to an environmentally relevant phthalate mixture disrupts testicular steroidogenesis in adult male mice. Environmental research, 2019. **172**: p. 194-201.

28. Kassotis, C.D., et al., Adverse reproductive and developmental health outcomes following prenatal exposure to a hydraulic fracturing chemical mixture in female C57Bl/6 mice. Endocrinology, 2016. **157**(9): p. 3469-3481.

29. Stanko, J.P., et al., Effects of prenatal exposure to a low dose atrazine metabolite mixture on pubertal timing and prostate development of male Long-Evans rats. Reproductive toxicology, 2010. **30**(4): p. 540-549.

30. Zhou, R., et al., Interactions between three typical endocrine-disrupting chemicals (EDCs) in binary mixtures exposure on myocardial differentiation of mouse embryonic stem cell. Chemosphere, 2017. **178**: p. 378-383.

31. Davidsen, N., et al., Exposure to human relevant mixtures of halogenated persistent organic pollutants (POPs) alters neurodevelopmental processes in human neural stem cells undergoing differentiation. Reproductive Toxicology, 2021. **100**: p. 17-34.

32. Christiansen, S., et al., Synergistic disruption of external male sex organ development by a mixture of four antiandrogens. Environmental health perspectives, 2009. **117**(12): p. 1839-1846.

33. Seiler, A.E. and H. Spielmann, The validated embryonic stem cell test to predict embryotoxicity *in vitro*. Nature protocols, 2011. **6**(7): p. 961-978.

34. Spielmann, H., et al., The embryonic stem cell test, an *in vitro* embryotoxicity test using two permanent mouse cell lines: 3T3 fibroblasts and embryonic stem cells. *In Vitro* Toxicology, 1997. **10**(1): p. 119-128.

35. Genschow, E., et al., The ECVAM international validation study on *in vitro* embryotoxicity tests: results of the definitive phase and evaluation of prediction models. Alternatives to laboratory animals, 2002. **30**(2): p. 151-176.

36. van Oostrom, C.T., W. Slob, and L.T. van der Ven, Defining embryonic developmental effects of chemical mixtures using the embryonic stem cell test. Food and Chemical Toxicology, 2020. **140**: p. 111284.

37. Yamane, J., et al., Prediction of developmental chemical toxicity based on gene networks of human embryonic stem cells. Nucleic acids research, 2016. **44**(12): p. 5515-5528.

38. Palmer, J.A., et al., Establishment and assessment of a new human embryonic stem cell-based biomarker assay for developmental toxicity screening. Birth Defects Research Part B: Developmental and Reproductive Toxicology, 2013. **98**(4): p. 343-363.

39. Jung, E.M., et al., Evaluation of developmental toxicity using undifferentiated human embryonic stem cells. Journal of Applied Toxicology, 2015. **35**(2): p. 205-218.

40. Ceccatelli, S., E. Daré, and M. Moors, Methylmercury-induced neurotoxicity and apoptosis. Chemico-biological interactions, 2010. **188**(2): p. 301-308.

41. Koos, B.J. and L.D. Longo, Mercury toxicity in the pregnant woman, fetus, and newborn infant: a review. American Journal of Obstetrics and Gynecology, 1976. **126**(3): p. 390-409.

42. Castoldi, A.F., et al., Neurodevelopmental toxicity of methylmercury: Laboratory animal data and their contribution to human risk assessment. Regulatory Toxicology and Pharmacology, 2008. **51**(2): p. 215-229.

43. Muckle, G., et al., Prenatal exposure of the northern Québec Inuit infants to environmental contaminants. Environmental health perspectives, 2001. **109**(12): p. 1291-1299.

44. Kuhnlein, H.V. and H.M. Chan, Environment and contaminants in traditional food systems of northern indigenous peoples. Annual review of nutrition, 2000. **20**: p. 595.

45. Van Oostdam, J., et al., Human health implications of environmental contaminants in Arctic Canada: a review. Science of the total environment, 2005. **351**: p. 165-246.

46. Donaldson, S., et al., Environmental contaminants and human health in the Canadian Arctic. Science of the Total Environment, 2010. **408**(22): p. 5165-5234.

47. Florian, M., et al., Interplay of Obesity, Ethanol, and Contaminant Mixture on Clinical Profiles of Cardiovascular and Metabolic Diseases: Evidence from an Animal Study. Cardiovascular Toxicology, 2022. **22**(6): p. 558-578.

48. Florian, M., et al., Northern contaminant mixtures induced morphological and functional changes in human coronary artery endothelial cells under culture conditions typifying high fat/sugar diet and ethanol exposure. Toxicology, 2013. **313**(2-3): p. 103-112.

49. Mailloux, R., et al., A Northern contaminant mixture impairs pancreas function in obese and lean JCR rats and inhibits insulin secretion in MIN6 cells. Toxicology, 2015. **334**: p. 81-93.

50. Mailloux, R.J., et al., Exposure to a northern contaminant mixture (NCM) alters hepatic energy and lipid metabolism exacerbating hepatic steatosis in obese JCR rats. PloS one, 2014. **9**(9): p. e106832.

51. Bowers, W.J., et al., Early developmental neurotoxicity of a PCB/organochlorine mixture in rodents after gestational and lactational exposure. Toxicological Sciences, 2004. **77**(1): p. 51-62.

52. Chu, I., et al., Toxicological effects of gestational and lactational exposure to a mixture of persistent organochlorines in rats: systemic effects. Toxicological Sciences, 2005. **88**(2): p. 645-655.

53. Beyrouty, P. and H.M. Chan, Co-consumption of selenium and vitamin E altered the reproductive and developmental toxicity of methylmercury in rats. Neurotoxicology and Teratology, 2006. **28**(1): p. 49-58.

54. Chu, I., et al., Toxicological effects of *in utero* and lactational exposure of rats to a mixture of environmental contaminants detected in Canadian Arctic human populations. Journal of Toxicology and Environmental Health, Part A, 2008. **71**(2): p. 93-108.

55. Pelletier, G., et al., Contribution of methylmercury, polychlorinated biphenyls and organochlorine pesticides to the toxicity of a contaminant mixture based on Canadian Arctic population blood profiles. Toxicology letters, 2009. **184**(3): p. 176-185.

56. Elabbas, L.E., et al., *In utero* and lactational exposure to a mixture of environmental contaminants detected in Canadian Arctic human populations alters retinoid levels in rat offspring with low margins of exposure. Journal of Toxicology and Environmental Health, Part A, 2014. **77**(5): p. 223-245.

57. Padhi, B., et al., Gene expression profiling in rat cerebellum following *in utero* and lactational exposure to mixtures of methylmercury, polychlorinated biphenyls and organochlorine pesticides. Toxicology letters, 2008. **176**(2): p. 93-103.

58. Mokra, K., Endocrine disruptor potential of short-and long-chain perfluoroalkyl substances (PFASs)—a synthesis of current knowledge with proposal of molecular mechanism. International Journal of Molecular Sciences, 2021. **22**(4): p. 2148.

59. Mora, A.M., et al., Prenatal exposure to perfluoroalkyl substances and adiposity in early and mid-childhood. Environmental health perspectives, 2017. **125**(3): p. 467-473.

60. Halldorsson, T.I., et al., Prenatal exposure to perfluorooctanoate and risk of overweight at 20 years of age: a prospective cohort study. Environmental health perspectives, 2012. **120**(5): p. 668-673.

61. Schjenken, J.E., et al., Endocrine disruptor compounds—a cause of impaired immune tolerance driving inflammatory disorders of pregnancy? Frontiers in endocrinology, 2021. **12**: p. 607539.

62. Senut, M.-C., et al., Lead exposure disrupts global DNA methylation in human embryonic stem cells and alters their neuronal differentiation. Toxicological Sciences, 2014. **139**(1): p. 142-161.

63. Furgal, C., et al., Exposure to food chain contaminants in Nunavik: Evaluating spatial and time trends among pregnant women & implementing effective health communication for healthy pregnancies and children (Year 2 of 3)

64. Zhou, F., et al., Lead, cadmium, arsenic, and mercury combined exposure disrupted synaptic homeostasis through activating the Snk-SPAR pathway. Ecotoxicology and environmental safety, 2018. **163**: p. 674-684.

65. Marabini, L., R. Calò, and S. Fucile, Genotoxic effects of polychlorinated biphenyls (PCB 153, 138, 101, 118) in a fish cell line (RTG-2). Toxicology *in Vitro*, 2011. **25**(5): p. 1045-1052.

66. Tang, L., et al., PCB 118-induced endothelial cell apoptosis is partially mediated by excessive ROS production. Toxicology Mechanisms and Methods, 2017. **27**(5): p. 394-399.

67. Shain, W., B. Bush, and R. Seegal, Neurotoxicity of polychlorinated biphenyls: structure-activity relationship of individual congeners. Toxicology and applied pharmacology, 1991. **111**(1): p. 33-42.

68. Zuluaga, M., et al., Metabolite profiling to monitor organochlorine pesticide exposure in HepG2 cell culture. Chromatographia, 2016. **79**(17): p. 1061-1068.

69. Tiemann, U., *In vivo* and *in vitro* effects of the organochlorine pesticides DDT, TCPM, methoxychlor, and lindane on the female reproductive tract of mammals: a review. Reproductive Toxicology, 2008. **25**(3): p. 316-326.

70. Sørli, J.B., et al., Per-and polyfluoroalkyl substances (PFASs) modify lung surfactant function and pro-inflammatory responses in human bronchial epithelial cells. Toxicology *in Vitro*, 2020. **62**: p. 104656.

71. Tachachartvanich, P., et al., *In Vitro* characterization of the endocrine disrupting effects of per-and poly-fluoroalkyl substances (PFASs) on the human androgen receptor. Journal of Hazardous Materials, 2022. **429**: p. 128243.

72. Fukami-Kobayashi, J. and Y. Mitsui, Cyclin D1 inhibits cell proliferation through binding to PCNA and cdk2. Experimental cell research, 1999. **246**(2): p. 338-347.

73. Pagano, M., et al., Cyclin D1-mediated inhibition of repair and replicative DNA synthesis in human fibroblasts. Genes & Development, 1994. **8**(14): p. 1627-1639.

74. Rodríguez Varela, M.S., et al., Regulation of cyclin E1 expression in human pluripotent stem cells and derived neural progeny. Cell Cycle, 2018. **17**(14): p. 1721-1744.

75. Dugina, V., et al., Divergent impact of actin isoforms on cell cycle regulation. Cell Cycle, 2018. **17**(23): p. 2610-2621.

76. Teo, A.K.K., et al., Pluripotency factors regulate definitive endoderm specification through eomesodermin. Genes & development, 2011. **25**(3): p. 238-250.

77. Probst, S. and S. Arnold, Eomesodermin—at dawn of cell fate decisions during early embryogenesis. Current topics in developmental biology, 2017. **122**: p. 93-115.

78. Weidgang, C.E., et al., TBX3 directs cell-fate decision toward mesendoderm. Stem cell reports, 2013. **1**(3): p. 248-265.

79. Esmailpour, T. and T. Huang, TBX3 promotes human embryonic stem cell proliferation and neuroepithelial differentiation in a differentiation stage-dependent manner. Stem cells, 2012. **30**(10): p. 2152-2163.

80. El-Khairi, R. and L. Vallier, The role of hepatocyte nuclear factor 1β in disease and development. Diabetes, Obesity and Metabolism, 2016. **18**: p. 23-32.

81. Lee, K., et al., FOXA2 is required for enhancer priming during pancreatic differentiation. Cell reports, 2019. **28**(2): p. 382-393. e7.

82. Munthe-Fog, L., et al., Immunodeficiency associated with FCN3 mutation and ficolin-3 deficiency. New England Journal of Medicine, 2009. **360**(25): p. 2637-2644.

83. De Smedt, J., et al., PU. 1 drives specification of pluripotent stem cell-derived endothelial cells to LSEC-like cells. Cell death & disease, 2021. **12**(1): p. 1-18.

84. Kim, D.-K., et al., Lefty1 and lefty2 control the balance between self-renewal and pluripotent differentiation of mouse embryonic stem cells. Stem cells and development, 2014. **23**(5): p. 457-466.

85. Bigsby, R., et al., Evaluating the effects of endocrine disruptors on endocrine function during development. Environmental health perspectives, 1999. **107**(suppl 4): p. 613-618.

86. Luo, Z.-C., et al., Birth outcomes in the Inuit-inhabited areas of Canada. CMAJ, 2010. **182**(3): p. 235-242.

87. Plusquellec, P., et al., The relation of low-level prenatal lead exposure to behavioral indicators of attention in Inuit infants in Arctic Quebec. Neurotoxicology and Teratology, 2007. **29**(5): p. 527-537.

88. Boucher, O., et al., Prenatal methylmercury, postnatal lead exposure, and evidence of attention deficit/hyperactivity disorder among Inuit children in Arctic Quebec. Environmental health perspectives, 2012. **120**(10): p. 1456-1461.

89. Plusquellec, P., et al., The relation of environmental contaminants exposure to behavioral indicators in Inuit preschoolers in Arctic Quebec. Neurotoxicology, 2010. **31**(1): p. 17-25.

3.7 Tables and Figures

Table 3.1. Nunavik Contaminant Mixture (NCM) components and their geometric mean (GM) concentrations detected in human maternal blood/plasma samples.

Compound group	Compound	1X (µg/L)	1X (nM)	Solvent
Metals	Lead	12.000	57.915	DMSO
	Mercury	4.200	20.937	DMSO
Polychlorinated Biphenyls (PCBs)	PCB99	0.043	0.132	DMSO
	PCB118	0.038	0.116	DMSO
	PCB138	0.110	0.305	DMSO
	PCB153	0.220	0.610	DMSO
	PCB170	0.029	0.073	DMSO
	PCB180	0.100	0.253	DMSO
	PCB183	0.015	0.038	DMSO
Organochlorines (OCs) and Pentachlorophenol (PCP)	β-HCH	0.016	0.055	DMSO
	cis-nonachlor	0.034	0.077	DMSO
	HCB	0.140	0.492	DMSO
	Mirex	0.021	0.038	DMSO
	Oxychlordane	0.120	0.283	DMSO
	PCP	0.160	0.601	DMSO
	p'p-DDE	0.730	2.296	DMSO
	trans-nonachlor	0.240	0.540	DMSO
	PFOA	0.600	1.449	H_2O

Perfluoroalkyl and Polyfluoroalkyl Substances (PFASs)	PFOS	3.300	6.599	H_2O
	PFHxS	0.260	0.650	H_2O
	PFDA	0.520	1.011	DMSO
	PFuDA	0.590	1.046	DMSO
	PFNA	2.400	5.171	DMSO
Sum(Σ)		25.886	100.687	

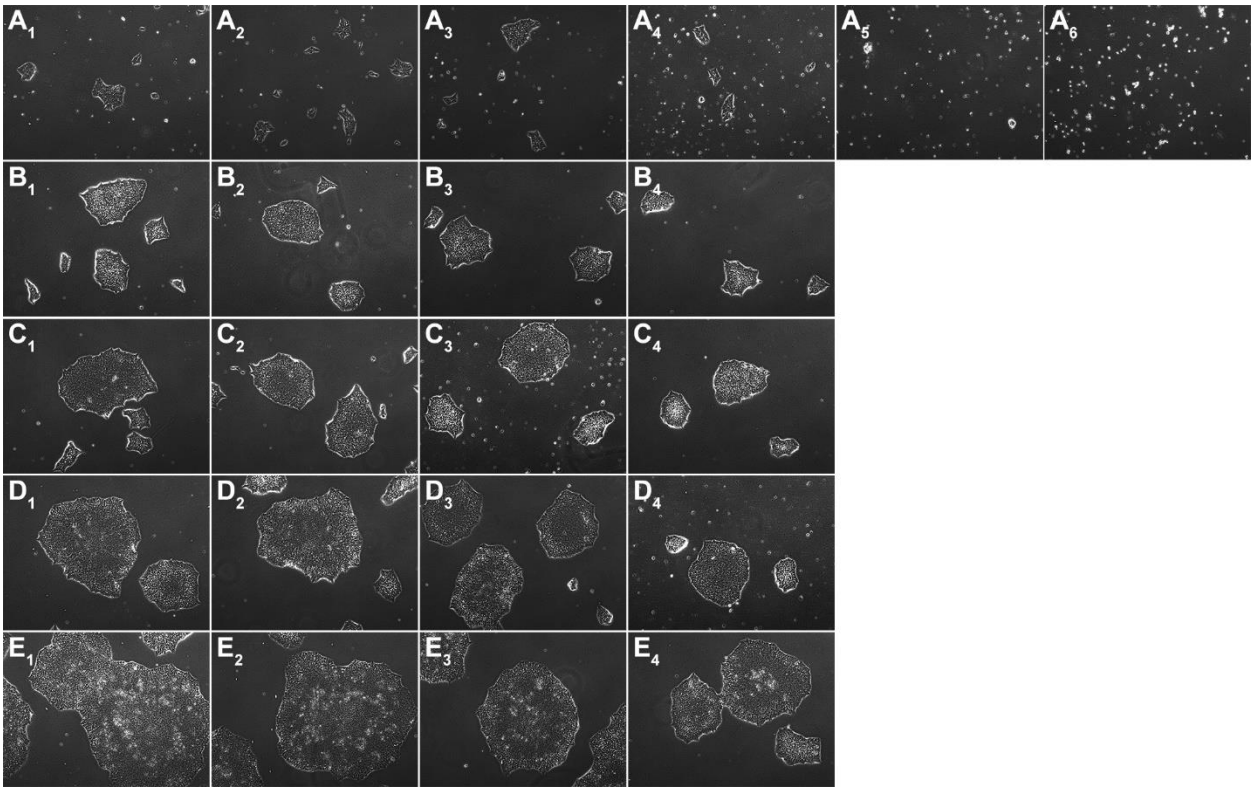

Figure 3.1. The effects of Nunavik Contaminant Mixture (NCM) exposure on the cell attachment, colony formation, and morphology of human embryonic stem cells (hESCs). Representative images showing cellular attachment and colony formation of hESCs after (A) 24 h, (B) 48 h, (C) 72 h, (D) 96 h, and (E) 120 h of [$(A\text{-}E)_1$] control, [$(A\text{-}E)_2$] 0.16X, [$(A\text{-}E)_3$] 0.8X, [$(A\text{-}E)_4$] 4X, (A_5) 20X, and (A_6) 100X NCM exposure. All images were taken under a 10X objective.

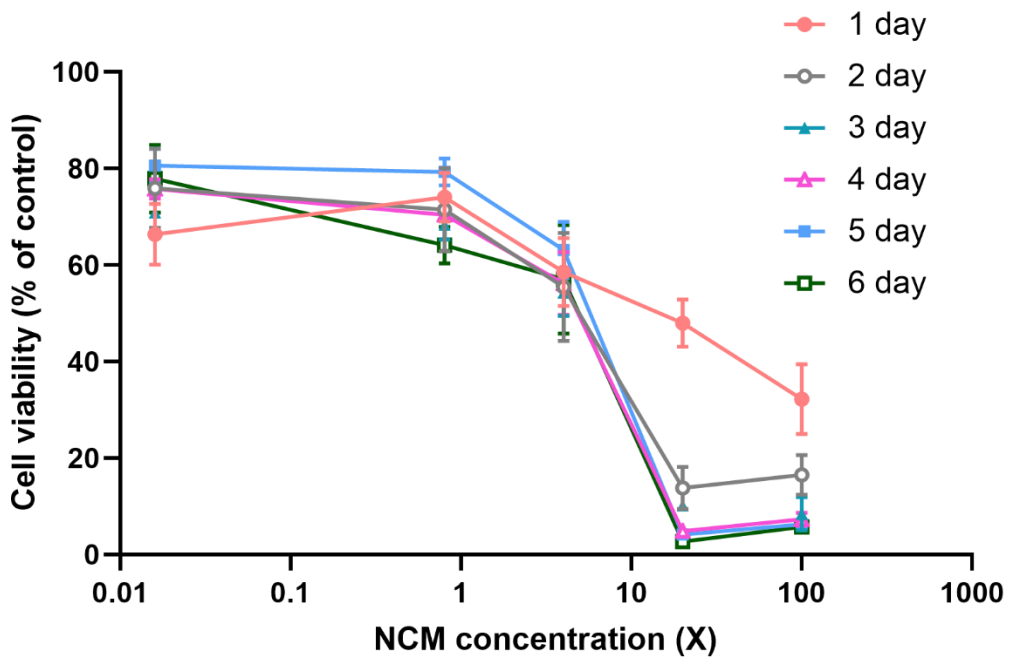

Figure 3.2. Cell viability (as percentage of control) of human embryonic stem cells (hESCs) exposed to Nunavik Contaminant Mixture (NCM) at 0.16X, 0.8X, 4X, 20X, and 100X, respectively, for 24 h to 6 d. One-way ANOVA and Dunnett's post hoc test were used at each time point to compare differences between treatment and control groups with $p<0.05$ being considered as significant. Data are presented as means ± SEMs with n=4 for each group.

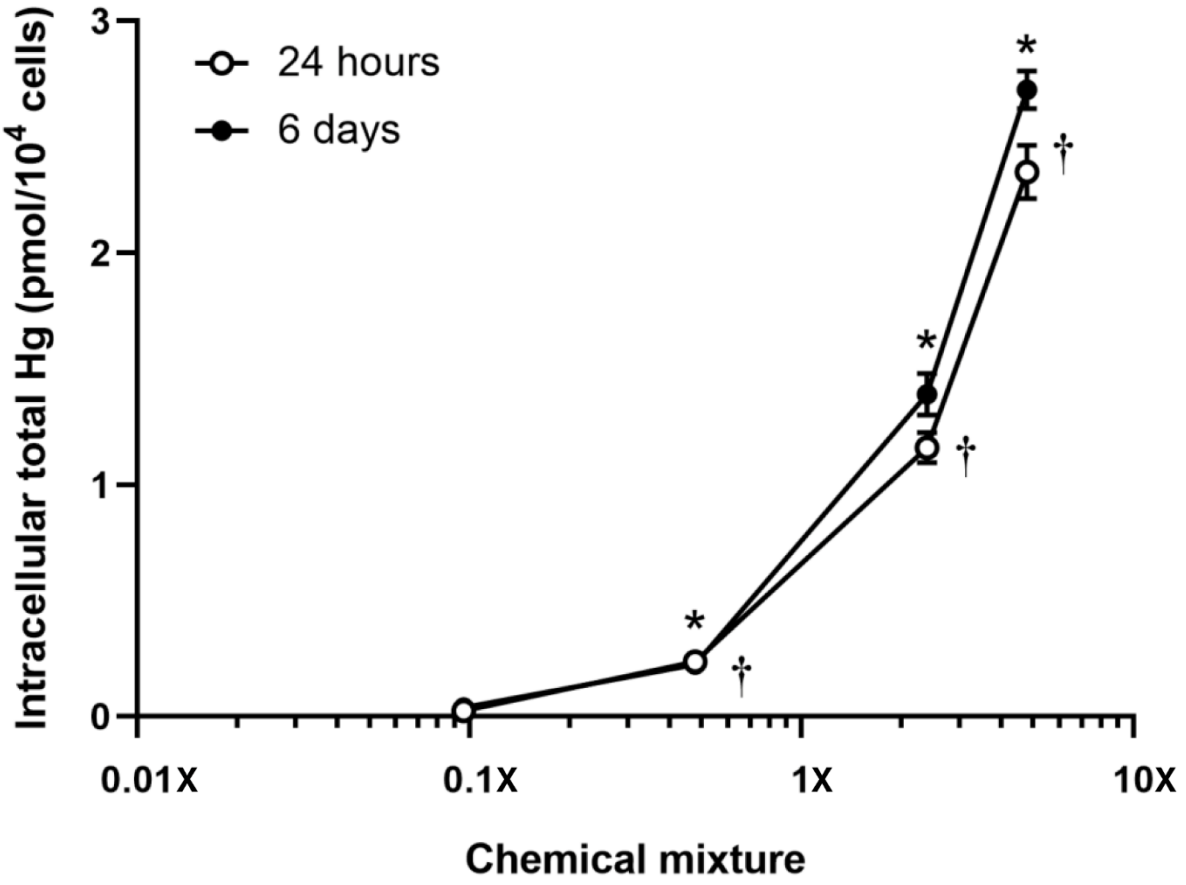

Figure 3.3. Intracellular total mercury content in human embryonic stem cells (hESCs) exposed to Nunavik Contaminant Mixture (NCM) at 0X, 0.096X, 0.478X, 2.388X and 4.776X, respectively, for 24 h and 6 d. One-way ANOVA and Dunnett's post hoc test were used at each time point to compare differences between treatment and control groups with $p<0.05$ being considered as significant. Data are presented as means ± SEMs with N=3 for each group. †, $p<0.05$ within 24 h. *, $p<0.05$ within 6 d.

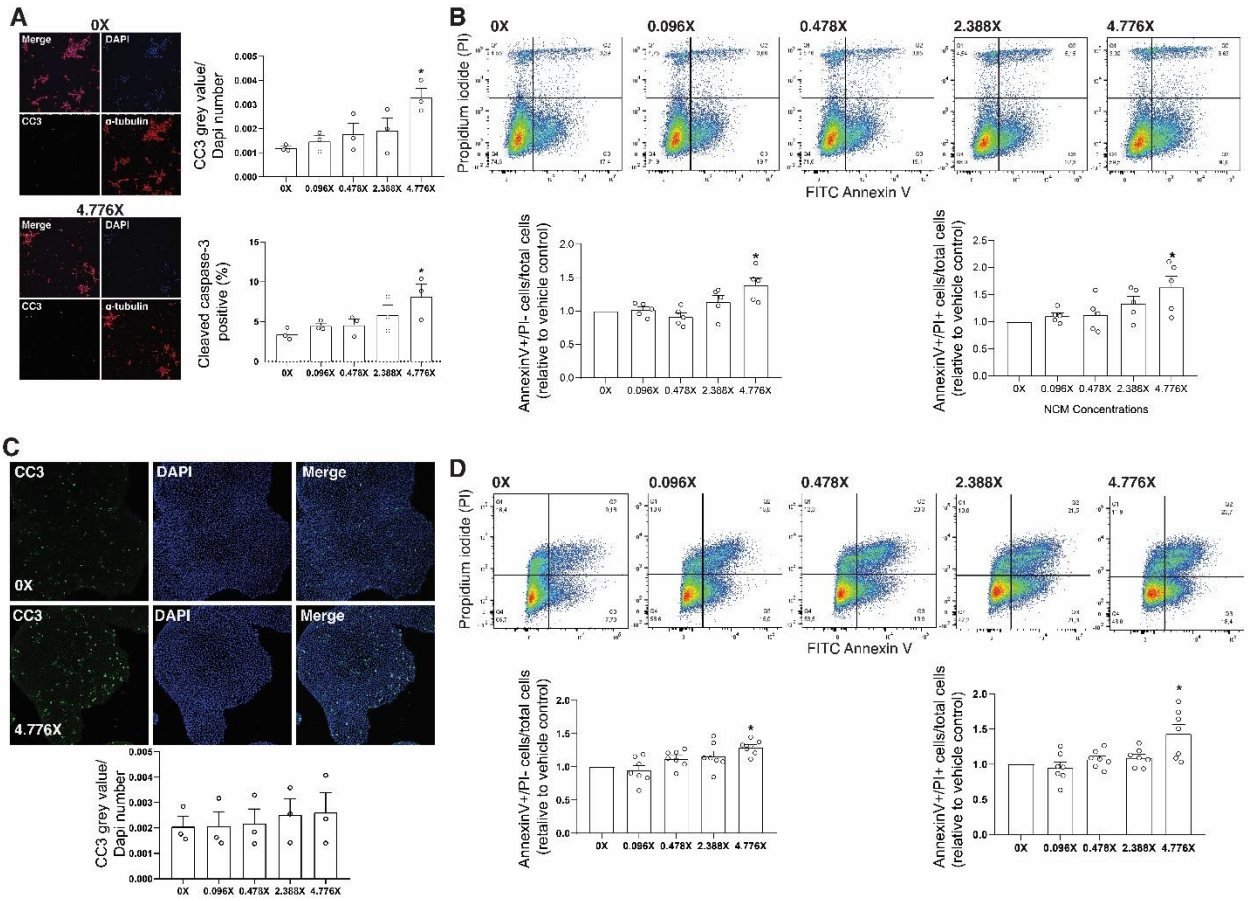

Figure 3.4. Measures of apoptosis in human embryonic stem cells (hESCs) exposed to Nunavik Contaminant Mixture (NCM) at 0X, 0.096X, 0.478X, 2.388X and 4.776X, respectively, for 24 h and 6 d. (A) Representative image of positive staining of cleaved caspase-3 (CC3) (green), nuclei (DAPI, blue) and α-tubulin (red) and quantification of CC3-positive cells (as either percentage of CC3 positive cells or CC3 positive grey value normalized to cell number measured by DAPI) in hESCs exposed to 5 doses of NCM for 24 h. (B) Flow cytometry analysis of cell population (percentage) positively stained for Annexin V-FITC and propidium iodide (PI) as measures of early apoptosis and necrosis after 24 h of NCM treatment, respectively. (C) Representative image of positive staining of CC3 (green) and nuclei (DAPI, blue) following 6 d of NCM exposure and quantification of CC3 grey value normalized to cell number measured by DAPI.

(D) Flow cytometry analysis of cell population (percentage) positively stained for Annexin V-FITC and PI as measures of early apoptosis and necrosis after 6 d of NCM treatment, respectively. Data are presented as means ± SEMs with N=3 for immunostaining and N=5 for flow cytometry at 24 h, and N=3 for immunostaining and N=7 for flow cytometry at 6 d. One-way ANOVA and Dunnett's post hoc test were used at each time point to compare differences between treatment and control groups with $p<0.05$ being considered as significant.

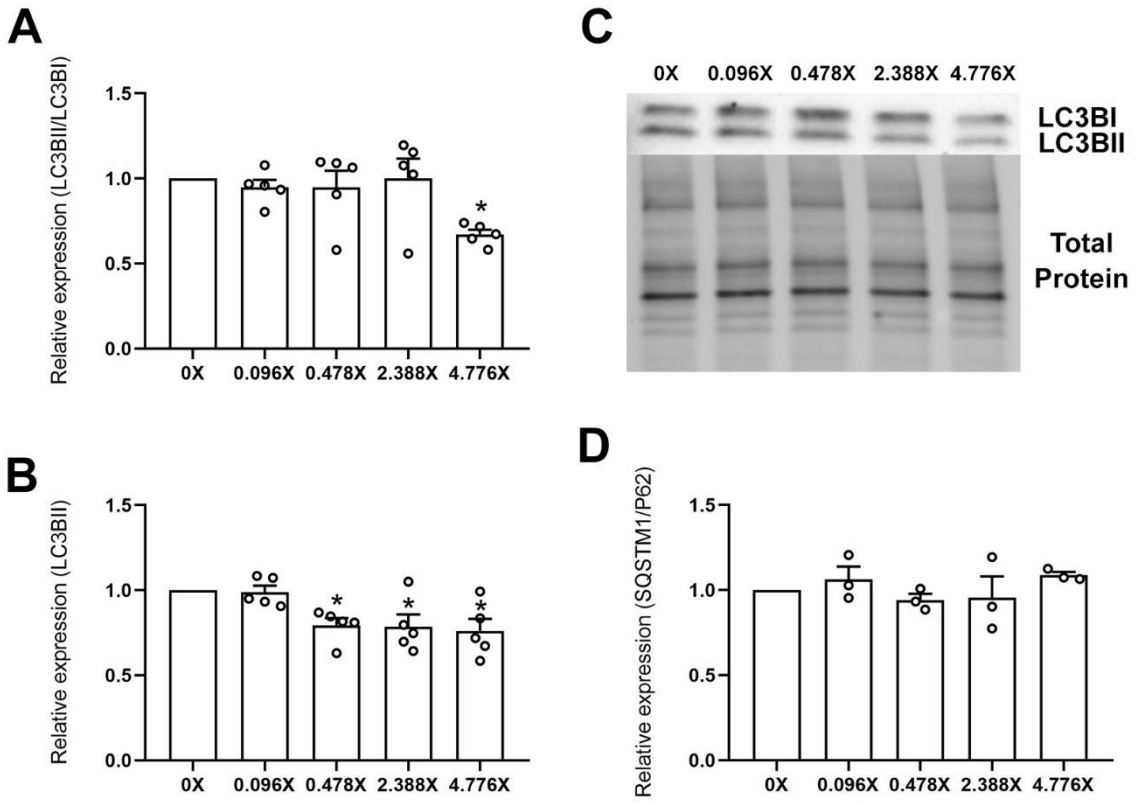

Figure 3.5. Protein expressions of LC3B (LC3BI and LC3BII) and SQSTM1 (p62) were measured in human embryonic stem cells (hESCs) at 0X, 0.096X, 0.478X, 2.388X and 4.776X, respectively, after 6 d of exposure to Nunavik Contaminant Mixture (NCM). Data are presented as means ± SEMs with N=5 for LC3B and N=3 for SQSTM1 (p62). For LC3B, the ratio of LC3BII/LC3BI was calculated first before comparison. Each batch was first normalized to its vehicle control (0X) before comparison. One-way ANOVA and Dunnett's post hoc test were used at each time point to compare differences between treatment and control groups with $p<0.05$ being considered as significant.

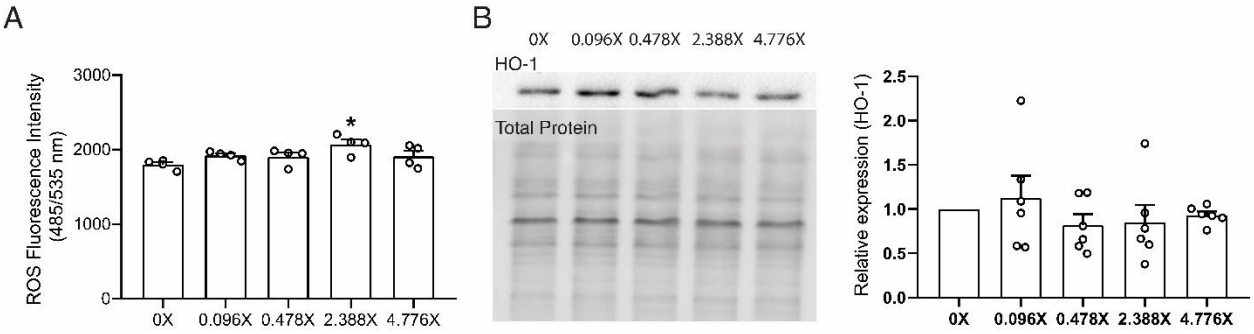

Figure 3.6. Presence of (A) reactive oxygen species (ROS) and (B) protein expression of HO-1 in human embryonic stem cells (hESCs) exposed to Nunavik Contaminant Mixture (NCM) at 0X, 0.096X, 0.478X, 2.388X and 4.776X, respectively, for 24 h and 6 d, respectively. Data are presented as means ± SEMs with N=4 for ROS fluorescence intensity and N=6 for HO-1 Western blots. For Western blots, each batch was first normalized to its vehicle control (0X) before comparison. One-way ANOVA and Dunnett's post hoc test were used at each time point to compare differences between treatment and control groups with $p<0.05$ being considered as significant.

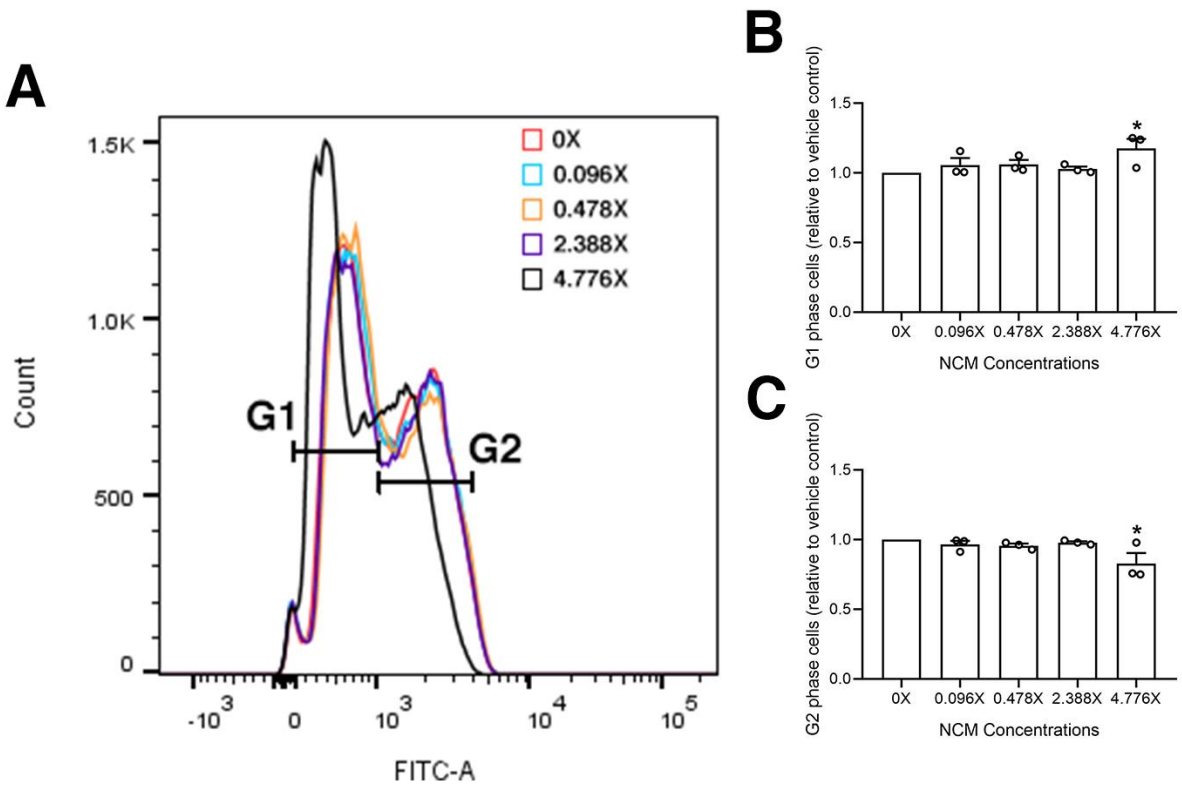

Figure 3.7. Analysis of the cell cycle of human embryonic stem cells (hESCs) at 0X, 0.096X, 0.478X, 2.388X and 4.776X, respectively after 6 d of exposure to Nunavik Contaminant Mixture (NCM). (A) Flow cytometry analysis of cell cycle phases, with a histogram showing the peak for FITC-staining of DNA content as identifications of cell phases and (B-C) bar graphs showing the percentage of cells in different cell cycle phases of hESCs after 6 d of exposure to NCM. Each batch was first normalized to its vehicle control (0X) before comparison. One-way ANOVA and Dunnett's post hoc test were used at each time point to compare differences between treatment and control groups with $p<0.05$ being considered as significant.

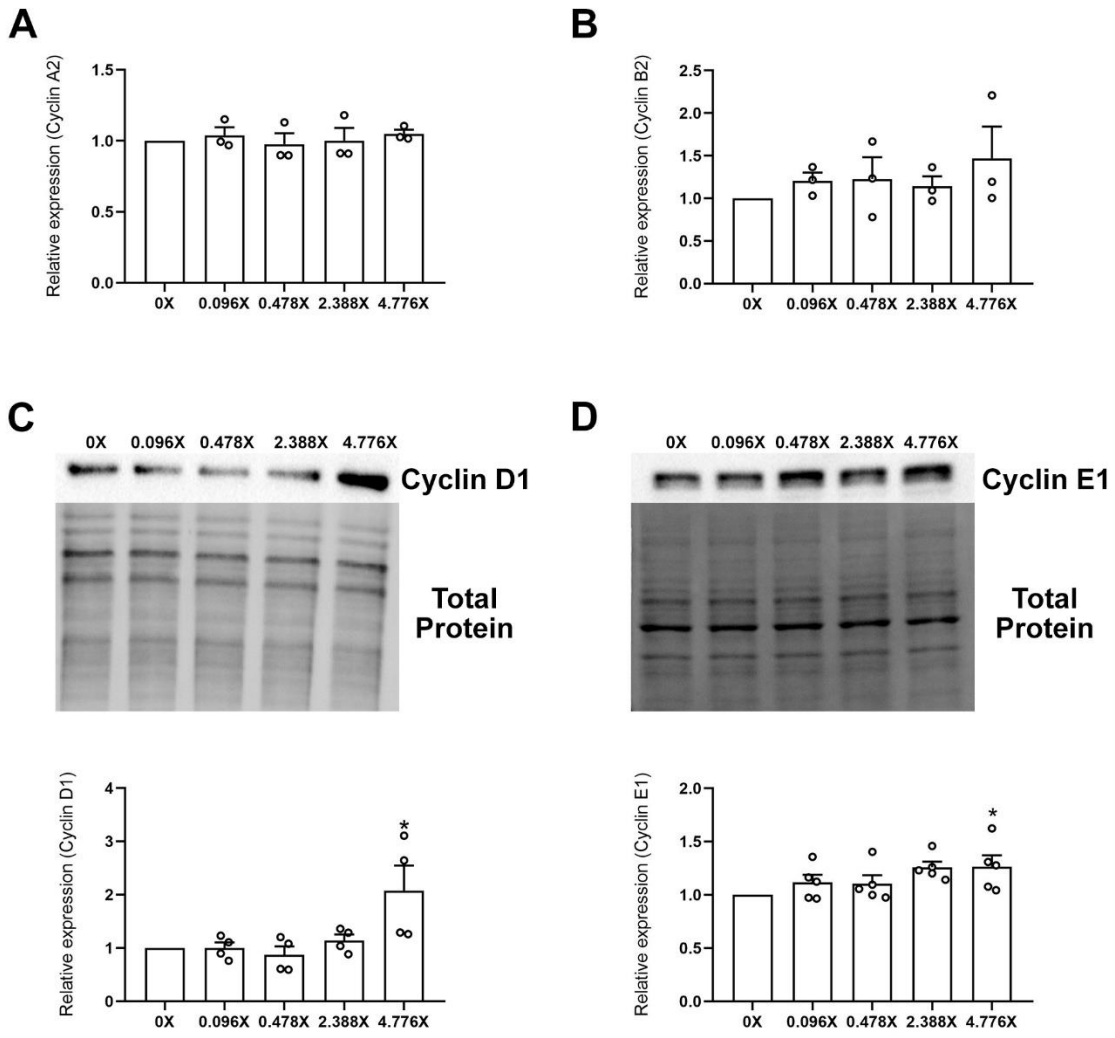

Figure 3.8. Protein expression of cyclin A2, B2, D1, and E1 measured in human embryonic stem cells (hESCs) at 0X, 0.096X, 0.478X, 2.388X and 4.776X, respectively, after 6 d of exposure to Nunavik Contaminant Mixture (NCM). Data are presented as means ± SEMs with N=3 for cyclin A2 and B2, N=4 for cyclin D1, and N=5 for cyclin E1. For Western blots, each batch was first normalized to its vehicle control (0X) before comparison. One-way ANOVA and Dunnett's post hoc test were used at each time point to compare differences between treatment and control groups with $p<0.05$ being considered as significant.

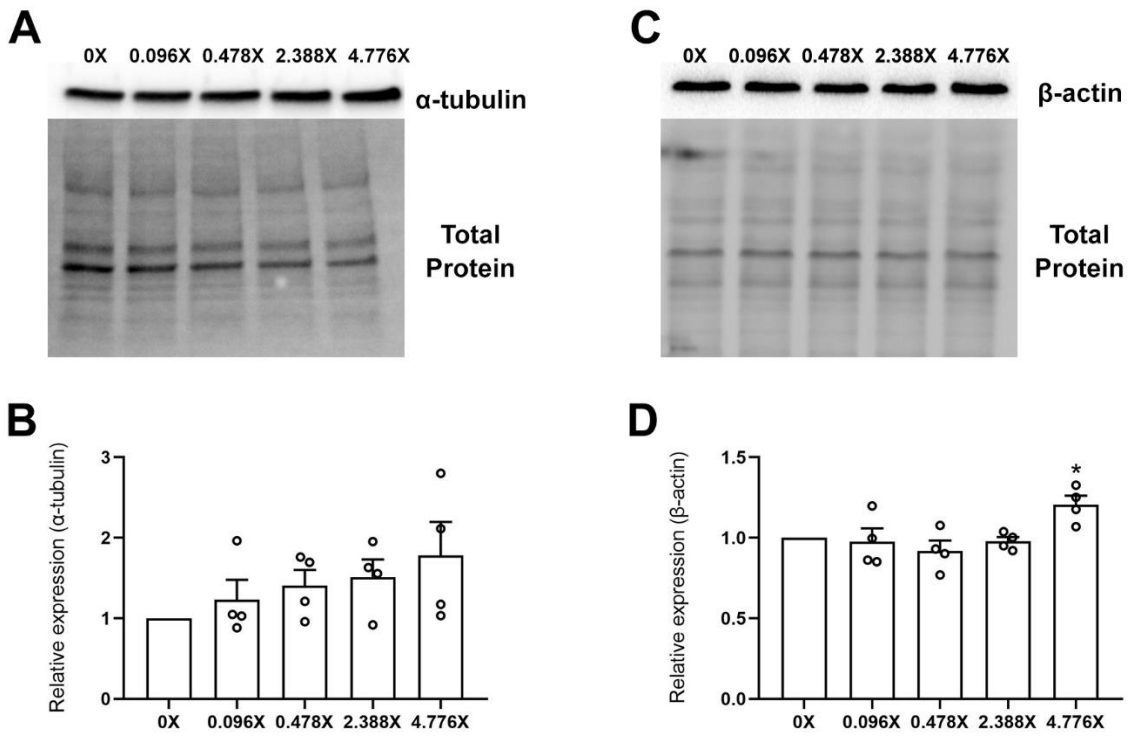

Figure 3.9. Expressions of (A-B) α-tubulin and (C-D) β-actin proteins in human embryonic stem cells (hESCs) exposed to Nunavik Contaminant Mixture (NCM) at 0X, 0.096X, 0.478X, 2.388X and 4.776X, respectively, for 6 d. Data are presented as means ± SEMs with N= for α-tubulin and β-actin. Each batch was first normalized to control (0X) before comparison. One-way ANOVA and Dunnett's post hoc test were used at each time point to compare differences between treatment and control groups with $p<0.05$ being considered as significant.

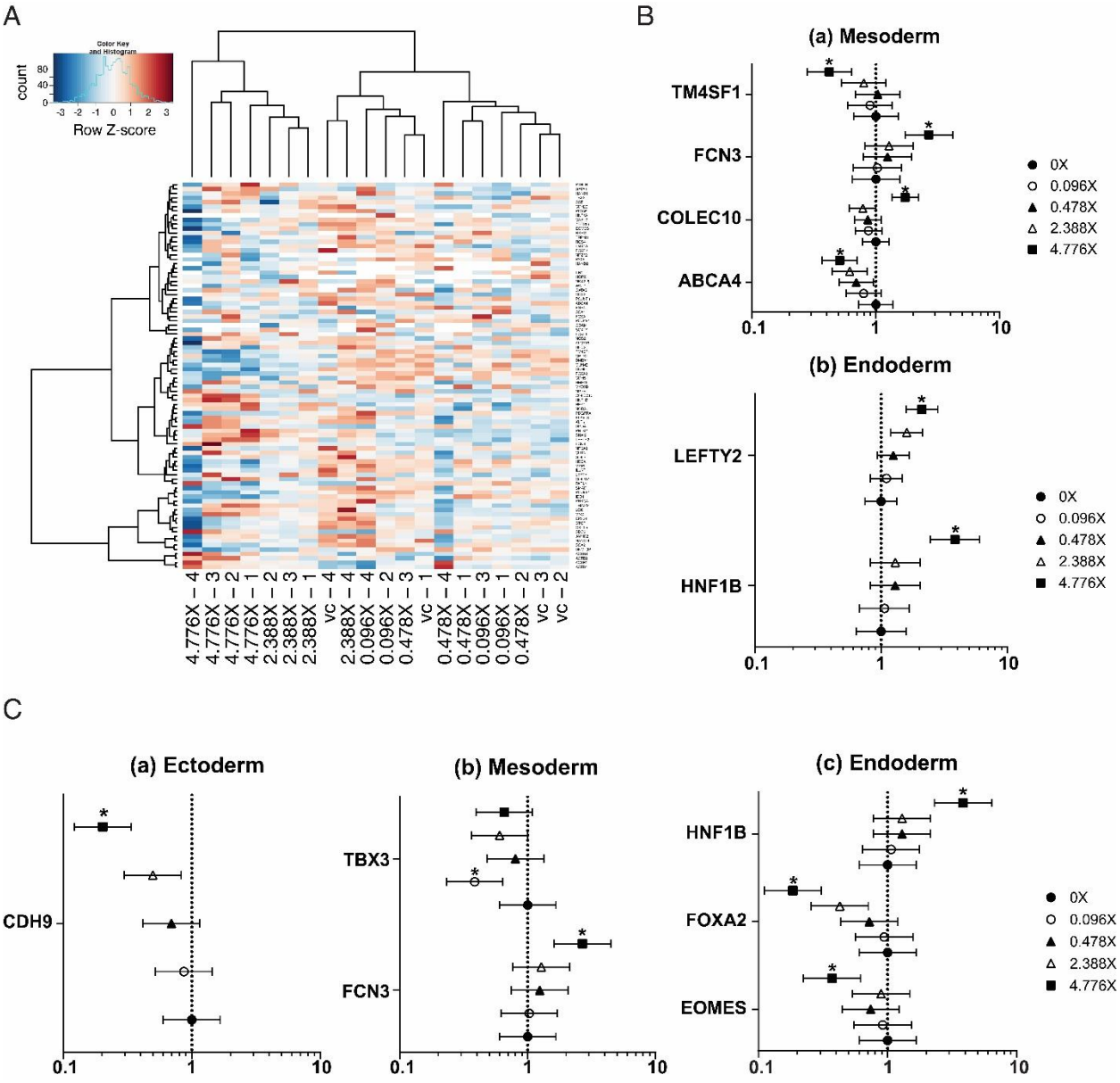

Figure 3.10. Hierarchical cluster analysis and fold change estimates of cell lineage marker gene expression in human embryonic stem cells (hESCs) exposed to Nunavik Contaminant Mixture (NCM) at 0X, 0.096X, 0.478X, 2.388X and 4.776X, respectively, for 6 d. (A) Heatmap of cell lineage marker gene expression in the various treatment groups. Rows represent genes, and columns represent samples. Red and blue blocks represent high and low expression relative to the reference gene respectively, whereas white blocks indicate equal expression. (B-C) The

expression of genes with significant difference between the NCM-treatment groups and the control group, with (C) or without (B) taking into account potential interactions within lineage genes. Fold change was estimated using the function of $2^{(-\text{least square mean for MeHg dose group})/2(-\text{least square mean for control})}$. Data are presented as mean fold change ± 95% CI with N=4 for each group. The dashed line in each panel represents the line of no fold change. Asterisks (*) represent significance compared to the control.

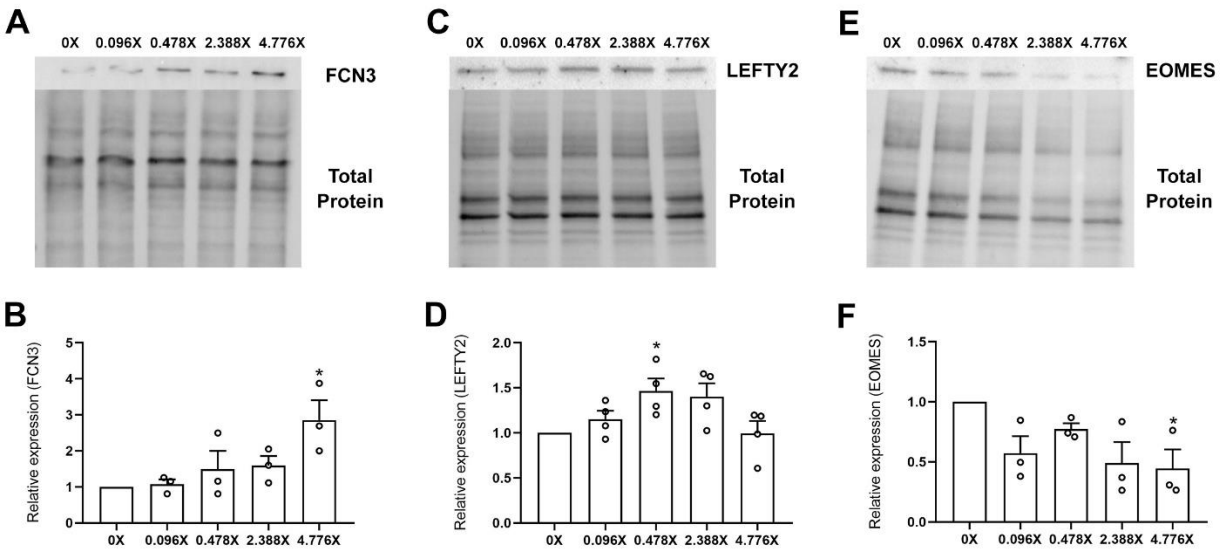

Figure 3.11. Expressions of selected cell lineage marker proteins, (A-B) FCN3, (C-D) LEFTY2, and (E-F) EOMES, as measured using Western blots, in human embryonic stem cells (hESCs) exposed) to northern contaminant mixture (NCM) at 0X, 0.096X, 0.478X, 2.388X and 4.776X, respectively, for 6 d. Data are presented as means ± SEMs with N=3 for FCN3 and EOMES, and N=4 for LEFTY2. Each batch was first normalized to its vehicle control (0X) before comparison. One-way ANOVA and Dunnett's post hoc test were used at each dose point to compare differences between treatment and control groups with $p<0.05$ being considered as significant

3.8 Supplemental Tables and Figures

Table S3.1. Antibody information used for Western blot.

Marker	Catalog No.	Company
LC3B	PA5-32254	Thermo Fisher Scientific
SQSTM1/p62	ab56416	Abcam
HO-1	ab13248	Abcam
Cyclin A2	ab181591	Abcam
Cyclin B2	Ab18250	Abcam
Cyclin D1	ab134175	Abcam
Cyclin E1	ab133266	Abcam
α-tubulin	ab4074	Abcam
β-actin	ab8227	Abcam
FCN3	SAB1402990	Sigma-aldrich
LEFTY2	PA5-21367	Thermo Fisher Scientific
EOMES	ab216870	Abcam
COLEC10	LS-C293446	Life Span Biosciences
HNF1B	ab128912	Abcam
TM4SF1	PA5-21119	Thermo Fisher Scientific
FOXA2	ab108422	Abcam
TBX3	ab154828	Abcam
TRIM56	ab154821	Abcam
ABCA4	LS-C354507	Life Span Biosciences

CDH9	ab124803	Abcam
Goat anti-Rabbit secondary antibody, HRP	G-21234	Thermo Fisher Scientific
Goat anti-Mouse secondary antibody, HRP	ab97023	Abcam

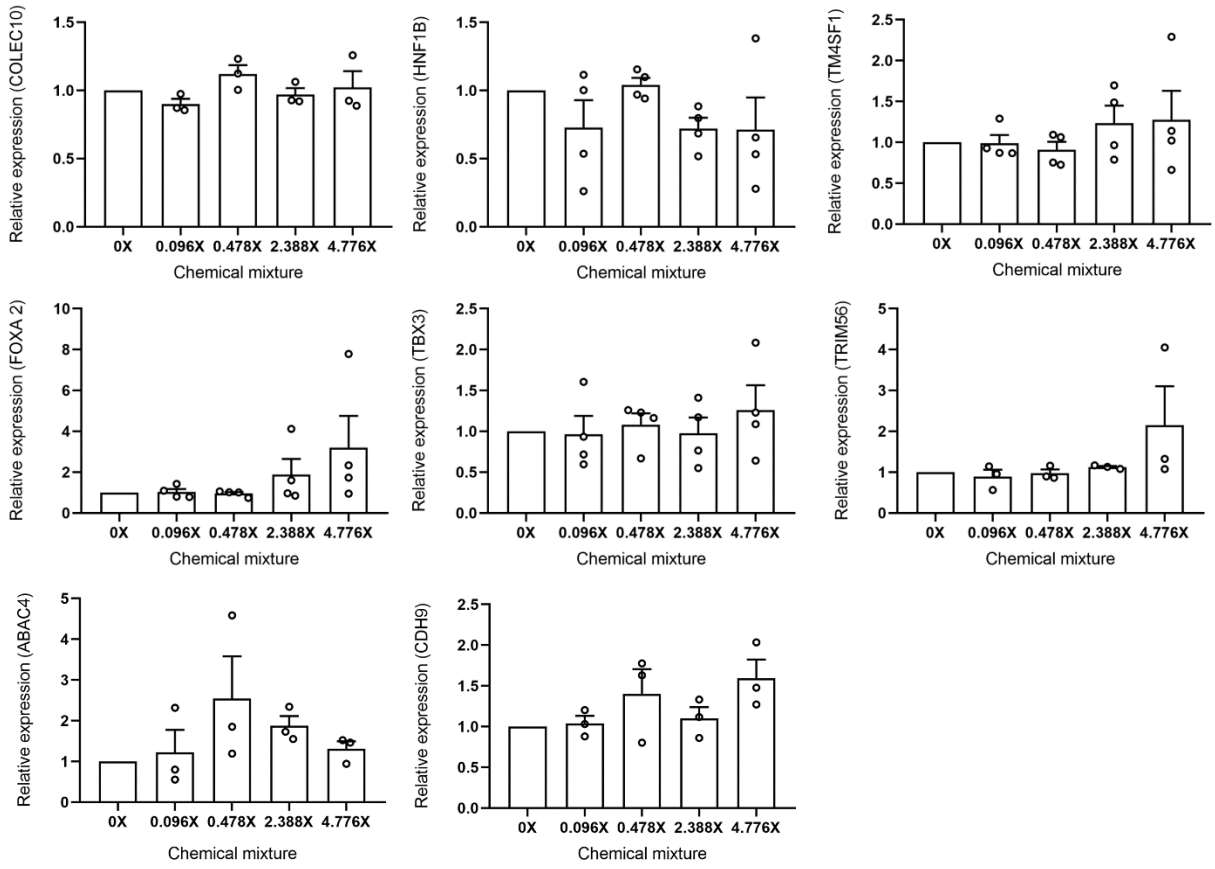

Figure S3.1. Expression of selected cell lineage marker proteins using Western blot that were not significant as measured by one-way ANOVAs.

Chapter 4: Effects of low doses of methylmercury (MeHg) exposure on definitive endoderm cell differentiation in human embryonic stem cells

Bai Li[1], Xiaolei Jin[2*], and Hing Man Chan[1*]

[1]Department of Biology, University of Ottawa, Ottawa, Ontario, Canada

[2]Regulatory Toxicology Research Division, Bureau of Chemical Safety, Food Directorate, HPFB, Health Canada, Ottawa, Ontario, Canada

Abstract

Fetal development is one of the most sensitive windows to methylmercury (MeHg) toxicity. Laboratory and epidemiological studies have shown a dose-response relationship between fetal MeHg exposure and neuro performance in different life stages from infants to adults. In addition, MeHg exposure has been reported to be associated with disorders in endoderm-derived organs, such as morphological changes in liver cells and pancreatic cell dysfunctions. However, the mechanisms of the effects of MeHg on non-neuronal organs or systems, especially during the early development of endoderm-derived organs, remain unclear. Here we determined the effects of low concentrations of MeHg exposure during the differentiation of definitive endoderm (DE) cells from human embryonic stem cells (hESCs). hESCs were exposed to MeHg (0, 10, 100 and 200 nM) that covers the range of Hg concentrations typically found in human maternal blood during DE cell induction. Transcriptomic analysis showed that sublethal doses of MeHg exposure could alter global gene expression patterns during hESC to DE cell differentiation, leading to increased expression of endodermal genes/proteins, which would likely promote endodermal fate. This effect of MeHg seemed to have occurred partly through disrupting calcium homeostasis and generating ROS. Bioinformatic analysis results suggested that MeHg exerts its developmental toxicity mainly by disrupting ribosome biogenesis during early cell lineage differentiation. This disruption, if *in vivo*, could lead to aberrant growth or dysfunctions of the developing endoderm-derived organs, and it may be the underlying mechanism for the observed congenital diseases later in life. Based on the results, we proposed an adverse outcome pathway for the effects of MeHg exposure during human embryonic stem cell to definitive endoderm differentiation.

4.1 Introduction

Mercury (Hg) is a well-recognized environmental contaminant that is of global concern [1]. In the environment, Hg (Hg^0) occurs in its elemental form, as inorganic salts (Hg^+ or Hg^{2+}), and as organic compounds such as methylmercury (MeHg) [2]. Anthropogenic effects have increased Hg emission dramatically into the environment [3], which is further converted to MeHg through anaerobic microorganisms, typically sulphur-reducing bacteria, in aquatic environments [2, 4]. Methylmercury can then bioaccumulate along the aquatic food chains into top marine/freshwater predators, making communities or populations that rely heavily on fish consumption in their diets susceptible to MeHg exposure [1, 5]. Also, rice which grows in moist, anaerobic soil that is ideal for microbial methylation of mercury, can also accumulate MeHg, and affect the rice-consuming populations [6].

The main target site for MeHg is the central nervous system, with clinical findings showing MeHg-induced neurobehavioral and cognitive function impairments in the victims of the Japanese and Iraqi MeHg poisoning events [7-10]. Animal studies under well-controlled laboratory conditions have also confirmed the neurotoxic effects of MeHg, with the developing central nervous systems being especially susceptible, causing more severe effects in prenatal exposure compared to exposure in later life stages [11]. This is in part attributed to MeHg-induced negative effects on neuronal migration and differentiation [12-14], and also MeHg-induced cell death due to distortion of intracellular calcium and glutamate homeostasis, oxidative stress generation, as well as mitochondrial dysfunction [15, 16].

In addition to the well-characterized neurotoxic effects of MeHg, MeHg exposure can also lead to adverse effects in tissues other than the brain. In victims of the MeHg poisoning event in Japan, erosive inflammation of the digestive tract, fatty degeneration of the liver and

kidney, and disturbance of pancreatic islet cells were all observed in addition to neuronal disturbances [8, 17, 18]. Furthermore, hepatic disorder was also identified as a cause of death for MeHg poisoning victims, with comparable levels of MeHg accumulation in the liver compared to the brain [8]. Multiple cohort studies have shown a positive correlation between mercury exposure levels and elevated insulin levels accompanied by decreased pancreatic β-cell function [19, 20]. Animal studies have also corroborated epidemiology findings, showing that MeHg accumulated within the liver to comparable levels of the brain [21, 22], resulting in imbalanced redox, hepatic glycogen accumulation, disruption of energy metabolism pathways, as well as alteration of global gene expression profiles within the liver [23-26]. Apoptosis and dysfunction in pancreatic β-cells through oxidative stress were also observed [27-29]. *In vitro* studies on non-brain derived cell lines exposed to MeHg, though limited, have shown that MeHg-induced oxidative stress resulted in apoptosis in liver derived HepG2 cells [30] and altered cell morphology in human induced pluripotent stem cell derived hepatocytes [31]. Despite these observations, the mechanism of the effects of MeHg exposure on non-brain related organs are still poorly understood compared to the effects of MeHg on the brain, and studies examining the developmental effects of MeHg exposure on non-brain related organs is still lacking.

In recent years, there is a growing trend of reducing the use of animals for testing of hazardous compounds, and *in vitro* toxicity testing that relies on cultured cells has emerged as an alternative tool for toxicity assessment. Among these, embryonic stem cells, and especially human embryonic stem cells (hESCs), which have the potential to differentiate into all fetal cell lineages represent an attractive cellular system for *in vitro* studies in developmental toxicology [32], and has been utilized to examine the embryotoxicity of MeHg [33-35]. As the effects of MeHg on neuronal differentiation has been extensively studied [36-41], our objective is to

examine the developmental toxicity of MeHg on other non-neural derived organs using hESCs as a model. Since the potentially affected organs such as liver, pancreas and the digestive tract [8, 17, 18] are endoderm derived, and the endoderm is the first germ layer to develop out of the three germ layers [42], we hypothesized that MeHg exposure affects the early differentiation of the endoderm in the hESCs. Using a transcriptomics approach, we aim to not only characterize the effects of MeHg during definitive endoderm formation but also explore the potential cellular mechanisms that lead to developmental toxicity due to MeHg exposure. We hypothesized that MeHg could disrupt the differentiation of endoderm formation in human stem cells by distortion of intracellular calcium and glutamate homeostasis, oxidative stress generation, as well as mitochondrial dysfunction.

4.2 Materials and Methods

4.2.1 Ethics Review and Approval

This project was reviewed and approved by the Health Canada and Public Health Agency of Canada's Research Ethics Board (File No. REB 2016-027H) and by the Office of Research Ethics and Integrity of the University of Ottawa (File No. H-05-19-4084).

4.2.2 Cell Maintenance and Induction

Human embryonic stem cells (H9; passage 30; WiCell Research Institute) were maintained according to the protocols established in our previous study [35]. Briefly, hESCs were maintained and expanded in six-well plates, which were precoated with Matrigel (Catalog no. 354 230; BD Biosciences). Cells were cultured under 37°C, 4% oxygen (O_2) and 10% carbon dioxide (CO_2) in a tri-gas incubator (Thermo Fisher Scientific) and fresh Essential 8 Flex

Medium (Catalog no. A2858501; Thermo Fisher Scientific) was changed daily. On the first day of seeding, 10 μM Rho-associated kinase inhibitor (Catalog no. 72304; StemCell Technologies) was added to the medium to enhance the survival of the cells. Cells were gently detached with Gibco StemPro Accutase cell dissociation reagent (Catalog no. A1110501; Thermo Fisher Scientific) and seeded onto new plates for subsequent experiments when the confluency reached around 85%. Only hESCs under passage 40 (within 10 passages from purchase) were used to avoid any serious genetic instability associated with prolonged passaging.

The hESCs were seeded in 6-well plates at a density of 2×10^4 cells/mL with the growth medium (Essential 8 Flex Medium) and incubated at 37°C, 4% oxygen (O_2) and 10% carbon dioxide (CO_2) with daily medium change. When the cell confluency reached around 20%~30%, the growth medium was replaced with the definitive endoderm induction medium A from Gibco™ PSC Definitive Endoderm Induction Kit (A3062601, Thermo Fisher Scientific). 24 h later, the culture medium was disposed of, and the definitive endoderm induction medium B was used for another 24 h of incubation. The hESC-derived DE cells were verified by immunostaining for both self-renewal (OCT4) and endodermal protein markers (SOX17 and CXCR4) (Figure S4.1). In brief, the cells were washed twice with phosphate-buffered saline (PBS) after disposing the induction medium B and fixing with 4% paraformaldehyde (Santa Cruz Biotechnology). The cells were then blocked and permeabilized with 5% bovine serum albumin (BSA) diluted in PBS containing 0.3% Triton X-100 (Sigma-Aldrich). The cells were respectively incubated with rabbit anti-human OCT4 antibody (Catalog no. C30A3; Cell Signaling Technology), goat anti-human SOX17 antibody (Catalog no. AF1924; R&D systems) and rabbit anti-human CXCR4 antibody (Catalog no. ab124824; Abcam) diluted at 1:200 in 5% BSA, and incubated overnight at 4°C. The cells were then gently washed with PBS for three

times and respectively incubated with Alexa Fluor 488 goat anti-rabbit IgG (Catalog no. A11008; Thermo Fisher Scientific), and Alexa Fluor 594 donkey anti-goat IgG (Catalog no. A11058; Thermo Fisher Scientific) diluted at 1:500 in 5% BSA at 4°C, overnight. Prolong Gold antifade reagent containing 4',6-diamidino-2-phenylindole (DAPI; Catalog no. S36939; Thermo Fisher Scientific) was added and the immunofluorescent images were taken with a Nikon A1RsiMP confocal microscope (Nikon Instruments Inc.) with Nikon's Imaging Software NIS-Elements.

4.2.3 Chemical Preparation and Exposure

MeHg chloride (purity: 99.9%) was obtained from Sigma-Aldrich and dissolved in dimethyl sulfoxide (DMSO, Sigma) to obtain 1000 × stock solutions (i.e., 0.001, 0.01, 0.1, 0.2, 0.3, 0.4, 0.5, 1, 5 and 10 mM). hESCs were seeded in 6-well plates and allowed for growth until they reached a confluency of around 20%~30%. The cells were then exposed to 0 (DMSO as vehicle control), 0.001, 0.01, 0.1, 0.2, 0.3, 0.4, 0.5, 1, 5 or 10 μM MeHg by 1000 × dilution of the stock solutions in induction medium for the initial cell viability assay. The experimental doses were narrowed down according to the results of cell viability and the cells were treated with 0 (DMSO as vehicle control), 10, 100 or 200 nM MeHg by 1000 × dilution of the stock solutions in induction medium for the rest of assays. The cells were repeatedly dosed each day throughout the induction process.

4.2.4 Cell Viability and Morphology

Cell viability was determined by a Cell Counting Kit 8 (WST-8 / CCK8) (Catalog no. ab228554, Abcam Inc.) according to the manufacturer's instructions. In brief, hESCs were seeded, induced, and exposed to MeHg as described above. At the end of induction and

exposure, 200 µL of WST-8 solution was added into each well of on the 6-well culture plate followed by 10 s of shaking and incubation at 37°C for 1.5 h in the dark. The absorbance at 460 nm wavelength was read on a BioTek Cytation 3 Cell Imaging Multi-Mode Reader (Fisher Scientific). The effects of 0, 10, 100 and 200 nM MeHg on cell viability was also checked by cell counting. Briefly, hESCs were seeded, induced, and exposed to MeHg as described above. At the end of induction and exposure, the medium was disposed, cells were gently lifted by StemPro Accutase cell dissociation reagent after rinsing by PBS. Then the cells were centrifuged and resuspended in 1 ml of PBS and gently pipetted to generate a single cell suspension. 10 µL of the cell suspension was taken for cell counting and the cell numbers were counted with a Countess Automated Cell Counter (Invitrogen, Thermo Fisher Scientific) after 1:1 dilution of cell suspension in Trypan blue solution (Catalog no. T10282; ThermoFisher Scientific).

For morphology observations, hESCs were seeded, induced to DE, and treated with MeHg as described above. The cell morphology was observed and imaged at each time point (before induction, during induction and after induction) with a 10× objective on a Zeiss Axiovert 40 CFL inverted microscope (Carl Zeiss Microscopy LLC) with a SPOT RT3 digital camera and SPOT basic software (Diagnostic Instruments Inc.).

4.2.5 RNA sample preparation and next generation sequencing

MeHg doses used for RNA sequencing was chosen based on cell viability and morphology results, as well as a literature review on the Hg concentrations found in maternal blood (Table 4.1). The final doses of 0, 10, 100 and 200 nM of MeHg exposure was chosen for RNA sequencing as these doses did not induce significant cell death and covered the range of Hg concentrations typically found within human blood. hESCs were cultured, induced, and treated as described above. RNA samples were extracted and purified with a RNeasy Plus Mini kit

(Catalog no. 74134, Qiagen) following the manufacturer's protocol. In brief, the culture medium was completely removed, and cells were lysed directly with Buffer RLT Plus containing 10% β-mercaptoethanol (β-ME). The cell lysates were gently pipetted into microcentrifuge tubes and mixed by vortexing. Lysates were homogenized by centrifugation for two minutes at maximum speed (14800 rpm) in QIAshredder spin columns placed in 2 ml collection tubes and were transferred to gDNA eliminator spin columns for gDNA removal. After centrifuging for 30 seconds at 10,000 rpm, 70% ethanol was added to the flow-through, and mixed well by pipetting. The mixed sample solutions were transferred to RNeasy spin columns and centrifuged for 15 seconds at 10,000 rpm. The flow-through was discarded, and spin column membranes were washed by centrifuging for 15 seconds at 10,000 rpm in Buffer RW1 and discarding the flow-through. The spin column membranes were then washed by centrifuging for 15 seconds at 10,000 rpm in Buffer RPE, followed by a second wash in Buffer RPE for 2 minutes at 10,000 rpm. The spin columns were carefully placed in new collection tubes and centrifuged for 1 minute at maximum speed (14800 rpm) to eliminate any possible residual Buffer RPE. To elute the RNA samples, the spin columns were placed in 1.5 mL collection tubes and 30 µL RNase-free water was added directly to the column membrane. The collection tubes were centrifuged for 1 minute, and the eluted RNA samples were stored immediately at -80°C.

The RNA samples were sent to Genome Quebec for quality check and whole genome-scale mRNA sequencing by Illumina NovaSeq 6000. Sequencing was performed by paired end reading with a sequencing depth of 50 M reads for each sample and 3 biological replicates for each treatment group.

4.2.6 Sequencing Data analysis and marker selection for verification

The raw data were obtained from Genome Quebec and quality control was conducted with FastQC (https://www.bioinformatics.babraham.ac.uk/projects/fastqc/). All analysis were conducted in R (https://www.r-project.org/). Gene sequences were aligned to the reference human genome database GRCh38 (https://www.ncbi.nlm.nih.gov/data-hub/genome/GCF_000001405.26/), and reads counted using the "Rsubread" package [43]. Data were then normalized, and lowly expressed genes were filtered out using the "edgeR" package [44]. Filtered data were shown by boxplots to reflect quantile normalization, and principal component analysis (PCA) were used to demonstrate clustering of samples in different groups. The R package "edgeR" [44] was used to identify differentially expressed genes (DEGs) with cut-off for DEGs set as adjusted p-value <0.05 and absolute log2 [fold change (FC)] >1. Significant DEGs were further visualized in volcano plots and heat maps generated with the "ggplot2" package.

Gene set testing for DEGs was performed with the "clusterProfiler" package [45] for gene ontology (GO) functional enrichment and Kyoto Encyclopedia of Genes and Genomes (KEGG) pathway analysis. Adjusted p-value < 0.05 and count ≥ 30 was set as the cut-off for GO functional enrichment, whereas adjusted p-value < 0.05 was used as the cut-off for KEGG pathway analysis. Data were visualized using the "ggplot2" package.

GO functional enrichment analysis identified 32 GO terms that were significant, of which seven were related to early development. A protein-protein interaction network analysis of the genes within each of these seven early development related GO terms were conducted using Cytoscape (https://cytoscape.org/) to identify hub genes for each of these GO terms. Lineage genes classified based on the TaqMan hPSC scorecard assay [46] were also identified in the dataset, and a cross comparison of hub genes identified from GO terms and DEGs from lineage

genes with genes driving endoderm differentiation in the literature [47-51] narrowed down genes for further downstream qPCR and Western blot verification.

We explored the potential mechanisms of the developmental toxicity of MeHg on hESCs while differentiating toward DE cells by identifying the sequence of responses to the increasing dose of MeHg. We entered the DEGs into a web-based tool, FastBMD (https://www.fastbmd.ca/) [52] to calculate the benchmark doses (BMD). The DEGs were then ranked by their BMDs, and the enriched KEGG pathways were ranked based on the average rank of DEGs involved in each pathway (cut-off of involved DEG number ≥ 5).

4.2.7 Reverse Transcription Quantitative Polymerase Chain Reaction (RT-qPCR)

RNA samples were prepared as described above. RNA concentration was determined using NanoDrop™ 2000 spectrophotometer (Thermo Scientific) and RNA quality was verified using gel electrophoresis and qualitative assessment of the relative intensities of the 28 and 18s ribosomal RNA bands. RNA was treated with DNaseI (Catalog no. 18068015, Invitrogen, ThermoFisher Scientific) prior to cDNA synthesis from 900 ng total RNA using a high-capacity cDNA reverse transcription kit (Catalog no. 4368814; ThermoFisher Scientific). Real-time PCR was performed in 20 µl reactions containing 10 µl SsoFast EvaGreen supermix (Catalog no. 1725201, Bio-Rad), 500 nM forward and reverse primers (Table S4.1) and 0.5 µl cDNA template obtained from cDNA synthesis. Controls (no template added) were run in every assay and non-reverse transcribed samples were run for every primer pair. Reaction efficiency for all primer pairs was between 90% and 110%. Final data were normalized to the geometric mean of the three reference genes (gapdh, hddc2 and znf324b) and the 0 nM group using the delta-delta CT method [53].

4.2.8 Western blotting

To determine whether the effects of MeHg on gene expressions also occur at the protein level, we measured protein expression of the selected markers by Western blots.

hESCs were cultured, induced, and exposed to MeHg as described above. Culture medium was discarded, and the cells were washed with PBS and lysed with Pierce radioimmunoprecipitation assay buffer (RIPA buffer; Thermo Fisher Scientific) containing proteinase and phosphatase inhibitor cocktails (Catalog no. 5872S; Cell Signaling Technology). The cell lysates were then sonicated with a Microson Ultrasonic Cell Disruptor XL2000 (Misonix Inc.). The whole process of protein extraction was conducted on ice. Protein concentrations of the lysates were quantified with a Pierce Bicinchoninic Acid Protein Assay kit (Thermo Fisher Scientific). The cell lysates were then denatured by heating at 100°C for 4 min after mixing with 4× Laemmli sample buffer (Catalog no. 1610747; Bio-Rad).

Cell lysate samples were electrophoresed on 4-20% Mini-Protein TGX Stain-Free Precast Gels (Catalog no. 17000436, Bio-Rad). The same amount of protein was loaded for each batch, and the amount of total protein loaded ranged from 20 to 24 μg between different batches. Gels were then activated under ultraviolet light using the ChemiDoc XRS+ imaging system (Bio-Rad), and proteins were electro-transferred from gels to polyvinylidene difluoride (PVDF) membranes with the Mini Trans-Blot Cell (Catalog no. 1703930; Bio-Rad). Membranes were then blocked with 5% non-fat dry milk (NFDM, Catalog no. 1706404; Bio-Rad) or 3% bovine serum albumin (BSA, Catalog no. BSA-50; Rockland Immunochemicals, Inc.) depending on the protein targets for 1 h at room temperature and incubated with antibodies of interest (Table S4.2) diluted in their corresponding blocking buffer at 4°C overnight. Then the membranes were washed three times with Tris-buffered saline containing 0.1% Tween 20 (TBST) on a shaker for

5 min and incubated with 1:5,000 dilution of horseradish peroxidase (HRP)–linked secondary antibodies (Table S4.2) diluted in corresponding blocking buffer at 4°C overnight. The membranes were washed again for three times with TBST and incubated with enhanced chemiluminescence substrate (ECL, Catalog no. 1705062; Bio-Rad) in the dark and imaged with the ChemiDoc XRS+ imaging system. The Image Lab software (Bio-Rad) was used to quantify the band intensities and all target band intensities were normalized against the total protein band intensities.

As autophagy plays a critical role in the differentiation of stem cells [54], the expression of autophagic protein markers (LC3B and SQSTM1, antibody information is shown in Table S4.2) was also measured by Western blots as described above.

4.2.9 Statistical Analysis

All data were displayed as the means plus or minus the standard errors of the mean (means ± SEMs) and were tested for statistical significance with one-way ANOVA, followed by Dunnett's post hoc tests. The differences were considered significant if $p < 0.05$. Except for the RNA sequencing data, which was analyzed with R as described above, all statistical analyses were performed using GraphPad Prism (version 8).

4.3 Results

4.3.1 Effects on morphology and cell viability of MeHg exposure during definitive endoderm (DE) differentiation

To determine sublethal doses of MeHg exposure during hESC to DE differentiation, cell viability was measured following 0 – 10 μM of MeHg exposure. Differentiating cells exposed to

300 nM of MeHg showed a significant reduction in cell viability, and exposure to higher than 1 μM of MeHg resulted in almost complete cell death (Figure 4.1). Exposure to concentrations at or below 200 nM of MeHg did not have a significant impact on cell viability, and differentiated DE cells showed no morphological difference when compared to the controls (Figure 4.2). Therefore, the doses of 0, 10, 100 and 200 nM MeHg were identified as the sub-lethal doses for further transcriptomic analysis.

4.3.2 Identification of differentially expressed genes (DEGs)

Differentially expressed genes were identified with the "edgeR" package following data cleanup and quantile normalization of the samples (Figure 4.3A & B). Based on the cut-off for DEGs (adjusted p-value <0.05 and absolute log2 FC >1), a total of 1163 DEGs were identified, with 26 DEGs in the 10 nM treatment group, 393 DEGs in the 100 nM treatment group and 1136 DEGs in the 200 nM treatment group. A total of 16 genes were differentially expressed in all three treatment groups. These DEGs were further visualized via heat map (Figure 4.3C) and volcano plot (Figure 4.3D). The heat map showed a clear clustering of each MeHg treatment group.

4.3.3 Functional analysis of DEGs

The 1163 DEGs were analyzed for GO functional enrichment with a cut-off of p-adj < 0.05. A total of 87 GO terms were identified to be significant, and among those 32 GO terms with greater than 30 count number were kept for further analysis (Figure 4.4A). The clustering of these 32 significant GO terms were organized into an enrichment map (Figure 4.4B), showing that many of the significant GO terms were related to RNA metabolic processes including ribonucleoprotein complex biogenesis (GO:0022613), ribosome biogenesis (GO:0042254),

ncRNA metabolic process (GO:0034660), ncRNA processing (GO:0034470), rRNA processing (GO:0006364), rRNA metabolic process (GO:0016070), and nuclear-transcribed mRNA catabolic process, nonsense-mediated decay (GO:0000184) or protein synthesis/transport such as mRNA catabolic process (GO:0006402), protein targeting (GO:0006605), establishment of protein localization to membrane (GO:0090150), translation initiation (GO:0006413), and protein targeting to membrane (GO:0006612). In addition, seven of these GO terms, including negative regulation of cell differentiation (GO:0045596), gland development (GO: 0048732), urogenital system development (GO: 0001655), stem cell differentiation (GO: 0048863), renal system development (GO:0072001), mesenchyme development (GO:0060485), and kidney development (GO:0001822) were GO terms that were linked to the GO term developmental process (GO:0032502), and the genes that are linked to these seven GO terms are shown in Figure 4.4C. To select gene markers of interest for verification, a protein-protein interaction (PPI) network analysis of the genes within each of these seven development-related GO terms was conducted, and the top 10 hub genes were identified from each of these seven GO terms. A total of 27 hub genes were identified after accounting for repetitions, with BMP4 being a hub gene in all seven GO terms, and BMP2, WNT4, and SMAD3 appearing as hub genes in six out of the seven GO terms.

The KEGG pathway enrichment analysis (Figure 4.5) also yielded similar results as the GO functional enrichment, with multiple ribosome-related pathways such as ribosome (hsa03010), ribosome biogenesis in eukaryotes (hsa03008), spliceosome (hsa03040), and RNA polymerase (hsa03020) being upregulated in all three MeHg treatment groups (Figure 4.5A-C). In addition, pathways that are known to be perturbed by MeHg [55-58], such as calcium signaling pathway (hsa04020), nucleotide excision repair (hsa03420), and chemical

carcinogenesis – reactive oxygen species (hsa05208), are also reflected in the KEGG pathway enrichment analysis (Figure 4.5E). In addition, according to the average rank of DEGs based on their BMDs, 21 KEGG pathways were successfully ranked with protein digestion and absorption (hsa04974) and calcium signaling pathway (hsa04020) considered as the early responses triggered by increasing doses of MeHg.

Lineage marker genes within DEGs were also identified based on previously published lineage genes [46, 59], and 10 lineage genes were found to be differentially expressed (Figure 4.6). These included meso-/endodermal genes PDGFRA, FOXA2, GATA6, CLDN1, EOMES, and LEFTY2, ectodermal genes COL2A1 and MAP2, and self-renewal genes DNMT3B and SOX2. Of these genes, CLDN1, LEFTY2, and COL2A1 were downregulated following 200 nM of MeHg exposure during DE differentiation, whereas all the other lineage genes were upregulated.

As BMP4, SMAD3, FOXA2, GATA6, EOMES, and LEFTY2 were also major genes involved in the endoderm differentiation [47-51], these genes were chosen for further downstream qPCR and Western blot verification. In addition to the above genes, two other genes BHMT and URB1 were also selected for downstream verification. BHMT was chosen based on the justification that it has the highest fold change among all DEGs and BHMT itself is highly expressed in the endoderm-derived organs such as the liver and pancreas [60], and URB1 was chosen as it is a ribosome biogenesis protein that can modulate endoderm derived organ development [61], and ribosomal pathways were top enriched in both GO functional analysis and KEGG pathway analysis.

4.3.4 RT-qPCR and Western blot verification

Gene expression of the above-mentioned genes were further verified using RT-qPCR. Significant downregulation of bmp4 (Figure 4.7A) and smad3 (Figure 4.7B) were observed in the 200 nM MeHg treatment group, showing the same trends as the transcriptomics dataset. However, the other four genes [eomes, foxa2, gata6, urb1 (Figure 4.7C-F))] tested which showed a significant but low fold change difference in the transcriptomics dataset did not show any statistical differences when analyzed using RT-qPCR.

At the protein level, BHMT (Figure 4.8A) showed a significant downregulation following 200 nM of MeHg exposure, phosphorylated SMAD3 (p-SMAD3) (Figure 4.8B) and URB1 (Figure 4.8C) showed a significant upregulation following 200 nM of MeHg exposure, whereas FOXA2 (Figure 4.8D) was significantly upregulated at all three MeHg doses. BMP4, EOMES, GATA6, LEFTY2, and SMAD3 (Figure 4.8E-I) did not show any significant differences following MeHg treatment, and neither did any of the autophagy markers [SQSTM1, LC3BII/LC3BI (Figure S4.2)].

4.4 Discussion

The main goal of the present study was to assess the influence of MeHg exposure on the development of human embryonic stem cells (hESCs) during definitive endoderm (DE) cell differentiation using a transcriptomics approach. Our results showed that MeHg targeted mainly ribosomal processes to alter protein synthesis and translocation during hESCs to DE cell differentiation, resulting in an overall enhancement of cell differentiation.

The viability of differentiating cells was not affected when exposed to MeHg doses below or at 200 nM, whereas MeHg doses above 200 nM decreased its viability in a dose-

dependent manner. In contrast, undifferentiated hESCs showed close to 50% reduction in cell viability when exposed to 200 nM of MeHg for the same duration [35], suggesting that the hESCs which are differentiating towards DE cells have a higher tolerance for MeHg exposure in terms of cell viability when compared to undifferentiated hESCs. However, this does not indicate that MeHg exposure under 200 nM has no effect on these differentiating hESCs, as sublethal doses of MeHg exposure have been shown to alter protein expression and induce cognitive deficits in animal models [62]. This is supported by findings in this study that the effects of MeHg at sublethal doses on the altered gene and protein expressions of hESCs during the differentiation towards DE cells.

The transcriptomics dataset showed that MeHg exposure at 10 nM affected the least number of genes, with only 26 genes showing a significant difference in expression pattern compared to the vehicle control. The number of differentially expressed genes (DEGs) increased as MeHg concentrations increased, but the genes that were affected remained mostly consistent, as 85% of DEGs in the 10 nM MeHg dosed group and 93% of DEGs in the 100 nM MeHg dosed group were also DEGs in the 200 nM MeHg dosed group, suggesting a generally similar manner in gene pattern alterations among the three doses. Functional analysis of DEGs via GO functional enrichment or KEGG pathway analysis also confirmed that MeHg disrupted hESCs differentiation into DE cells via similar pathways, with ribosomal and protein synthesis/translocation pathways consistently appearing in all three MeHg-dosed groups. Thus, it is likely that MeHg exerts its developmental toxicity mainly by disrupting ribosome biogenesis during early cell lineage differentiation.

It is well recognized that ribosome biogenesis is important for the maintenance of stem cell pluripotency and its subsequent differentiation [63-65]. In undifferentiated stem cells,

ribosome biogenesis is generally at a high level, though global protein synthesis rates tend to be low, which primes the undifferentiated stem cell for rapid and efficient reassembly of their proteome into the target cell types during differentiation. During differentiation, rates of protein synthesis and ribosome biogenesis are tightly and dynamically regulated in accordance with the needs of the differentiating cells, with protein synthesis rates increasing during differentiation. In contrast, ribosome biogenesis transiently decreases only during the early phases of differentiation and then rises back up to high levels [66, 67]. Following MeHg exposure, upregulation of genes within ribosomal-related processes enriched from GO terms, upregulation of the ribosome biogenesis homolog URB1, and the upregulation of the KEGG pathway ribosome biogenesis in eukaryotes (hsa03008) all suggest that MeHg upregulates ribosomal biogenesis during hESC to DE cell differentiation. Despite undifferentiated stem cells having high ribosome biogenesis, and MeHg exposure on undifferentiated hESCs showing enhanced pluripotency [35], it is not likely that MeHg exposure during hESC to DE cell differentiation inhibited differentiation and enhanced hESCs' pluripotency. Firstly, despite "negative regulation of cell differentiation" being enriched through GO functional enrichment, the majority of genes within the GO term were downregulated following MeHg exposure (39 downregulated vs 27 upregulated), suggesting inhibition of negative regulation and thus enhancement of cell differentiation. Secondly, multiple pieces of evidence within the dataset also point to an upregulation of protein synthesis, translocation, and turnover. This includes genes within the GO terms "translational inhibition" (seven upregulated and none downregulated) and "protein targeting" (nine upregulated and six downregulated) being mostly upregulated, and core enriched genes within the KEGG pathways for "spliceosome", "RNA polymerase", and "aminoacyl-tRNA biosynthesis" being upregulated. In addition, MeHg is capable of inducing protein synthesis in animal models, with increases in

levels of liver ribosomes, ribosomal subunits and polyribosomes, along with a three-fold increase in the incorporation of labeled amino acids in the livers of rats exposed to MeHg [68]. Thus the combination of ribosome biosynthesis and protein synthesis upregulation suggests that MeHg upregulates ribosome biogenesis leading to increased global protein translation and enhancing differentiation which could further lead to the overgrowth of specific organs. For example, in zebrafish, MeHg caused upregulation of URB1 during DE differentiation, leading to alterations in ribosome biogenesis and overgrowth of digestive organs [61].

What is seemingly contradictory to this conclusion is that nine proteosome subunits (PSMA5, PSMA7, PSMB3, PSMB6, PSMD1, PSMD3, PSMD8, PSMD11, PSME3), and the KEGG pathway proteosome (hsa03050) were all upregulated following MeHg exposure during hESC to DE cell differentiation, as high levels of proteosome activity has been associated with the maintenance of pluripotency [69-71]. However, studies have shown that the ubiquitin proteosome pathway is critical in modulating the toxicity of MeHg. Specifically, overexpression of the ubiquitin-protein ligase CDC34 significantly increased cellular-ubiquitinated protein levels in yeast and human cells lines, increasing their resistance to MeHg exposure [72, 73]. Thus, the upregulation of the proteosome pathway may be due to cells resisting MeHg toxicity and not maintaining pluripotency. Considering that calcium signaling pathway (hsa04020) is one of the most sensitive responses to MeHg exposure in the ranked KEGG pathways based on BMDs of the gene set involved, a reasonable inference would be that disrupted calcium homeostasis leads to imbalanced $Ca2^{+}$, which can be utilized by mitochondria to generate excessive amounts of ROS [74]. This is supported in our data with KEGG pathways chemical carcinogenesis – reactive oxygen species (hsa05208) and oxidative phosphorylation (hsa00190) ranking behind the KEGG pathway calcium signaling pathway. Proteasome [(hsa03050) ranked

behind chemical carcinogenesis – reactive oxygen species and oxidative phosphorylation] would then need to be upregulated to clean up the damaged proteins caused by the elevated oxidative stress. Meanwhile, the overproduction of ROS has also been linked to hyperactive ribosome biogenesis, and protein synthesis in animal embryos and human cell lines [75, 76], and is considered to promote stem cell differentiation [77], including towards the DE fate [78].

Under normal circumstances, antioxidants such as glutathione can prevent oxidative stress through the removal of ROS. However, glutathione is also involved in Hg detoxification by specifically binding with MeHg to form a complex that prevents Hg from binding to cellular proteins and causing cellular damage [79] and by forming a glutathione-mercury complex in the liver for the excretion of mercury [80], depleting existing glutathione concentrations resulting in the lack of antioxidants for the removal of ROS and subsequent cell death. To counteract this depletion of glutathione by Hg and Hg-induced oxidative stress, upregulation of the trans-sulfuration pathway that synthesizes glutathione from homocysteine (Hcy) has been observed [81]. Within our dataset, this upregulation of glutathione synthesis is reflected as a downregulation of betaine-homocysteine S-methyltransferase (BHMT), one of the genes with the highest fold change following MeHg exposure. BHMT normally plays an important role in the regulation of Hcy metabolism by catalyzing the resynthesis of methionine from Hcy [60]. Thus downregulation of BHMT would facilitate Hcy in entering the trans-sulfuration pathway for glutathione synthesis. Interestingly though, folate biosynthesis (hsa00790), which produces folate that also catalyzes the resynthesis of methionine from Hcy was significantly upregulated following MeHg exposure. This could partly reflect the lack of methionine within the cell due to Hcy being directed for glutathione synthesis to protect against oxidative stress induced by MeHg exposure.

As MeHg resulted in enhanced differentiation during hESC to DE cell differentiation, it is likely endodermal fate was overpromoted. Under normal conditions, three major extracellular signals, Wnt, Nodal/Activin, and BMPs, regulate definitive endoderm differentiation. These signals all, in turn, phosphorylate SMAD2/3 proteins [47, 48, 82], which depending on the transcriptional regulator it binds to either activate endodermal fate genes when bound to SMAD4 [83] or activate mesodermal fate genes when bound to FOXH1 [84]. In addition, BMP4 can act synergistically with activin to further upregulate the expression of transcription factors involved in endoderm differentiation and promote the endodermal fate [85]. BMP4 itself can also cooperate with FGF2 via ERK to further induce mesoderm and inhibit the endoderm differentiation [86]. To understand how MeHg may have disrupted stem cell specification during the differentiation towards DE cells, we examined lineage gene markers within our dataset. We found that the most significantly affected genes by MeHg were meso- or endodermal genes, including pdgfra, foxa2, gata6, cldn1, eomes and lefty2. Most notably, the expression of endodermal genes foxa2, eomes and gata6 were upregulated, and FOXA2 was confirmed to be upregulated at the protein level as well. FOXA2 is an important transcription factor that is expressed during early endoderm differentiation and, when overexpressed, can lead to the expression of genes associated with endodermal lineage, but does not induce the expression of genes involved in late endoderm differentiation [87]. EOMES, on the other hand, interacts with SMAD2/3 to initiate the transcriptional network governing endoderm formation and, when overexpressed, leads to the expression of DE markers such as FOXA2 [47, 48]. These changes are likely initiated by an upregulation of phosphorylated SMAD3 (p-SMAD3) though smad3 gene expression was significantly downregulated in this study, suggestive of a negative feedback loop between p-SMAD3 and smad3 gene expression. Similar to smad3 gene and p-SMAD3

protein, there might be a negative feedback loop for BMP4 regulation as well, as bmp4 gene was downregulated, yet BMP4 protein showed an increasing though non-significant trend following MeHg exposure, which could further promote endoderm differentiation. Thus, MeHg exposure during hESC to DE cell differentiation leads to overexpression of endodermal genes, which may ultimately result in the overpromotion of endodermal fate (Figure 4.9).

In conclusion, our study showed that MeHg exposure during hESC to DE differentiation could affect cell viability and human-relevant concentrations of MeHg which did not cause lethal effects could cause global gene expression changes, leading to calcium dyshomeostasis and ROS overproduction, resulting in an upregulation of ribosome biogenesis and global protein synthesis/translocation to promote hESC differentiation. Considering that the key transcription factors such as EOMES and FOXA2, which are critical in endodermal development, are overexpressed following MeHg exposure, hESC specification could be affected with endodermal fate being overpromoted, abnormal organ development, and subsequently congenital diseases later in life. A summary of this effect is presented in the form of an adverse outcome pathway in Figure 4.10. It is not possible to extrapolate the dose-response relationship observed in this *in vitro* study to humans. However, the treatment doses covered a range of total Hg typically found in human maternal blood [0.1 – 150 nM] (Table 4.1). Our results suggest that the risk of MeHg during pregnancy, especially the newfound effects on endodermal development, needs more consideration for public health promotion and disease prevention.

4.5 References

1. Driscoll, C.T., et al., Mercury as a global pollutant: sources, pathways, and effects. Environmental science & technology, 2013. **47**(10): p. 4967-4983.

2. Clarkson, T.W., The three modern faces of mercury. Environmental health perspectives, 2002. **110**(suppl 1): p. 11-23.
3. Streets, D.G., Q. Zhang, and Y. Wu, Projections of global mercury emissions in 2050. Environmental science & technology, 2009. **43**(8): p. 2983-2988.
4. Parks, J.M., et al., The genetic basis for bacterial mercury methylation. Science, 2013. **339**(6125): p. 1332-1335.
5. Van Oostdam, J., et al., Human health implications of environmental contaminants in Arctic Canada: a review. Science of the total environment, 2005. **351**: p. 165-246.
6. Feng, L., P. Li, and X. Feng, Methylmercury bioaccumulation in rice and health effects: A systematic review. Current Opinion in Environmental Science & Health, 2021. **23**: p. 100285.
7. Amin-Zaki, L., et al., Methylmercury poisoning in the Iraqi suckling infant: a longitudinal study over five years. Journal of Applied Toxicology, 1981. **1**(4): p. 210-214.
8. Harada, M., Minamata disease: methylmercury poisoning in Japan caused by environmental pollution. Critical reviews in toxicology, 1995. **25**(1): p. 1-24.
9. Bakir, F., et al., Methylmercury Poisoning in Iraq: An interuniversity report. Science, 1973. **181**(4096): p. 230-241.
10. Harada, M., Congenital Minamata disease: intrauterine methylmercury poisoning. Teratology, 1978. **18**(2): p. 285-288.
11. Castoldi, A.F., et al., Neurodevelopmental toxicity of methylmercury: Laboratory animal data and their contribution to human risk assessment. Regulatory Toxicology and Pharmacology, 2008. **51**(2): p. 215-229.

12. Tamm, C., et al., High susceptibility of neural stem cells to methylmercury toxicity: effects on cell survival and neuronal differentiation. Journal of neurochemistry, 2006. **97**(1): p. 69-78.
13. Bose, R., et al., Inherited effects of low-dose exposure to methylmercury in neural stem cells. Toxicological Sciences, 2012. **130**(2): p. 383-390.
14. Fujimura, M. and F. Usuki, Low concentrations of methylmercury inhibit neural progenitor cell proliferation associated with up-regulation of glycogen synthase kinase 3β and subsequent degradation of cyclin E in rats. Toxicology and Applied Pharmacology, 2015. **288**(1): p. 19-25.
15. Nagashima, K., A review of experimental methylmercury toxicity in rats: neuropathology and evidence for apoptosis. Toxicologic Pathology, 1997. **25**(6): p. 624-631.
16. dos Santos, A.A., et al., Methylmercury and brain development: A review of recent literature. Journal of trace elements in medicine and biology, 2016. **38**: p. 99-107.
17. Eto, K., Pathology of Minamata disease. Toxicologic Pathology, 1997. **25**(6): p. 614-623.
18. Eto, K., M. Marumoto, and M. Takeya, The pathology of methylmercury poisoning (Minamata disease) The 50th Anniversary of Japanese Society of Neuropathology. Neuropathology, 2010. **30**(5): p. 471-479.
19. Chang, J.-W., et al., Simultaneous exposure of non-diabetics to high levels of dioxins and mercury increases their risk of insulin resistance. Journal of Hazardous Materials, 2011. **185**(2-3): p. 749-755.
20. He, K., et al., Mercury exposure in young adulthood and incidence of diabetes later in life: the CARDIA Trace Element Study. Diabetes care, 2013. **36**(6): p. 1584-1589.

21. Carneiro, M.F.H., et al., A systematic study of the disposition and metabolism of mercury species in mice after exposure to low levels of thimerosal (ethylmercury). Environmental Research, 2014. **134**: p. 218-227.

22. Gonzalez, P., et al., Comparative effects of dietary methylmercury on gene expression in liver, skeletal muscle, and brain of the zebrafish (Danio rerio). Environmental science & technology, 2005. **39**(11): p. 3972-3980.

23. Ung, C.Y., et al., Mercury-induced hepatotoxicity in zebrafish: *in vivo* mechanistic insights from transcriptome analysis, phenotype anchoring and targeted gene expression validation. Bmc Genomics, 2010. **11**(1): p. 1-14.

24. da Rosa-Silva, H.T., et al., Hepatic and neurobiological effects of foetal and breastfeeding and adulthood exposure to methylmercury in Wistar rats. Chemosphere, 2020. **244**: p. 125400.

25. Yadetie, F., et al., Global transcriptome analysis of Atlantic cod (Gadus morhua) liver after *in vivo* methylmercury exposure suggests effects on energy metabolism pathways. Aquatic toxicology, 2013. **126**: p. 314-325.

26. Mela, M., et al., Effects of dietary methylmercury on liver and kidney histology in the neotropical fish Hoplias malabaricus. Ecotoxicology and Environmental Safety, 2007. **68**(3): p. 426-435.

27. Yang, C.-Y., et al., Methylmercury Induces Mitochondria-and Endoplasmic Reticulum Stress-Dependent Pancreatic β-Cell Apoptosis via an Oxidative Stress-Mediated JNK Signaling Pathway. International Journal of Molecular Sciences, 2022. **23**(5): p. 2858.

28. Schumacher, L. and L.C. Abbott, Effects of methyl mercury exposure on pancreatic beta cell development and function. Journal of Applied Toxicology, 2017. **37**(1): p. 4-12.

29. Chen, Y.W., et al., Methylmercury induces pancreatic β-cell apoptosis and dysfunction. Chemical research in toxicology, 2006. **19**(8): p. 1080-1085.

30. Cuello, S., et al., Molecular mechanisms of methylmercury-induced cell death in human HepG2 cells. Food and chemical toxicology, 2010. **48**(5): p. 1405-1411.

31. Jamalpoor, A., et al., A novel human stem cell-based biomarker assay for *in vitro* assessment of developmental toxicity. Birth Defects Research, 2022.

32. Visan, A., et al., Neural differentiation of mouse embryonic stem cells as a tool to assess developmental neurotoxicity *in vitro*. Neurotoxicology, 2012. **33**(5): p. 1135-1146.

33. Seiler, A.E. and H. Spielmann, The validated embryonic stem cell test to predict embryotoxicity *in vitro*. Nature protocols, 2011. **6**(7): p. 961-978.

34. Stummann, T., L. Hareng, and S. Bremer, Embryotoxicity hazard assessment of methylmercury and chromium using embryonic stem cells. Toxicology, 2007. **242**(1-3): p. 130-143.

35. Li, B., et al., Characterizing the Low-Dose Effects of Methylmercury on the Early Stages of Embryo Development Using Cultured Human Embryonic Stem Cells. Environmental health perspectives, 2021. **129**(7): p. 077007.

36. Theunissen, P.T., et al., Time-response evaluation by transcriptomics of methylmercury effects on neural differentiation of murine embryonic stem cells. Toxicological Sciences, 2011. **122**(2): p. 437-447.

37. He, X., et al., Effects of methylmercury exposure on neuronal differentiation of mouse and human embryonic stem cells. Toxicology letters, 2012. **212**(1): p. 1-10.

38. Zimmer, B., et al., Sensitivity of dopaminergic neuron differentiation from stem cells to chronic low-dose methylmercury exposure. Toxicological Sciences, 2011. **121**(2): p. 357-367.

39. Stummann, T.C., L. Hareng, and S. Bremer, Hazard assessment of methylmercury toxicity to neuronal induction in embryogenesis using human embryonic stem cells. Toxicology, 2009. **257**(3): p. 117-126.

40. Tamm, C., et al., Methylmercury inhibits differentiation of rat neural stem cells via Notch signalling. Neuroreport, 2008. **19**(3): p. 339-343.

41. Prince, L.M., et al., Environmentally relevant developmental methylmercury exposures alter neuronal differentiation in a human-induced pluripotent stem cell model. Food and Chemical Toxicology, 2021. **152**: p. 112178.

42. Muhr, J. and K.M. Ackerman, Embryology, gastrulation. 2020.

43. Liao, Y., G.K. Smyth, and W. Shi, The R package Rsubread is easier, faster, cheaper and better for alignment and quantification of RNA sequencing reads. Nucleic acids research, 2019. **47**(8): p. e47-e47.

44. Robinson, M.D., D.J. McCarthy, and G.K. Smyth, edgeR: a Bioconductor package for differential expression analysis of digital gene expression data. bioinformatics, 2010. **26**(1): p. 139-140.

45. Yu, G., et al., clusterProfiler: an R package for comparing biological themes among gene clusters. Omics: a journal of integrative biology, 2012. **16**(5): p. 284-287.

46. Tsankov, A.M., et al., A qPCR ScoreCard quantifies the differentiation potential of human pluripotent stem cells. Nature biotechnology, 2015. **33**(11): p. 1182.

47. Teo, A.K.K., et al., Pluripotency factors regulate definitive endoderm specification through eomesodermin. Genes & development, 2011. **25**(3): p. 238-250.

48. Faial, T., et al., Brachyury and SMAD signalling collaboratively orchestrate distinct mesoderm and endoderm gene regulatory networks in differentiating human embryonic stem cells. Development, 2015. **142**(12): p. 2121-2135.

49. Xuan, S. and L. Sussel, GATA4 and GATA6 regulate pancreatic endoderm identity through inhibition of hedgehog signaling. Development, 2016. **143**(5): p. 780-786.

50. Aksoy, I., et al., Klf4 and Klf5 differentially inhibit mesoderm and endoderm differentiation in embryonic stem cells. Nature communications, 2014. **5**(1): p. 1-15.

51. Chu, L.-F., et al., Single-cell RNA-seq reveals novel regulators of human embryonic stem cell differentiation to definitive endoderm. Genome biology, 2016. **17**(1): p. 1-20.

52. Ewald, J., et al., FastBMD: an online tool for rapid benchmark dose–response analysis of transcriptomics data. Bioinformatics, 2021. **37**(7): p. 1035-1036.

53. Rao, X., et al., An improvement of the 2ˆ (–delta delta CT) method for quantitative real-time polymerase chain reaction data analysis. Biostatistics, bioinformatics and biomathematics, 2013. **3**(3): p. 71.

54. Sharma, K., et al., Autophagy modulates cell fate decisions during lineage commitment. Autophagy, 2022. **18**(8): p. 1915-1931.

55. Roos, D., et al., Role of calcium and mitochondria in MeHg-mediated cytotoxicity. Journal of Biomedicine and Biotechnology, 2012. **2012**.

56. Novo, J.P., et al., Cellular and molecular mechanisms mediating methylmercury neurotoxicity and neuroinflammation. International journal of molecular sciences, 2021. **22**(6): p. 3101.

57. Farina, M., J.B. Rocha, and M. Aschner, Mechanisms of methylmercury-induced neurotoxicity: evidence from experimental studies. Life sciences, 2011. **89**(15-16): p. 555-563.

58. Grotto, D., et al., Low levels of methylmercury induce DNA damage in rats: protective effects of selenium. Archives of toxicology, 2009. **83**(3): p. 249-254.

59. Bock, C., et al., Reference Maps of human ES and iPS cell variation enable high-throughput characterization of pluripotent cell lines. Cell, 2011. **144**(3): p. 439-452.

60. Pajares, M.A. and D. Pérez-Sala, Betaine homocysteine S-methyltransferase: just a regulator of homocysteine metabolism? Cellular and Molecular Life Sciences CMLS, 2006. **63**(23): p. 2792-2803.

61. He, J., et al., Ribosome biogenesis protein Urb1 acts downstream of mTOR complex 1 to modulate digestive organ development in zebrafish. Journal of Genetics and Genomics, 2017. **44**(12): p. 567-576.

62. Bittencourt, L.O., et al., Proteomic approach underlying the hippocampal neurodegeneration caused by low doses of methylmercury after long-term exposure in adult rats. Metallomics, 2019. **11**(2): p. 390-403.

63. Tahmasebi, S., M. Amiri, and N. Sonenberg, Translational control in stem cells. Frontiers in genetics, 2019. **9**: p. 709.

64. Gabut, M., F. Bourdelais, and S. Durand, Ribosome and translational control in stem cells. Cells, 2020. **9**(2): p. 497.

65. Saba, J.A., et al., Translational control of stem cell function. Nature Reviews Molecular Cell Biology, 2021. **22**(10): p. 671-690.

66. Baser, A., et al., Onset of differentiation is post-transcriptionally controlled in adult neural stem cells. Nature, 2019. **566**(7742): p. 100-104.

67. Corsini, N.S., et al., Coordinated control of mRNA and rRNA processing controls embryonic stem cell pluripotency and differentiation. Cell stem cell, 2018. **22**(4): p. 543-558. e12.

68. Brubaker, P., G. Lucier, and R. Klein, The effects of methylmercury on protein synthesis in rat liver. Biochemical and Biophysical Research Communications, 1971. **44**(6): p. 1552-1558.

69. Schröter, F. and J. Adjaye, The proteasome complex and the maintenance of pluripotency: sustain the fate by mopping up? Stem Cell Research & Therapy, 2014. **5**(1): p. 1-9.

70. Saez, I., et al., Insights into the ubiquitin-proteasome system of human embryonic stem cells. Scientific reports, 2018. **8**(1): p. 1-21.

71. Yan, P., et al., Protein quality control of cell stemness. Cell Regeneration, 2020. **9**(1): p. 1-11.

72. Hwang, G.-W., Ubiquitin-proteasome system as a factor that determine the sensitivity to methylmercury. Yakugaku Zasshi: Journal of the Pharmaceutical Society of Japan, 2007. **127**(3): p. 463-468.

73. Hwang, G.W., T. Furuchi, and A. Naganuma, Ubiquitin-proteasome system is responsible for the protection of yeast and human cells against methylmercury. The FASEB journal, 2002. **16**(7): p. 709-711.

74. Farina, M. and M. Aschner, Methylmercury-induced neurotoxicity: focus on pro-oxidative events and related consequences. Neurotoxicity of Metals, 2017: p. 267-286.

75. Huang, Y., et al., Oxidative damage-induced hyperactive ribosome biogenesis participates in tumorigenesis of offspring by cross-interacting with the Wnt and TGF-β1 pathways in IVF embryos. Experimental & Molecular Medicine, 2021. **53**(11): p. 1792-1806.

76. Oliveira, V., et al., The snoRNA target of t (4; 14) in multiple myeloma regulates ribosome biogenesis. FASEB BioAdvances, 2019. **1**(7): p. 404-414.

77. Bigarella, C.L., R. Liang, and S. Ghaffari, Stem cells and the impact of ROS signaling. Development, 2014. **141**(22): p. 4206-4218.

78. Lv, J., et al., Mitochondrial homeostasis regulates definitive endoderm differentiation of human pluripotent stem cells. Cell death discovery, 2022. **8**(1): p. 1-13.

79. Kromidas, L., L.D. Trombetta, and I.S. Jamall, The protective effects of glutathione against methylmercury cytotoxicity. Toxicology letters, 1990. **51**(1): p. 67-80.

80. Zalups, R.K., Molecular interactions with mercury in the kidney. Pharmacological reviews, 2000. **52**(1): p. 113-144.

81. Woods, J.S. and M.E. Ellis, Up-regulation of glutathione synthesis in rat kidney by methyl mercury: Relationship to mercury-induced oxidative stress. Biochemical pharmacology, 1995. **50**(10): p. 1719-1724.

82. Funa, N.S., et al., β-Catenin regulates primitive streak induction through collaborative interactions with SMAD2/SMAD3 and OCT4. Cell stem cell, 2015. **16**(6): p. 639-652.

83. Yang, J. and W. Jiang, The role of SMAD2/3 in human embryonic stem cells. Frontiers in Cell and Developmental Biology, 2020. **8**: p. 653.

84. Charney, R.M., et al., Foxh1 occupies cis-regulatory modules prior to dynamic transcription factor interactions controlling the mesendoderm gene program. Developmental cell, 2017. **40**(6): p. 595-607. e4.

85. Teo, A.K., et al., Activin and BMP4 synergistically promote formation of definitive endoderm in human embryonic stem cells. Stem Cells, 2012. **30**(4): p. 631-642.

86. Bernardo, A.S., et al., BRACHYURY and CDX2 mediate BMP-induced differentiation of human and mouse pluripotent stem cells into embryonic and extraembryonic lineages. Cell stem cell, 2011. **9**(2): p. 144-155.

87. Levinson-Dushnik, M. and N. Benvenisty, Involvement of hepatocyte nuclear factor 3 in endoderm differentiation of embryonic stem cells. Molecular and Cellular Biology, 1997. **17**(7): p. 3817-3822.

4.6 Tables and Figures

Table 4.1. Maternal blood concentrations of Hg in different populations.

Population (Country)	Total Hg GM/AM/Median (range), ug/L	Total Hg GM/AM/Median (range), nM	MeHg GM/AM/Median (range), ug/L	MeHg GM/AM/Median(range), nM	Reference
Nunavik (Canada)	4.2 (3.4-4.9)	20.9 (16.9-24.4)			Nunavik study, 2017-2018
9 cities (Canada)	0.62	3.1			MIREC, 2018
South Carolina (USA)	0.87 (0.02-3.9)	4.3 (0.1-19.4)	0.58 (0.01-2.7)	2.7 (0.05-12.5)	Alexis Donohue, 2018
Lisbon (Portugal)	4.82 (1.03-12.0)	24.0 (5.13-59.8)	2.73 (0.47-9.12)	12.7 (2.2-42.3)	Timothy A, 2006
3 provinces (Korea)	5.27 (5.0-5.57)	26.3 (24.9-27.8)	4.05 (3.81-4.32)	18.8 (17.7-20.0)	Chang-Hun You, 2012
fifteen regional centers (Japan)	4.21 (0.334-30.1)	21.0 (1.7-150.1)			SumitakaKobayashi, 2019
2 northeastern areas (Japan)	5.42 (0.61-25.19)	27.0 (3.0-125.6)	5.15 (0.6-24.99)	23.9 (2.8-115.9)	Miyuki Iwai-Shimada, 2019
Zhoushan (China)	5.68	28.3			JinhuaWu, 2014
Guizhou (China)	3.0 (1.7-11)	15.0 (8.5-54.8)			Sarah E.Rothenberg, 2013

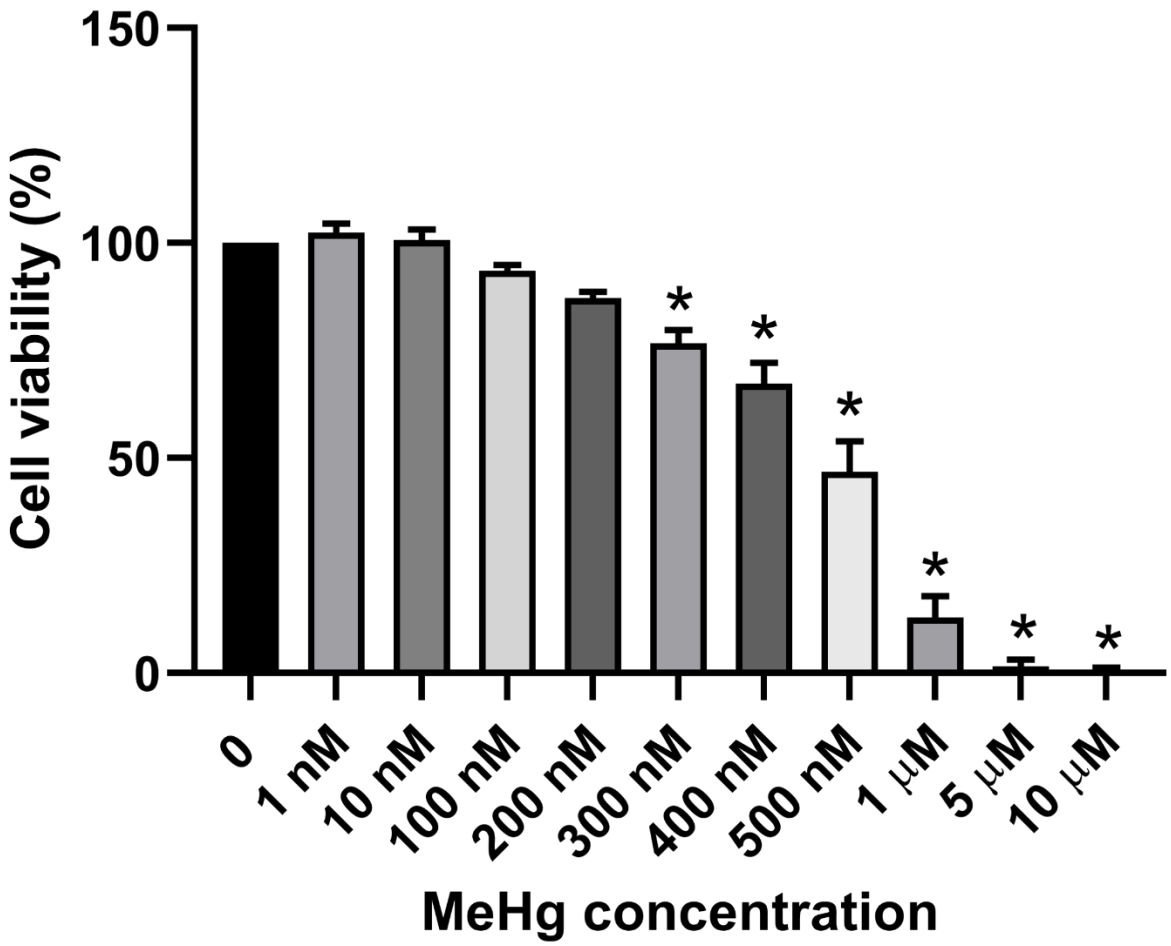

Figure 4.1. Cell viability (as percentage of control) of definitive endoderm (DE) cells differentiated from human embryonic stem cells (hESCs) exposed to 1 nM to 10 μM MeHg during DE differentiation. One-way ANOVA and Dunnett's post hoc test were used at each time point to compare differences between treatment and 0 nM group with $p < 0.05$ being considered as significant. Data are presented as means ± SEMs with N= 6-9 for each group.

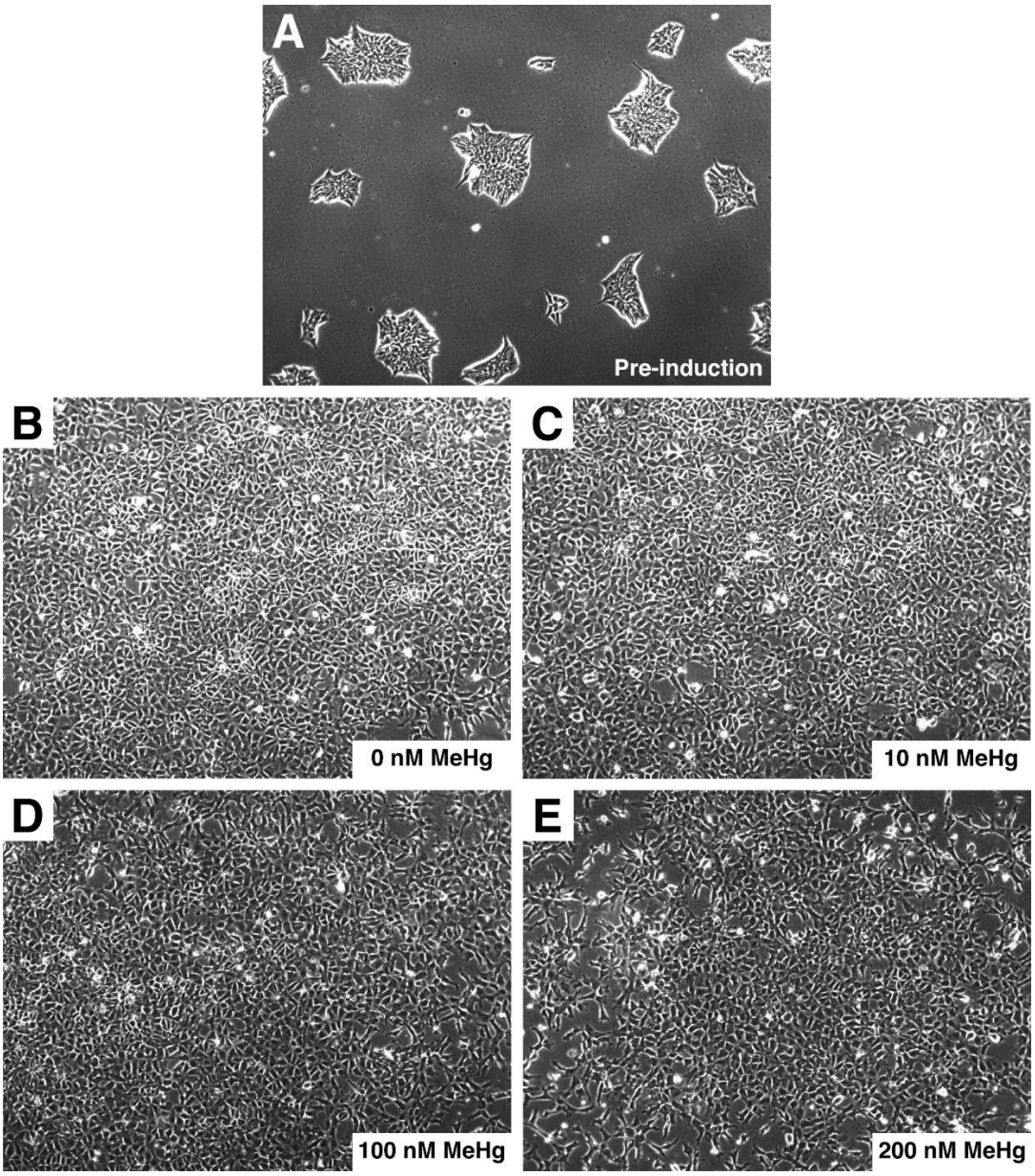

Figure 4.2. Cell attachment, colony formation, and morphology of definitive endoderm (DE) cells differentiated from human embryonic stem cells (hESCs) exposed to MeHg during DE differentiation. (A) Representative images of hESCs before induction. (B-E) Representative images of DE cells exposed to 0 nM, 10 nM, 100 nM and 200 nM MeHg during DE cell differentiation. All images were taken under a 10X objective.

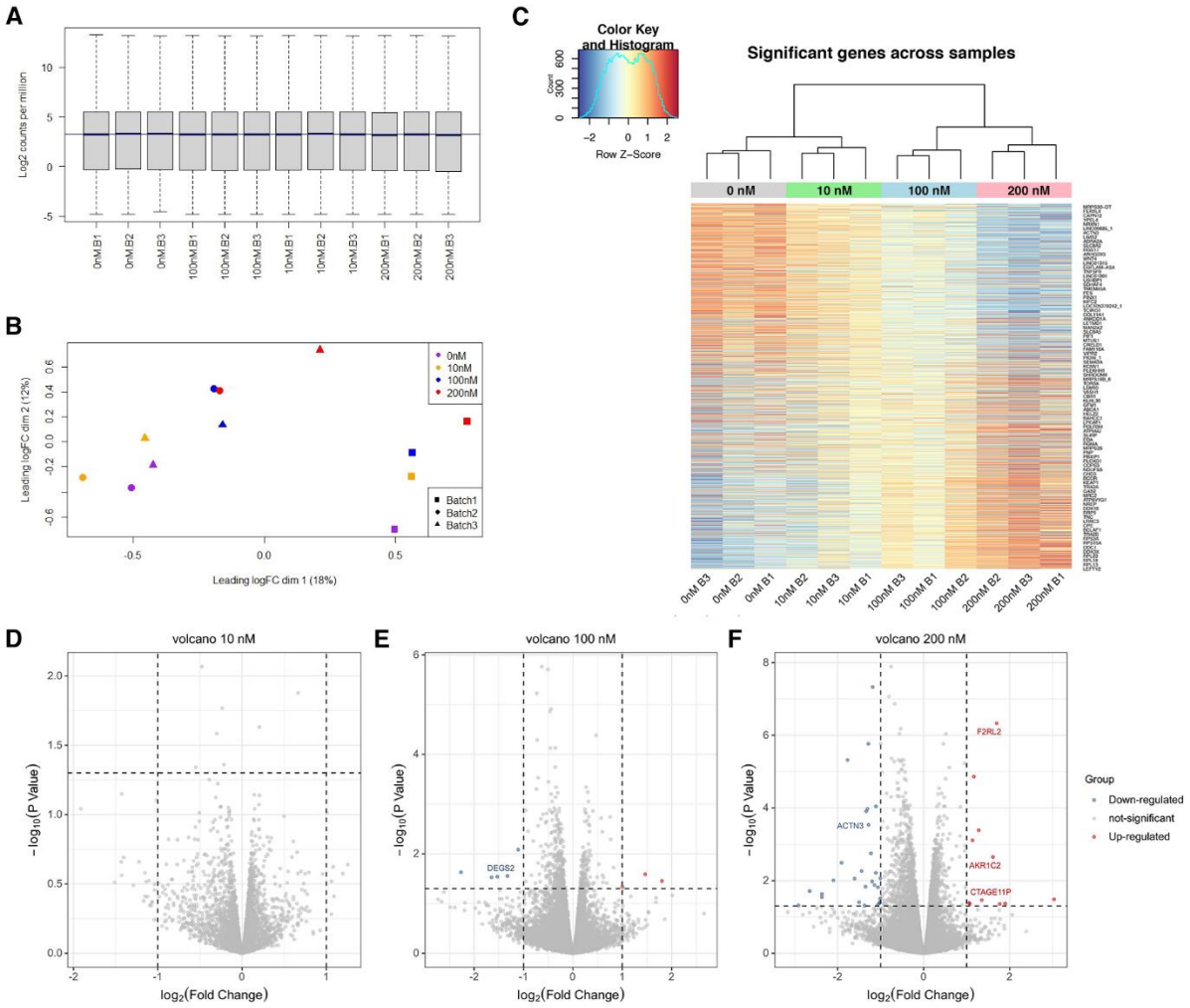

Figure 4.3. Data processing and identification of differentially expressed genes (DEGs). (A) Boxplot for transcriptomic samples after quantile normalization. (B) PCA for transcriptomic samples after quantile normalization. (C) The cluster heat map of DEGs with each row corresponding to a gene and each column corresponding to a sample. Light blue shows relatively low gene expression levels, whereas red represents relatively high gene expression levels. (D) Volcano plots of DEGs identified from 10 nM, 100 nM and 200 nM MeHg exposure during human embryonic stem cell (hESC) to DE differentiation.

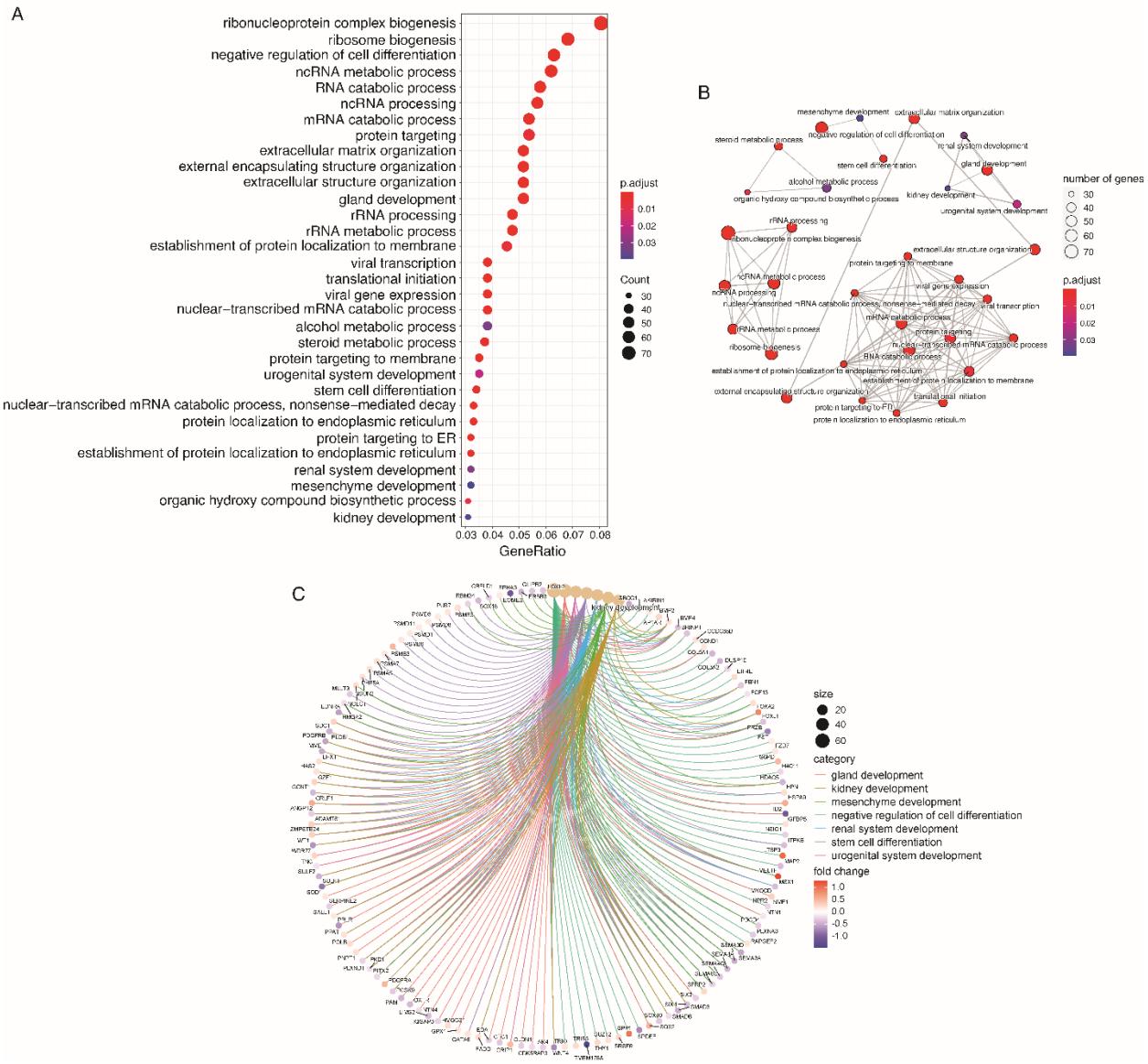

Figure 4.4. Significant enrichment GO terms of differentially expressed genes (DEGs). (A) GO functional enrichment dot plots of DEGs. The dots size represents the number of genes among the significant DEGs associated with the GO term. The color of the dots represents their significance in accordance with the adjusted P-value. (B) Enrichment map of the 32 GO terms identified. (C) Gene-concept network plot of the 7 GO terms related to early embryo development.

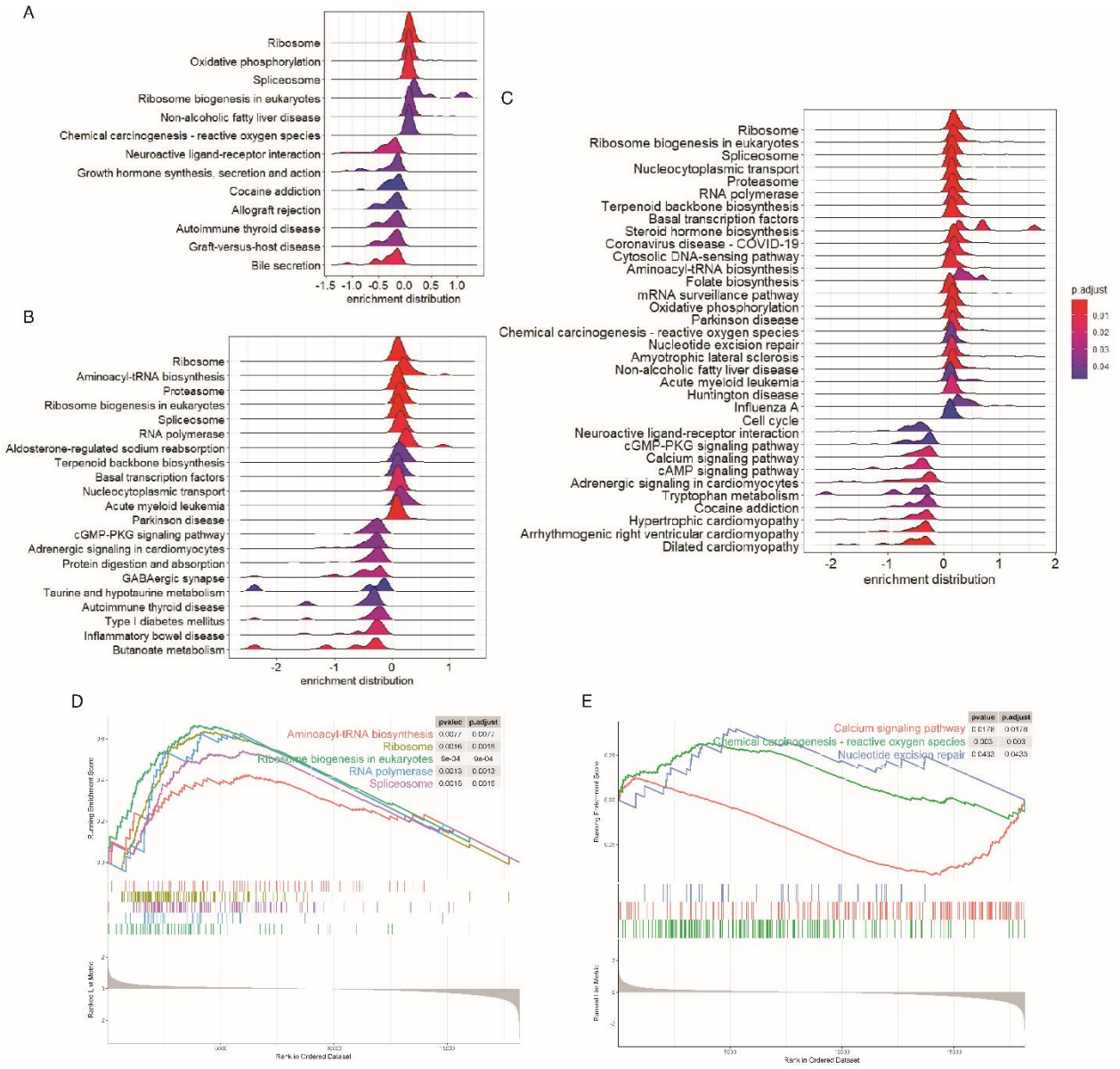

Figure 4.5. KEGG pathway enrichment of definitive endoderm (DE) cells expsored to (A) 10 nM, (B) 100 nM, and (C) 200 nM MeHg during human embryonic stem cell to DE cell differentiation. (D) Enrichment plot of ribosome and protein translation related KEGG pathways in 200 nM MeHg dosed group compared to the controls. (E) Enrichment plot of KEGG pathways known to be perturbed by MeHg in 200 nM MeHg dosed group compared to the controls.

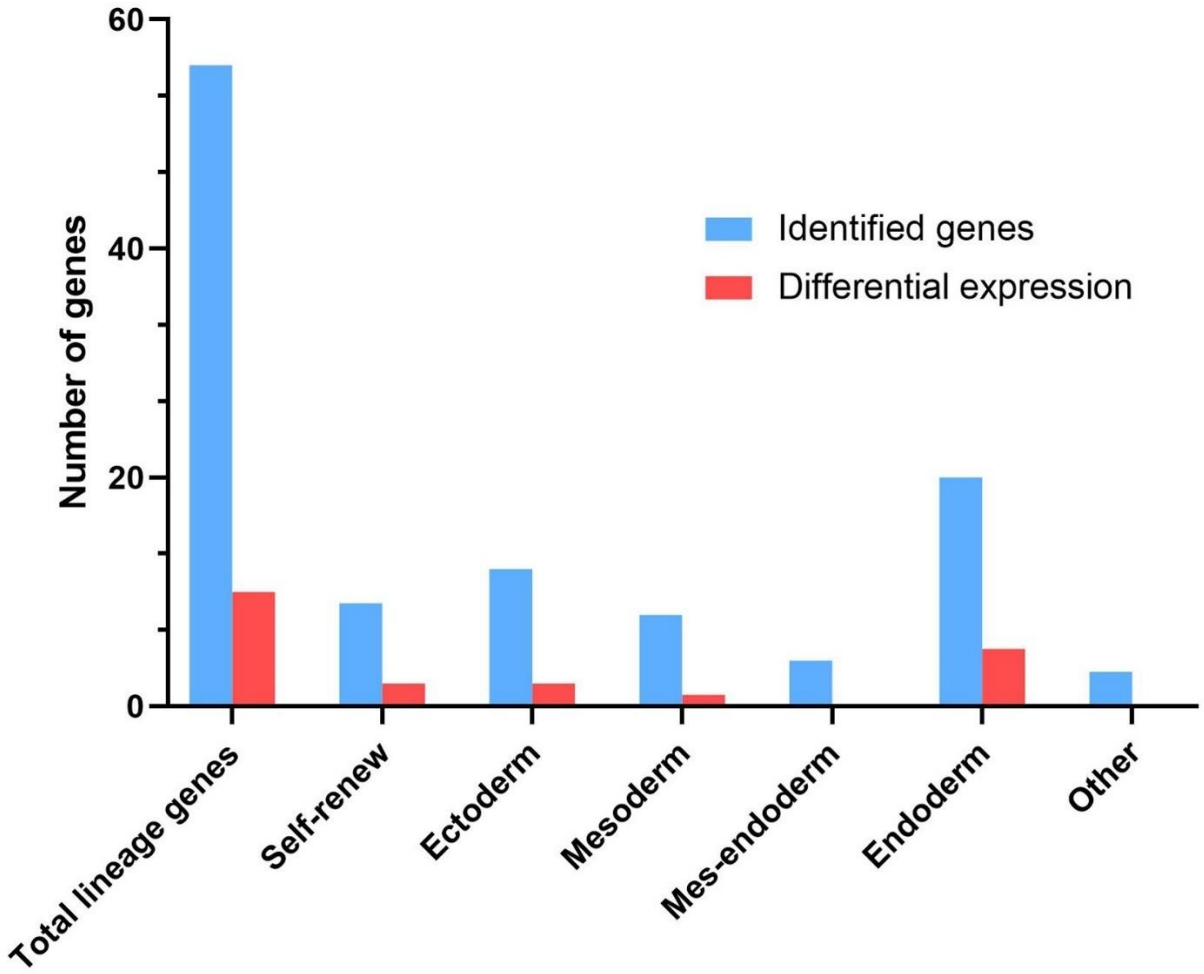

Figure 4.6. Lineage genes identified within the transcriptomics data set and the number of lineage genes that were differentially expressed following MeHg exposure during human embryonic stem cell to definitive endoderm differentiation.

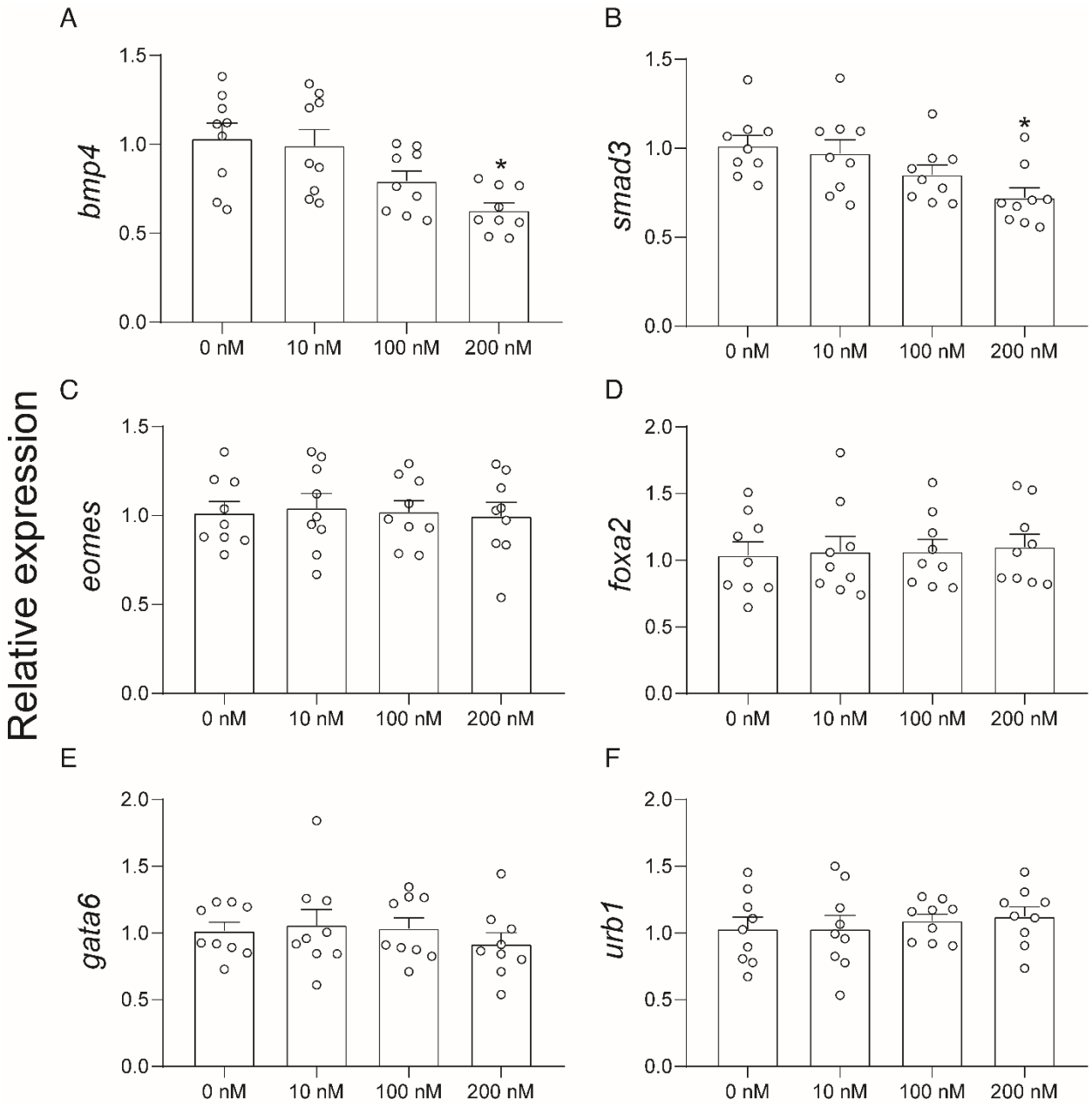

Figure 4.7. Expression of bmp4, smad3, eomes, foxa2, gata6, and urb1 genes in definitive endoderm (DE) cells exposed to MeHg during human embryonic stem cells to DE cell differentiation. Data are presented as means ± SEMs with N = 9 for each gene. One-way ANOVA and Dunnett's post hoc test were used at each time point to compare differences

between treatment and control groups with $p < 0.05$ being considered as significant marked by asterisk.

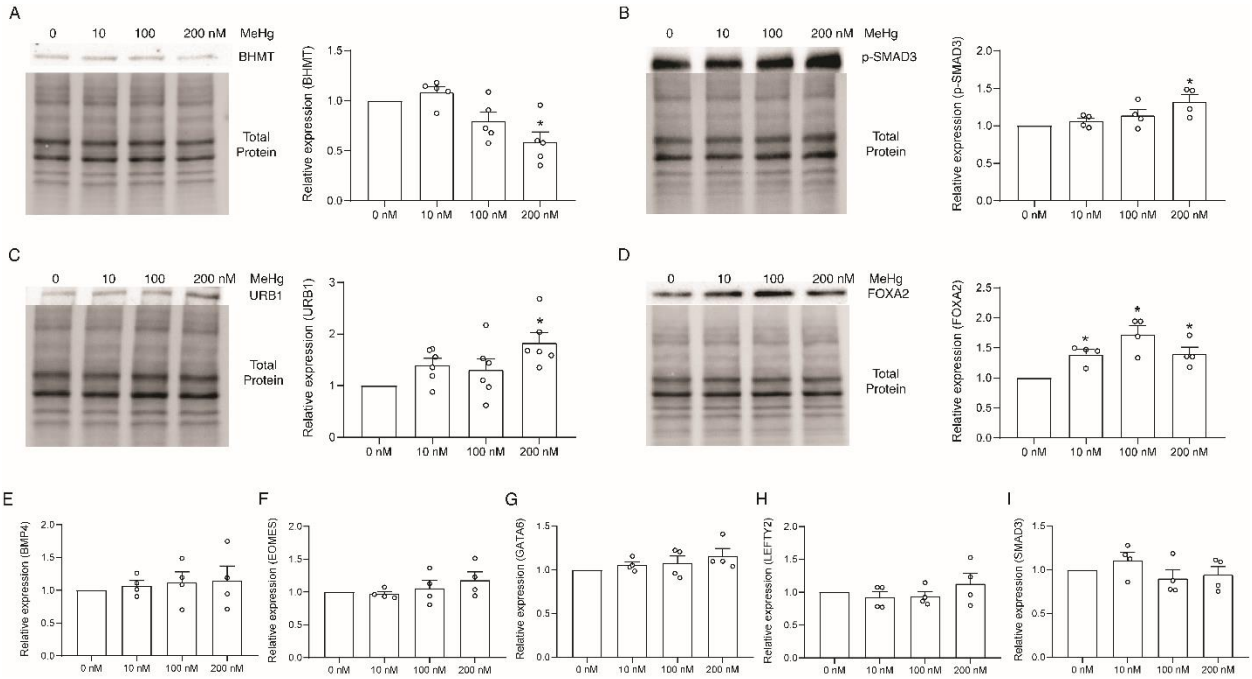

Figure 4.8. Expression of BHMT, p-SMAD3, URB1, FOXA2, BMP4, EOMES, GATA6, LEFTY2, and SMAD3 protein in definitive endoderm (DE) cells exposed to MeHg during human embryonic stem cells to DE cell differentiation. Data are presented as means ± SEMs with N = 4-6 for each protein. Each batch was first normalized to 0 nM exposure group before comparison. One-way ANOVA and Dunnett's post hoc test were used at each time point to compare differences between treatment and control groups with $p < 0.05$ being considered as significant marked by asterisk.

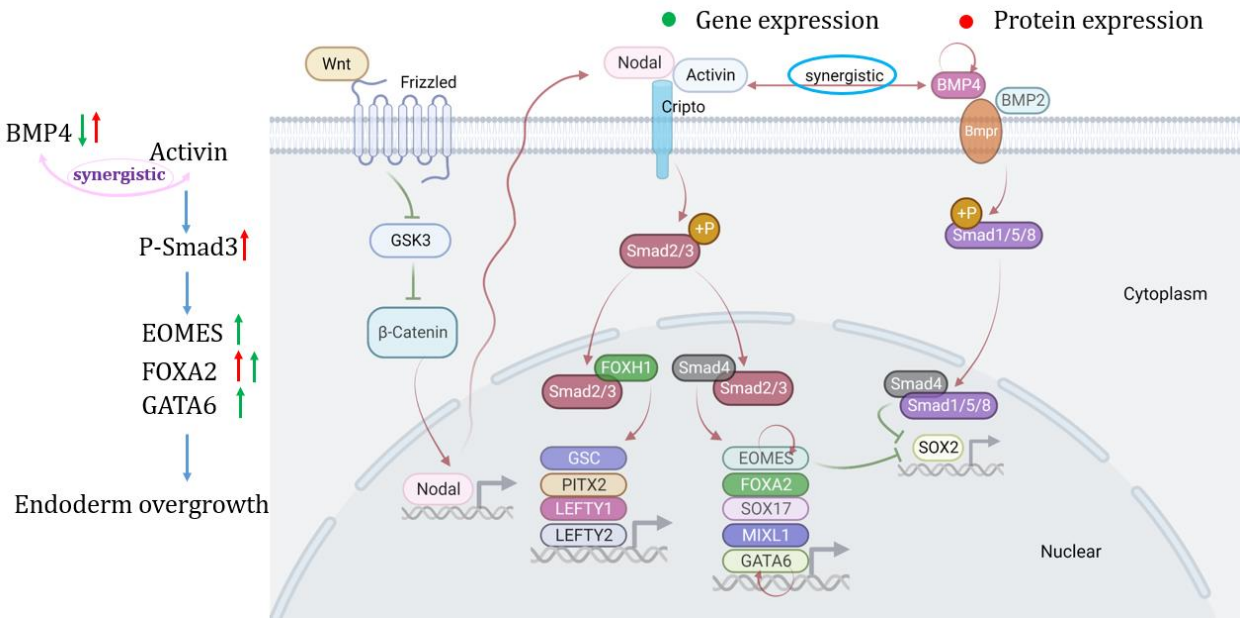

Figure 4.9. Summary of proteins involved in definitive endoderm differentiation and changes in these genes/proteins following MeHg exposure during differentiation. See text for more information.

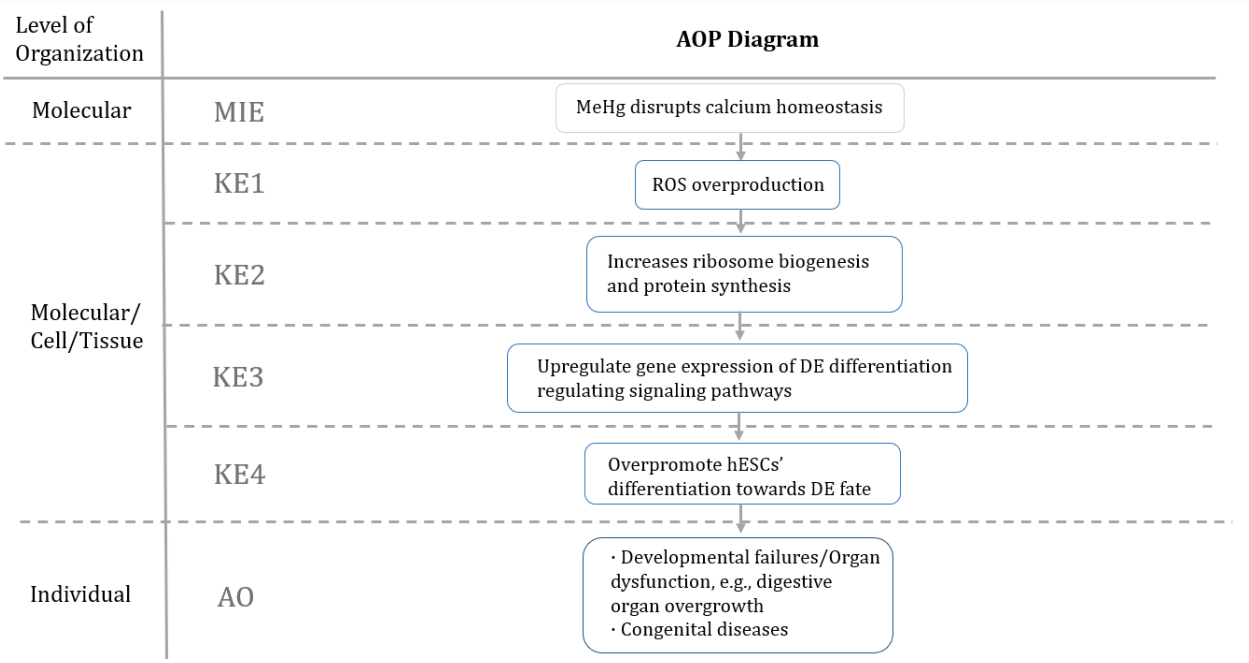

Figure 4.10. Adverse outcome pathway diagram of the effects of MeHg exposure during human embryonic stem cell to definitive endoderm differentiation.

4.7 Supplemental Tables and Figures

Table S4.1. Primer information for qPCR.

Gene name	Accession No./Reference	Sequence
URB1	NM_014825.3	F: 5'-CATCTGCCCGGACCCCATAG-3' R: 3'-TCCTGACAAAGCACTTCCTCTC-5'
SMAD3	PMID: 25140399	F: 5'-CCCCAGCACATAATAACTTGG-3' R: 3'-AGGAGATGGAGCACCAGAAG-5'
BMP4	NM_001202.6	F: 5'-GGGATTCCCGTCCAAGCTAT-3' R: 3'-ACGGAATGGCTCCATAGGTC-5'
GATA6	NM_005257.6	F: 5'-AGAAGCGCGTGCCTTCATC-3' R: 3'-ATAGCAAGTGGTCTGGGCAC-5'
EOMES	PMID: 29382828	F: 5'-CGGCCTCTGTGGCTCAAA-3' R: 3'-AAGGAAACATGCGCCTGC-5'
FOXA2	NM_021784.5	F: 5'-TGCACTCGGCTTCCAGTATG-3' R: 3'-CGTGTTCATGCCGTTCATCC-5'
GAPDH	NM_002046.7	F: 5'-TCGGAGTCAACGGATTTGGT-3' R: 3'-TTCCCGTTCTCAGAATTGAC-5'
HDDC2	NM_016063.3	F: 5'-GAAGCGGTCATGAAAGTGCC-3' R: 3'-ATGAACCTAGCCTTCGGGGA-5'
ZNF324B	PMID: 30927132	F: 5'-CATTGGAAGGACAAACCTAGGATGATG-3' R: 3'-CTTATCTGCTCCAAAGCTATCACTGTC-5'

Table S4.2. Antibody information used for Western blot.

Marker	Dilution	Catalog No.	Company
BHMT	1:1000 in NFDM	PA5-21466	Thermo Fisher Scientific
URB1	1:500 in NFDM	20023-1-AP	Thermo Fisher Scientific
SMAD	1:1000 in NFDM	MA5-14939	Thermo Fisher Scientific
p-SMAD	1:500 in BSA	ab52903	Abcam
BMP4	1:500 in BSA	MA5-15572	Thermo Fisher Scientific
GATA6	1:1000 in NFDM	PA5-40559	Thermo Fisher Scientific
EOMES	1:500 in NFDM	MA5-24291	Thermo Fisher Scientific
LEFTY2	1:1000 in NFDM	PA5-21367	Thermo Fisher Scientific
FOXA2	1:1000 in NFDM	ab108422	Abcam
PSMB3	1:1000 in NFDM	PA5-28999	Thermo Fisher Scientific
LC3B	1:1000 in NFDM	PA5-32254	Thermo Fisher Scientific
SQSTM1/p62	1:1000 in NFDM	ab56416	Abcam

Goat anti-Rabbit secondary antibody, HRP	1:5000 in BSA/NFDM	G-21234	Thermo Fisher Scientific
Goat anti-Mouse secondary antibody, HRP	1:5000 in BSA/NFDM	ab97023	Abcam

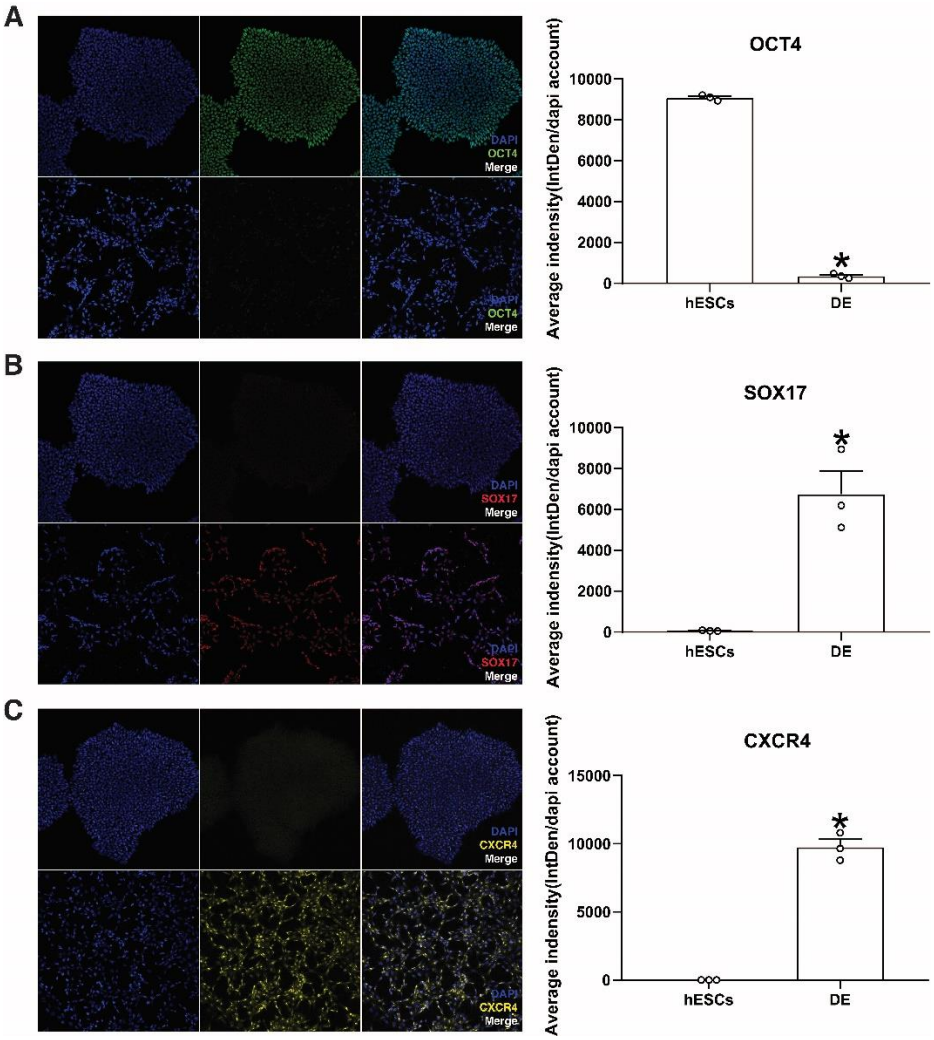

Figure S4.1. Verification of DE induction before conducting experiments. Pre-induction hESCs and induced DE cells were immunostained for both pluripotency marker (OCT4) and definitive endoderm markers (SOX17 and CXCR4). Green indicates positive staining of OCT4 (A). Red indicates positive staining of SOX17 (B). Yellow indicates positive staining of CXCR4 (C). Blue indicates positive staining of nuclei using DAPI. The fluorescent intensity was normalized to DAPI numbers. Data are presented as means ± SEMs with N = 3 for each group. T-test was conducted to compare differences between the average fluorescent intensity of hESCs and DE cells with $p < 0.05$ being considered as significant marked by asterisk.

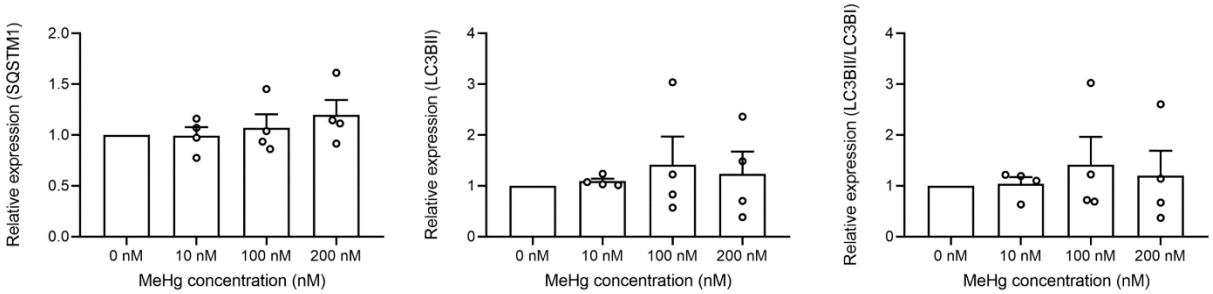

Figure S4.2. Expression of autophagy related proteins SQSTM1, LC3BII and ratio of LC3BII/LC3BI in definitive endoderm (DE) cells exposed to MeHg during human embryonic stem cells to DE cell differentiation. Data are presented as means ± SEMs with N = 4 for each protein. Each batch was first normalized to 0 nM exposure group before comparison. One-way ANOVA and Dunnett's post hoc test were used at each time point to compare differences between treatment and control groups with $p < 0.05$ being considered as significant marked by asterisk.

Chapter 5. General Discussion

5.1 Thesis summary and research contribution

The overall objective of this thesis was to investigate the embryo-/developmental toxicity of methylmercury (MeHg) and the Nunavik Chemical Mixture (NCM) using human embryonic stem cells (hESCs). Chapter 2 verified hESCs as an *in vitro* model for testing the toxicity of environmental chemicals and characterized the effects of low doses of MeHg on cultured hESCs. My findings suggest that hESCs are useful *in vitro* models in embryotoxicity screening of MeHg, and low doses of MeHg adversely affect hESCs when exposed during a period of time that models early stages of embryo development. In chapter 3, I examined the effects of NCM on early-developing embryos by using the same cell model under the same culture conditions. I then compared the effects of NCM exposure on hESCs to that of MeHg exposure alone (Chapter 2), or compared the effects of NCM exposure to the effects of similar environmental chemical mixtures from other studies. The main findings suggest that NCM is embryotoxic. Still, the effects caused by NCM exposure were different from that caused by the same doses of single MeHg exposure, indicating potential interactions among components within a mixture. Therefore, more is needed to assess the embryotoxicity of chemical mixtures than by simply looking at their individual effects.

My objective for Chapter 4 was to determine the effects of low doses of MeHg on the development and specification of hESCs during definitive endoderm (DE) differentiation. I induced hESCs towards DE cells and exposed MeHg during the induction process. Findings from this chapter show that exposure to MeHg during DE cell differentiation could affect cell specification towards endoderm, which may pose potential risks to subsequent embryo development *in vivo*. The altered ribosome biogenesis and global protein synthesis/translocation

status which could be due to calcium dyshomeostasis and ROS imbalance, could be the main underlying mechanisms based on the pathway analysis results.

Overall, the finding of this thesis verified the value of hESCs in embryotoxicity and developmental toxicity testing of environmental contaminants, identified the potential risks of MeHg and NCM exposures on human early-stage developing embryos and highlighted the importance of evaluating the effects of chemical mixtures, instead of assessing chemical mixtures by looking at the effects or NOAELs of the individual components. This thesis provided information in predicting the potential effects of prenatal environmental chemical exposures and in protecting specific populations from those exposures. Moreover, the potential toxicity of MeHg in the early development of non-neuronal systems was examined, and the underlying mechanisms were also inferred. This information advanced the understanding of MeHg's toxicity, made aware of the potential health concerns of MeHg's developmental toxic effects on other organs, such as the pancreas and liver, and provided new directions for the toxicity research of MeHg.

5.2 hESCs as an *in vitro* model for environmental chemical toxicity testing

Although hESCs is a promising model in the field of toxicity testing and have multiple advantages, such as unlimited proliferation and the potential to differentiate, the procedures of cell maintenance and toxicity testing methods are still not completely standardized, leading to unstable cell growth status and huge variances in testing results [1, 2]. Thus, the culture conditions and induction processes were optimized based on our own lab circumstances before conducting any treatments or endpoint measurements for more reliable results. Specifically, as I aimed to mimic the *in vivo* blastocyst, pre-, during, and early post-implantation stages using hESCs in Chapter 2 and 3, the cell seeding density, dissociation and cryopreservation methods,

and oxygen (O_2) and carbon dioxide (CO_2) concentrations were optimized to allow high viability and attachment without any visible differentiation upon 7 days of continuous culturing. In my thesis, the cells were cultured under 4% O_2 and 10% CO_2 with a seeding density of 1 x 10^4/ml for dosing experiments. Cell statuses were monitored by an optical microscope daily (Figure 5.1A-C showing typical hESC colonies and spontaneous differentiations), and the pluripotency of hESCs was verified by staining specific pluripotency markers (OCT4 and Tra-1-81) after culturing (Figure S2.2).

For Chapter 4, although a commercial induction kit for DE cells was used, multiple conditions were optimized, including feeder layer regents, cell density upon plating, cell status and colony size upon induction initiation, maximize the viability of target differentiation, and to ensure relatively uniform cell populations between batches for dosing experiments. Cell morphology changes during induction were observed with an optical microscope (Figure 5.2A-C) and DE cell differentiation was verified by staining of its specific cell markers (SOX17 and CXCR4) (Figure S4.1). For all chapters in this thesis, vails of frozen cells were first generated from the original cell supply to be used for experiments. Only cells within 15 passages from purchase were used to avoid genetic instabilities.

Although variances still existed, the findings of this thesis were consistent and comparable to the evidence from both epidemiological and animal studies. For example, previous animal studies have shown that MeHg is a potent neurotoxicant, especially during early development [3], and an improved version of the embryonic stem cell test using mouse embryonic stem cells has also classified MeHg as an embryo-toxicant [4, 5]. In comparison, my results showed that MeHg exposure is capable of increasing apoptosis in undifferentiated hESCs, enhancing self-renewal gene expression, and promoting endoderm differentiation during hESC

to DE differentiation. This suggests that hESCs are a useful tool in predicting the embryotoxicity of environmental chemicals, which can provide reliable results following the "3R" rules (Replacement, Reduction and Refinement) [6] without concerns of species-specific differences.

5.3 Comparison between the effects of MeHg and NCM on hESCs: importance of assessing mixture toxicity as a whole

Findings from Chapters 2 and 3 showed that both MeHg and NCM are toxic to hESCs, resulting in decreased cell viability, increased rate of apoptosis, disrupted cell cycle and altered expressions of lineage marker genes/proteins. However, the levels of changes, specific markers altered, and the doses which induced significant changes are different.

Firstly, the level of cell viability decrease was lower in MeHg-dosed hESCs than in hESCs dosed with NCM containing the same concentrations (10, 50 and 100 nM) of MeHg, reflecting other chemicals within the NCM may act synergistically with MeHg to enhance the cytotoxic effects of MeHg. Cell viability is usually used to reflect the "death effect" of a toxicant. However, in our case, viability is more likely represents the percentage of inhibition of mitochondrial dehydrogenase activity. There was no dramatical differences observed in the effects of colony size and numbers in the cells dosed with MeHg compared to cells dosed with NCM containing similar concentration of MeHg. Moreover, MeHg alone at 10 and 50 nM, but not 0.5X and 2.4X of NCM (containing 10 and 50 nM MeHg, respectively) significantly increased apoptosis in hESCs. These results suggest that other components within the NCM masked the effect of MeHg on apoptosis and at the same time, exerted/enhanced the inhibition of mitochondrial dehydrogenase activity in hESCs. On the other hand, as low doses of POPs within the NCM usually act as endocrine disruptors and do not induce significant cytotoxicity, and lead alone at the concentration levels within the NCM could not cause any reduction in cell viability

on hESCs according to previous evidence [7], it is suggesting that MeHg could be the main driver in decreasing cell viability in hESCs in this study.

Secondly, the effects of MeHg on apoptosis and cell cycle seemed to be lessened when MeHg is co-exposed with other environmental contaminants, as in the case of NCM. As mentioned above, MeHg at 10, 50, and 200 nM alone increased apoptosis in hESCs after both 24 h and 6 days of exposure. In contrast, the 4.8X CM dose containing 100 nM MeHg, but not the 0.5X and 2.4X doses containing 10 and 50 nM MeHg, respectively, increased apoptosis in hESCs after either 24h or 6 days of exposure. This suggests that the presence of other chemicals in the NCM diminished the effect of MeHg on apoptosis at both time points. In addition to the effect on apoptosis, the effect of MeHg on the cell cycle was also decreased by the presence of other chemicals in the NCM since MeHg at 10 and 50 nM alone, but not 0.5X and 2.4X CM containing 10 and 50 nM MeHg, increased the proportion of G1 phase cells and decreased proportion of G2 cells after 6 days of exposure. One key factor may be the difference in the internal dose of MeHg. The intracellular Hg content after 24 h of NCM exposure was much lower than that of MeHg alone exposure, suggesting that other chemicals in the NCM might either decrease the uptake or enhance the elimination of MeHg from the hESCs.

Thirdly, the effects of MeHg on lineage gene/protein expressions are different when exposed to MeHg alone or co-exposed with other environmental contaminants in NCM. A specific example is, MeHg alone at 50 nM increased protein expression of self-renewal gene OCT4 and decreased gene expression of an ectoderm marker PAX3 in hESCs after 6 days of exposure. In contrast, 2.4X NCM containing 50 nM MeHg had no influence on OCT4 and PAX3, but increased protein expression of an endoderm marker LEFTY2 in hESCs after 6 days of exposure. The 0.1X NCM containing 2 nM MeHg decreased gene expression of a mesoderm

marker TBX3. This suggests that endoderm and mesoderm differentiation may be a sensitive target of NCM, while MeHg alone could affect the potency of self-renewal and ectoderm development of hESCs. The different lineage marker changes could be more likely due to other chemicals, especially POPs, which usually act as endocrine disruptors when, at low doses, they interact with MeHg to drive the expressions of lineage genes/proteins towards distinct directions.

To my knowledge, Chapters 2 and 3 are the first studies to characterise the effects of MeHg and NCM using undifferentiated hESCs and compare the difference in embryotoxicity of MeHg alone and when exposed in an environmental contaminant mixture. The results from comparing the effects of single MeHg exposure and NCM exposure on hESCs are consistent with the findings from previous *in vivo* studies [8-10], showing that the effects of an individual chemical can be altered by the presence of other chemicals in the mixture and support the notion that it is insufficient to assess risks of chemical mixtures (especially at sublethal concentrations) by looking at the toxicity of its individual components.

Although risk assessment of mixtures is tricky, a concentration addition (CA) method is generally used as the default since it has been regarded to be more protective [11]. While based on the findings from this thesis, the components-based approach and the whole-mixture approach should be incorporated to address the potential interactions within the components of a chemical mixture. To better evaluate the effects of chemical mixtures, several advanced tools, such as adverse outcome pathways (AOPs), read-across and toxicokinetic and toxicodynamic (TKTD) approaches have emerged. These approaches are continuously been developed and have been used more widely. However, as the AOP approach is based on the same targets and the shared molecular initiating event (MIE) and key events (KE), when applying an AOP method, extra attention should be taken regarding the concentration/dose ranges of the components present in

the mixture. Chemicals usually produce different actions at different dose ranges, thus should follow different AOPs.

Findings from these two chapters provide valuable information to better understand the embryotoxicity of MeHg and NCM exposures during human early embryo development and provide helpful information in lowering the potential risks of adverse pregnancy outcomes among these sensitive populations.

5.4 Effects of MeHg on undifferentiated hESCs versus effects of MeHg on hESC to DE cell differentiation

It has been reported that undifferentiated human pluripotent stem cells are more sensitive to some types of stressors, including therapeutic agent [12] and drugs [13], than differentiated cells. This point is also supported by the findings in this thesis when comparing the effects of MeHg on undifferentiated hESCs to hESCs differentiating towards DE cells. In Chapter 2, cell viability of hESCs was reduced by close to 50% following two days of 200 nM MeHg exposure compared with the vehicle control, while no significant decrease in cell viability was observed in hESCs-derived DE cells exposed to the same concentrations of MeHg in Chapter 4, suggesting that undifferentiated hESCs could have a lower tolerance to MeHg toxicity than differentiating hESCs. This could be due to a change in cell type (hESCs vs DE cells derived from hESCs), which can result in a change in cellular integrity, membrane properties and mitochondrial sensitivity, which have been shown to result in a difference in the uptake and accumulation of MeHg [14] though this has not been verified specifically in the two cell types used in the current thesis. It has been found that undifferentiated mammalian embryonic stem cells contain high levels of damaged proteins, which were identified as the main targets of protein oxidation, such as chaperones and proteins of the cytoskeleton. However, upon differentiation, the cells have

been shown to rid themselves by efficiently eliminating these damaged proteins both *in vivo* and *in vitro*, probably by the increased activity of the 20S proteasome [15, 16]. This could also contribute to the difference in the effects of MeHg on cell viability or in the tolerance of MeHg toxicity of hESCs at the two different differentiated windows in this thesis.

In addition. the inhibited autophagy on undifferentiated hESCs could be another indicator of lower cell viability caused by MeHg exposure since a proper level of autophagy is critical for maintaining survival and dealing with cellular stress in stem cells [17]. Notably, the inhibition of autophagy was found to support long-term self-renewal and to suppress cell differentiation in hESCs [18, 19], which is consistent with the results of lineage marker expressions in Chapter 2, suggesting autophagy could be one of the potential mechanisms in MeHg's capability in enhancing the pluripotency of hESCs when exposed during the undifferentiated state. However, there was no significant change in autophagy level in the differentiating hESCs after the same exposure in Chapter 4. A possible reason is that enhanced differentiation promoted autophagy in stem cells [20, 21], which offset the autophagy inhibition caused by MeHg exposure.

Based on the effects of MeHg enhancing pluripotency in undifferentiated hESCs in Chapter 2, it would be expected that MeHg exposure during DE cell differentiation might inhibit the differentiation process. However, MeHg seems in contrast to enhance differentiation in the differentiating hESCs towards DE cells in Chapter 4. In undifferentiated hESCs, exposure to MeHg drives the expression of self-renewal genes such as OCT4, SOX2 and NANOG, resulting in the increased pluripotency of hESCs that were exposed to MeHg. This upregulation of many self-renewal genes, however, was no longer observed when MeHg was administered during the hESC to DE differentiation process. During differentiation, MeHg disrupted calcium homeostasis, which leads to elevated levels of ROS and could, in turn, increase ribosome

biogenesis and protein biosynthesis, enhancing the overall differentiation of hESCs mentioned in Chapter 4. Our results also showed that MeHg affected DNA repair, suggesting the presence of DNA damage which may further lead to the upregulation of mitochondrial oxidative phosphorylation that may also lead to ROS production [22]. Previous evidence has suggested that low levels of ROS are required for stem cells to maintain quiescence and self-renewal. In contrast, the overproduction of ROS could lead to stem cell differentiation [23] and specifically promote DE differentiation during directed hESC differentiation [24]. Thus, combined with the increased expression of transcription factors related to endoderm differentiation, such as EOMES and FOXA2, the cells could be ultimately overpromoted towards the endodermal fate when exposed to MeHg.

In addition, the International Agency on Research of Cancer (IARC) has classified MeHg as Group 2B compounds, which is possibly carcinogenic to humans [25], and Hg has also been suggested to promote carcinogenic risk through modulating cell proliferation, inducing oxidative DNA damage, and epigenetic modifications, though the evidence is still contradictory [26]. In our data, some significantly changed genes, such as E2F3, E2F6, CCND1, CCND2, and CCND3 which are involved in cell cycle regulation, also play a role in the formation and development of various human primary tumors [27], with many being tumors of mesodermal/endodermal-derived organs, such as urinary bladder, liver, colon and gastric cancers [27-29]. Thus, a potential link between these tumors and early developmental MeHg exposure cannot be ruled out. Considering that normal stem cells and cancer stem cells share many similar characteristics, such as extensive proliferation and expression of pluripotent and self-renewal markers [30, 31], studies on the relationship between MeHg exposure during early embryo development and organogenesis, and fetal tumor initiation is warranted.

In conclusion, these two chapters (Chapter 2 and Chapter 4) firstly suggest that undifferentiated hESCs could be more susceptible to MeHg toxicity compared to their differentiating counterparts towards DE cells, and the effects of low-dose of MeHg on cell fate decision of hESCs could be distinct from pluripotent to early differentiating stages, illustrating *in vivo* effects of MeHg exposure on the early developing embryos could be specific to the differentiation state of the cell. Findings from these two chapters enrich the understanding of embryotoxicity and developmental toxicity of MeHg and provide new directions in studying environmental chemical toxicity using stem cells.

5.5 Limitations and further directions

Although Chapters 2 and 3 have recognized hESCs as a promising *in vitro* model in testing environmental chemical toxicity and have provided valuable information in understanding the embryotoxicity of both MeHg and NCM, limitations still exist. First and foremost is that all findings in this thesis were obtained based on the hESC-H9 line, which was derived from one donor. Thus, all conclusions drawn from this thesis may only represent the biology of the donor. As various hESC lines have different karyotypes, self-renewal capacity and differentiation potential, which may affect the toxic response to environmental stimuli, multiple hESC lines derived from donors with different genetic and genders background, races, ages and even health conditions should be used and compared when screening the toxicity of environmental chemicals (not only MeHg and NCM) to make the extrapolation of the *in vitro* results to general populations more comprehensive and accurate.

Chapter 4 provided insights on predicting the potential effects of MeHg on the cell fate decision, particularly the development and specification of hESCs during the induction towards DE cells and speculated the underlying mechanisms. However, future inductions of the DE cells

into cells of later differentiated stages, such as progenitors and precursor cells of endoderm-derived organs, should be performed to verify these predicted developmental effects of MeHg exposure during their early differentiation.

Findings from Chapters 2 and 4 revealed that the effects of MeHg on hESCs are different based on the different differentiation status of the cell. Thus, one can reasonably induce that this differentiation stage-specific effects may also be present with other environmental contaminants or contaminant mixtures like NCM. In that case, the effects of multiple environmental chemicals on stem cells at various differentiation stages are valuable for further study to boost the knowledge of the embryotoxicity and developmental toxicity of the environmental toxicants.

In addition, this thesis focused more on the genetic alterations of MeHg and NCM on hESCs. As epigenetic status that can be affected by environmental stressors [32] also play an important role in the cell fate decision of hESCs [33, 34], the epigenetic effects of MeHg and NCM on hESCs should be further examined. The results from both genetic and epigenetic studies should be combined when explaining their toxicity on the development and differentiation of hESCs *in vitro*, as well as assessing the potential risks of adverse pregnancy and developmental outcomes related to such exposures *in vivo*.

Overall, findings from this thesis emphasized the value of hESCs in screening toxicity of environmental contaminants, enriched the understanding of potential pregnancy and developmental outcomes associated with MeHg and NCM exposure, and provided information that could help minimize the risks from such exposures among vulnerable populations. However, these contributions are only the beginning to understanding the toxicity of MeHg and NCM and exploring the underlying mechanisms of their toxicity.

5.6 References

1. Adler, S., et al., First steps in establishing a developmental toxicity test method based on human embryonic stem cells. Toxicology *in vitro*, 2008. **22**(1): p. 200-211.
2. Schwartz, P.H., et al., Traditional human embryonic stem cell culture, in Human Pluripotent Stem Cells. 2011, Springer. p. 107-123.
3. Castoldi, A.F., et al., Neurodevelopmental toxicity of methylmercury: Laboratory animal data and their contribution to human risk assessment. Regulatory Toxicology and Pharmacology, 2008. **51**(2): p. 215-229.
4. Baek, D.H., et al., Embryotoxicity assessment of developmental neurotoxicants using a neuronal endpoint in the embryonic stem cell test. Journal of Applied Toxicology, 2012. **32**(8): p. 617-626.
5. Stummann, T., L. Hareng, and S. Bremer, Embryotoxicity hazard assessment of methylmercury and chromium using embryonic stem cells. Toxicology, 2007. **242**(1-3): p. 130-143.
6. Flecknell, P., Replacement, reduction, refinement. ALTEX-alternatives to Animal Experimentation, 2002. **19**(2): p. 73-78.
7. Senut, M.-C., et al., Lead exposure disrupts global DNA methylation in human embryonic stem cells and alters their neuronal differentiation. Toxicological Sciences, 2014. **139**(1): p. 142-161.
8. Pelletier, G., et al., Contribution of methylmercury, polychlorinated biphenyls and organochlorine pesticides to the toxicity of a contaminant mixture based on Canadian Arctic population blood profiles. Toxicology letters, 2009. **184**(3): p. 176-185.

9. Elabbas, L.E., et al., *In utero* and lactational exposure to a mixture of environmental contaminants detected in Canadian Arctic human populations alters retinoid levels in rat offspring with low margins of exposure. Journal of Toxicology and Environmental Health, Part A, 2014. **77**(5): p. 223-245.
10. Padhi, B., et al., Gene expression profiling in rat cerebellum following *in utero* and lactational exposure to mixtures of methylmercury, polychlorinated biphenyls and organochlorine pesticides. Toxicology letters, 2008. **176**(2): p. 93-103.
11. Bopp, S., et al., Scientific methodologies for the assessment of combined effects of chemicals–a survey and literature.
12. Matsumoto, R., et al., Plasma-activated medium selectively eliminates undifferentiated human induced pluripotent stem cells. Regenerative Therapy, 2016. **5**: p. 55-63.
13. Panina, Y., et al., Human ES and iPS cells display less drug resistance than differentiated cells, and naïve-state induction further decreases drug resistance. The Journal of Toxicological Sciences, 2021. **46**(3): p. 131-142.
14. Morken, T.S., et al., Effects of methylmercury on primary brain cells in mono-and co-culture. Toxicological Sciences, 2005. **87**(1): p. 169-175.
15. Naujokat, C. and T. Šarić, Concise review: role and function of the ubiquitin-proteasome system in mammalian stem and progenitor cells. Stem cells, 2007. **25**(10): p. 2408-2418.
16. Hernebring, M., et al., Elimination of damaged proteins during differentiation of embryonic stem cells. Proceedings of the National Academy of Sciences, 2006. **103**(20): p. 7700-7705.
17. Chang, N.C., Autophagy and stem cells: self-eating for self-renewal. Frontiers in Cell and Developmental Biology, 2020. **8**: p. 138.

18. Wang, Y. and H. Zhang, Regulation of autophagy by mTOR signaling pathway. Autophagy: Biology and Diseases, 2019: p. 67-83.

19. Zhou, J., et al., mTOR supports long-term self-renewal and suppresses mesoderm and endoderm activities of human embryonic stem cells. Proceedings of the national academy of sciences, 2009. **106**(19): p. 7840-7845.

20. Tra, T., et al., Autophagy in human embryonic stem cells. PloS one, 2011. **6**(11): p. e27485.

21. Xu, Y., et al., Chaperone-mediated autophagy regulates the pluripotency of embryonic stem cells. Science, 2020. **369**(6502): p. 397-403.

22. Snezhkina, A.V., et al., ROS generation and antioxidant defense systems in normal and malignant cells. Oxidative medicine and cellular longevity, 2019. **2019**.

23. Zhou, D., L. Shao, and D.R. Spitz, Reactive oxygen species in normal and tumor stem cells, in Advances in cancer research. 2014, Elsevier. p. 1-67.

24. Lv, J., et al., Mitochondrial homeostasis regulates definitive endoderm differentiation of human pluripotent stem cells. Cell death discovery, 2022. **8**(1): p. 1-13.

25. Cancer, I.A.f.R.o., Beryllium, cadmium, mercury, and exposures in the glass. Apresentado em: IARC Working Group on the Evaluation of Carcinogenic Risks to Humans: Beryllium, Lyon, 1993.

26. Skalny, A.V., et al., Mercury and cancer: Where are we now after two decades of research? Food and Chemical Toxicology, 2022: p. 113001.

27. Fang, Y., et al., miR-449b inhibits the proliferation of SW1116 colon cancer stem cells through downregulation of CCND1 and E2F3 expression. Oncology reports, 2013. **30**(1): p. 399-406.

28. Chen, Z., et al., rtcisE2F drives liver TIC self-renewal and metastasis via m6A-modulated mRNA stability of E2F6 and E2F3. bioRxiv, 2021.
29. Shan, Y.S., et al., Cyclin D1 overexpression correlates with poor tumor differentiation and prognosis in gastric cancer. Oncology letters, 2017. **14**(4): p. 4517-4526.
30. Shackleton, M. Normal stem cells and cancer stem cells: similar and different. in Seminars in cancer biology. 2010. Elsevier.
31. Liu, A., X. Yu, and S. Liu, Pluripotency transcription factors and cancer stem cells: small genes make a big difference. Chinese journal of cancer, 2013. **32**(9): p. 483.
32. Worley, J.R. and G.C. Parker, Effects of environmental stressors on stem cells. World Journal of Stem Cells, 2019. **11**(9): p. 565.
33. Zhang, X., et al., Genome-wide analysis of epigenetic dynamics across human developmental stages and tissues. BMC genomics, 2019. **20**(2): p. 153-162.
34. Yu, Y., et al., Inhibition of EZH2 promotes human embryonic stem cell differentiation into mesoderm by reducing H3K27me3. Stem Cell Reports, 2017. **9**(3): p. 752-761.

5.7 Figures

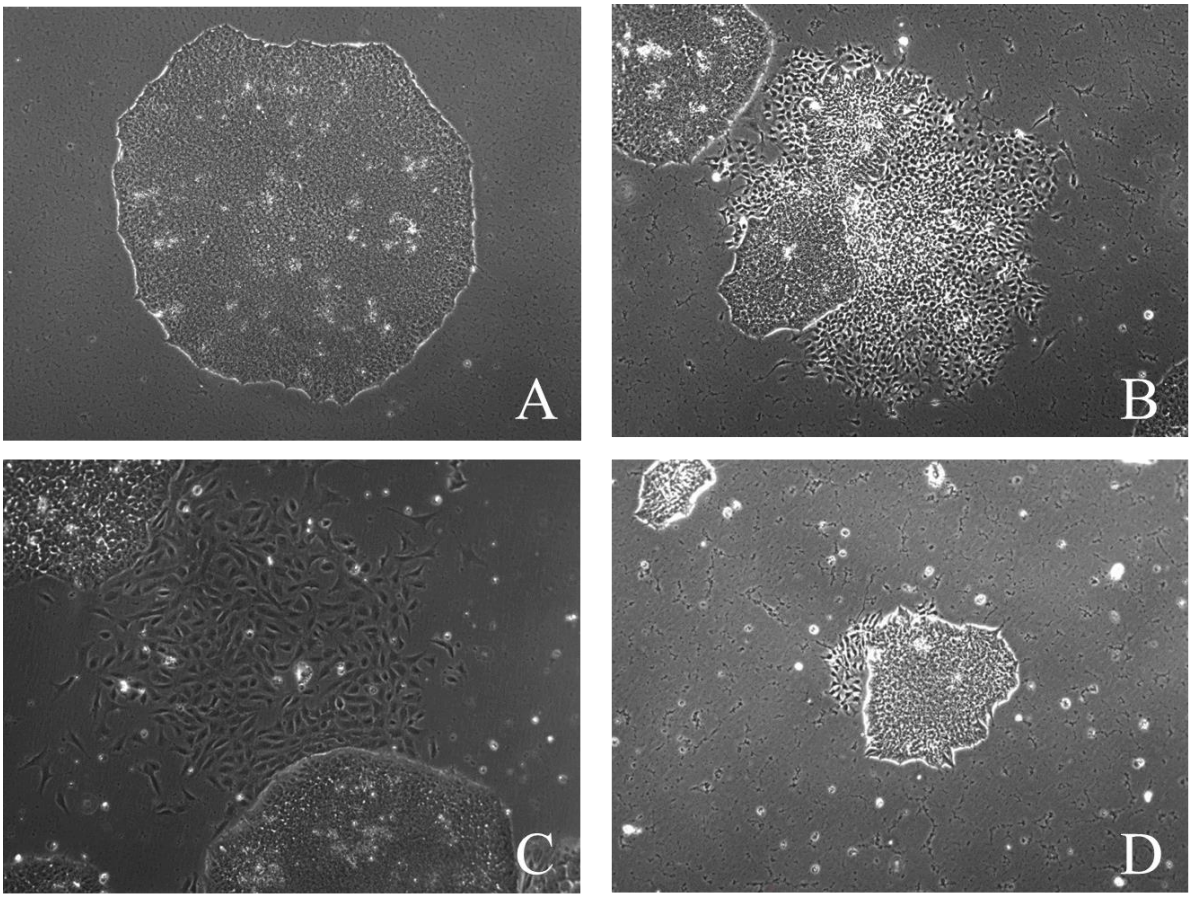

Figure 5.1 Representative culture images of typical hESC colony (A) and spontaneous differentiations (B, C, D). Images were taken under a 10x optical microscope.

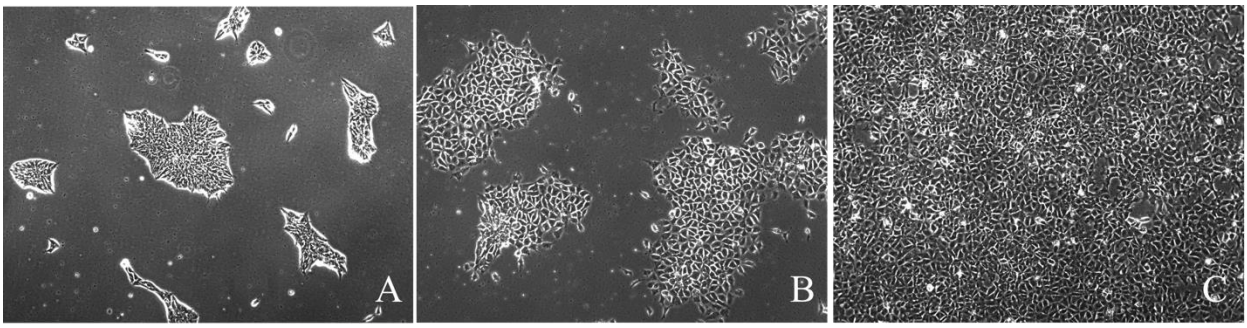

Figure 5.2 Representative culture images during definitive endoderm induction. hESCs before induction (A). Differentiating cells after 24 h of induction (B). Induced DE cells (C).